UNIVERSIDAD POLITÉCNICA DE MADRID

ESCUELA TÉCNICA SUPERIOR
DE INGENIEROS DE TELECOMUNICACIÓN

MASTER UNIVERSITARIO EN INGENIERÍA BIOMÉDICA

TRABAJO FIN DE MASTER

DESIGN, OPTIMISATION AND IMPLEMENTATION OF A ROBOTIC EXOSKELETON FOR LEG REHABILITATION

Camille Grand

2024

UNIVERSIDAD POLITÉCNICA DE MADRID

ESCUELA TÉCNICA SUPERIOR
DE INGENIEROS DE TELECOMUNICACIÓN

MASTER UNIVERSITARIO EN INGENIERÍA BIOMÉDICA

TRABAJO FIN DE MASTER

DESIGN, OPTIMISATION AND IMPLEMENTATION OF A ROBOTIC EXOSKELETON FOR LEG REHABILITATION

Autor

CAMILLE GRAND

Tutores

BLANCA LARRAGA GARCÍA
WILLINGTON JAIME ARCOS LEGARDA

2024

Resumen

Las lesiones neurológicas son lesiones físicas del tejido cerebral que alteran de forma transitoria o permanente la función cerebral. Los cambios físicos después de una lesión neurológica pueden incluir cambios en el tono muscular, que pueden endurecer las articulaciones y provocar movimientos anormales, reducción del equilibrio y la coordinación y debilidad muscular. Por ejemplo, la parálisis cerebral constituye la principal causa común de discapacidad física en los niños, con una prevalencia de aproximadamente 2 por 1.000 nacidos vivos. Es una condición permanente resultado de una lesión cerebral que describe un grupo de trastornos del movimiento y la postura que comienza en la primera infancia. El objetivo del tratamiento es proporcionar terapias tempranas para mejorar la funcionalidad y capacidades finales de los pacientes.

La integración de robots en programas de rehabilitación ofrece numerosas ventajas, tanto para los pacientes como para los terapeutas. Al reducir la carga física y la fatiga, aumentar la eficiencia y mejorar la precisión de las terapias, los robots permiten a los terapeutas centrarse más en tareas complejas y personalizadas. Esta sinergia entre tecnología y experiencia humana promete resultados de rehabilitación más rápidos y efectivos, al tiempo que mejora la calidad de vida de los pacientes y profesionales de la salud.

El proyecto de investigación ExoLeg del Consejo Superior de Investigaciones Científicas tiene como objetivo dar una solución para seguir desarrollando la integración de robots médicos en el campo de la rehabilitación de miembros inferiores.

Este Trabajo Fin de Máster colabora en este proyecto diseñando, optimizando e implementando un exoesqueleto robótico para la rehabilitación de piernas. El robot debe apoyar al paciente durante los ejercicios terapéuticos para ayudarle a recuperar su movilidad.

Al final de este proyecto, se ha probado el rendimiento del ExoLeg y se ha mejorado el diseño.

Palabras clave: Exoesqueleto, Robot médico, Rehabilitación de la marcha, Locomoción de miembros inferiores, Neurología, Robótica, Paciente.

Abstract

Neurological injuries are a physical injury to brain tissue which transiently or permanently alters brain function. Physical changes after a neurological injury can include changes in muscle tone, which can make the joints stiffer and cause abnormal movements, reduced balance and coordination, and muscle weakness. For instance, cerebral palsy constitutes the main common cause of physical impairment in children with a prevalence of approximately 2 per 1000 live births. It is a permanent condition result from brain injury that describes a group of movement and posture disorders that begins in early childhood. The treatment goal is to provide early therapies to improve the functionality and final capabilities of patients.

The integration of robots into rehabilitation programs offers numerous advantages, both for patients and therapists. By reducing physical load and fatigue, increasing efficiency and improving the precision of therapies, robots allow therapists to focus more on complex and personalized tasks. This synergy between technology and human expertise promises faster and more effective rehabilitation results, while improving the quality of life of patients and healthcare professionals.

The ExoLeg research project of the "Consejo Superior de Investigaciones Científicas" aims to provide a solution to continue to develop the integration of medical robots into the field of lower limb rehabilitation.

This Master Thesis collaborates in this project by designing, optimising and implementing a robotic exoskeleton for leg rehabilitation. The robot must support the patient during therapeutical exercises to help him or her regain its mobility.

At the end of this project, the performance of the ExoLeg has been tested and the design has been improved.

Keywords: Exoskeleton, Medical robot, Gait rehabilitation, Lower limb locomotion, Neurology, Robotics, Patient.

Acknowledgment

First of all, I would like to express my gratitude to my tutors for this Master Thesis, Willington Jaime Arcos Legarda and Blanca Larraga García. Thank you, Jaime, for your support and expertise, which were invaluable for the success of my Master Thesis. Thank you, Blanca, for your confidence in me and for helping me manage the project.

A special thank you goes to my two project partners, Clara Pinilla Nicolas and Elena Lopez Pulido. We formed a close-knit and supportive group, always helping and encouraging each other in times of doubt. I especially want to thank Elena, who was a great friend throughout the project and assisted me during the assembly of the exoskeleton.

I would also like to extend my heartfelt thanks to Rodrigo Saldaña Esteban, who was a great help during the last two months of the project. He assisted me significantly during the testing phase and provided excellent advice on improving the mechanical design and optimizing the ExoLeg.

Thank you to everyone in the laboratory at the University, with whom we had a great work environment and enjoyable breaks.

I am grateful to Gabriel Delgado for establishing a valuable connection with the CSIC and for spending some days in the laboratory to assist us with the project.

Finally, thank you to Alvaro Gutiérrez for giving me the opportunity and support to carry out this project in the field that led me to pursue this master's degree.

Contents

Figures index

Tables index

List of acronyms

ADV: Activities of Daily Living.

VR: Virtual Reality.

CP: Cerebral Palsy.

CSIC: Consejo Superior de Investigaciones Científicas.

CT: Computed Tomography.

CVRF: Cerebrovascular Risk Factors.

DOF: Degrees Of Freedom.

ETSIT: Escuela Técnica Superior de Ingenieros de Telecomunicación (Higher Technical School of Telecommunications Engineers).

INE: Instituto Nacional de Estadística (National Institute of Statistics in Spain).

MR: Magnetic Resonance.

PBWS: Partial Body Weight-Supported.

PBWSTT: Partial Body Weight-Supported Treadmill Training.

RAGT: Robot-Assisted Gait Therapy.

ROM: Range Of Motion.

SEN: Sociedad Española de Neurología (Spanish Society of Neurology).

Chapter 1

Introduction and objectives

This Master Thesis is a work carried out in collaboration with the Centro de Automática y Robótica (CAR) of the Centro Superior de Investigaciones Científicas (CSIC). It encompasses the development of a lower limb exoskeleton intended to support rehabilitation therapies in patients suffering from various conditions, such as spinal cord injuries, strokes, neurological disorders, or motor impairments. This Chapter reviews basic concepts about medical robotic rehabilitation devices, the work motivation, objectives, and the document layout.

1.1. Scope of the project and objectives

Robotic devices are increasingly part of modern medicine today. One of the areas where robotic technology is used is rehabilitation. Indeed, lower extremity rehabilitation exoskeletons represent a remarkable advancement in medicine technology [1]. These robotic devices provide physical assistance to individuals suffering from various conditions, such as spinal cord injuries, strokes, neurological disorders, or motor impairments. By combining advances in mechanical engineering, electronics and computing, exoskeletons provide personalized and adaptive support, allowing patients to recover more quickly and regain maximum functionality of their lower limbs.

The main objective of this Master Thesis is to develop an exoskeleton of the inferior limb for the rehabilitation of children. The first objective will be to study the actual mechanical design of the robot and to develop an analysis to explain its functioning. The mechanical conception should be functionable, safe, and comfortable for the user. This will include the selection of appropriate materials in order to ensure both the solidity and lightness of the structure. Then, the joint may to be created to allow natural human movements, while providing sufficient support. Additionally, motors will be integrated into the robot to help to amplify the user' s movements and to provide adaptive assistance based on individual needs.

The second objective will be to do a virtual representation of the ExoLeg using the software MATLAB and Simulink. This virtual model will allow the linking of different system components and the inclusion of the mathematical relationships necessary for optimal functioning of the device. Using these different software tools, along with a design software, will enable the simulation of various movements under different conditions, such as walking or rehabilitation exercises. This approach will allow the performance of the device to be evaluated and areas for improvement to be identified.

As a result of this second objective, the forces exerted on each component will be determined and analysed. These simulation results will enable the evaluation of the device's stability, efficiency, and safety. Additionally, potential design or performance issues will be identified, allowing for necessary adjustments and optimization of the robot.

The development of the exoskeleton for the lower limbs as part of this project could represent a significant advance in the field of medical rehabilitation. Currently, rehabilitation of patients with spinal cord injuries, stroke, neurological disorders or motor impairments often relies on traditional methods. These methods can be laborious and require intensive human assistance. That is why the integration of the ExoLeg could transform these practices by offering a great efficient solution that is less dependent on human resources. Moreover, in the long term, the use of exoskeletons in rehabilitation could lead to a substantial reduction in healthcare costs [2]. By reducing the need for constant assistance from therapists, exoskeletons could reduce the length of stays in rehabilitation centres and the frequency of consultations. In addition, patients’ increased autonomy could reduce their need for care at home or in a specialized establishment.

In summary, the ExoLeg project represents a major opportunity to transform medical rehabilitation, with significant potential impacts on patients’ quality of life and the effectiveness of care. The project’s prospects for improvement and expansion pave the way for continued innovation in this crucial area. However, before the ExoLeg can be used, it must be both functional and safe. Therefore, in this Master Thesis, the focus will be on the mechanical aspects of this exoskeleton, specifically by developing and refining its design and performance

1.2. Document layout

The document is organized in the following chapters:

- **Chapter 1**: In this chapter it is explained the problem statement, a review of the solution and the objectives of this Master Thesis.
- **Chapter 2**: In this chapter, the clinical problem is explored along with an overview of the various robotic solutions currently available on the market.
- **Chapter 3**: In the first subsection of this chapter, the design developed by Willington Jaime Arcos Legarda is presented, along with the various modifications that have been made. A theoretical study and dynamic analysis were then performed. These initial steps enabled the simulation of static forces and allowed conclusions to be drawn about potential optimizations for the current ExoLeg model design.
- **Chapter 4**: This chapter describes the assembly of the device, starting with the 3D printing of parts, followed by an explanation of the various mechanical components, and concluding with the final assembly of all the parts.
- **Chapter 5**: In this chapter it is explained the tests performed and the results that I obtained.
- **Chapter 6**: In this chapter are exposed the conclusions and future challenges drawn from this Master Thesis.

Chapter 2

State of the art

2.1. Clinical problem

This Master Thesis has for objective to develop a medical robot to help patients with their gait rehabilitation. A classification of patients can be made depending on the type of paralysis they suffer, as shown in Figure 2.1:

- **Monoplegia**: Paralysis of a single upper or lower limb.
- **Hemiplegia**: Paralysis of one side of the body, mainly effects the limbs.
- **Diplegia**: Paralysis of upper or lower limbs of both sides of the body.
- **Paraplegia**: Paralysis of lower limbs.
- **Quadriplegia**: Paralysis of all limbs.

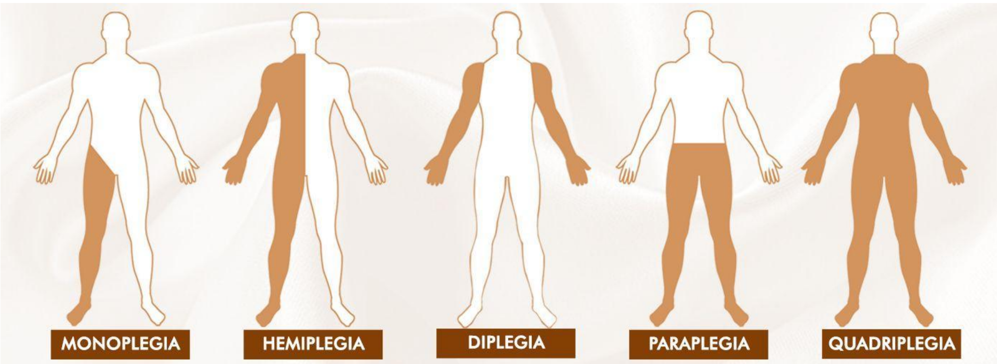

Figure 2.1 : Types of paralysis [3]

Many pathologies can have a repercussion on the proper functioning of locomotor muscles. This means that affected people may have difficulty moving around or completely lose the ability to walk, either temporarily or permanently. To reduce the effects of this loosing ability to walk, a rehabilitation therapy is prescribed to the patient [4]. Gait rehabilitation will be mainly used to fight the motor consequences of the neurological injuries. Neurological injuries are a physical injury to brain tissue which transiently or permanently alters brain function. The diagnosis is done clinically and confirmed by imaging (mainly by Computed Tomography (CT)). Larger injuries can lead to extensive brain oedema and increase intracranial pressure. Physical changes after a neurological injury can include changes in muscle tone, which can make the joints stiff and cause abnormal movements, reduced balance and coordination, and muscle weakness.

- **Spinal cord injury:** As shown in Figure 2.2, it is a damage to the axon of neurons and nerves that transmit incoming and outgoing messages between the brain and the rest of the body. When nerve damage occurs, the loss of muscle control or sensation may be temporary or permanent, partial or complete, depending on the severity of the injury. An injury that is linked to the spinal cord or destroys the nerve's conduit in the spinal cord, can results in permanent paralysis. However, another type of injury that violently impacts the spinal cord can cause temporary weakness that can last for days, weeks, or even months, but unlike the previous case, the consequences will not be permanent.

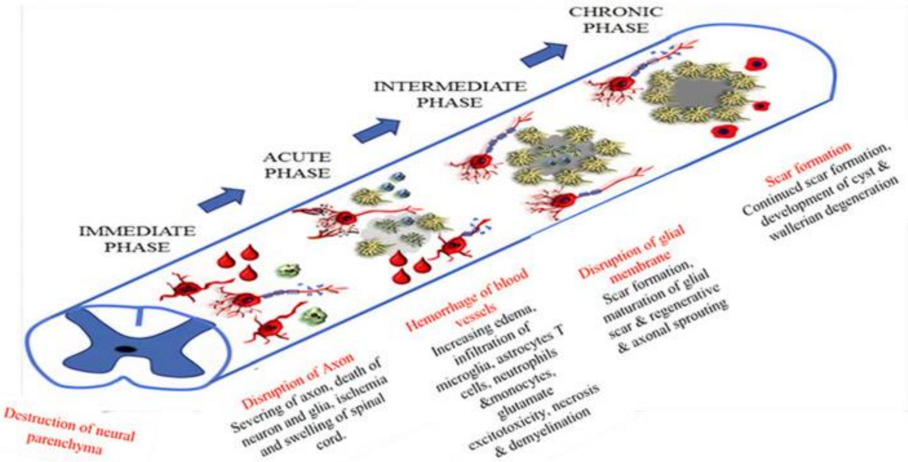

Figure 2.2 : Pathological events according to spinal cord injury phases [5]

- **Stroke:** sudden loss of brain function which occurs when blood circulation in a cerebral region is interrupted. The absence of oxygenated blood in this part of the brain leads to the destruction of the affected brain tissue within minutes of the interruption of circulation, as shown in Figure 2.3. Stroke has two main causes: blockage of a blood vessel carrying blood to the brain (ischemia); and rupture of such a blood vessel (haemorrhage). [6]

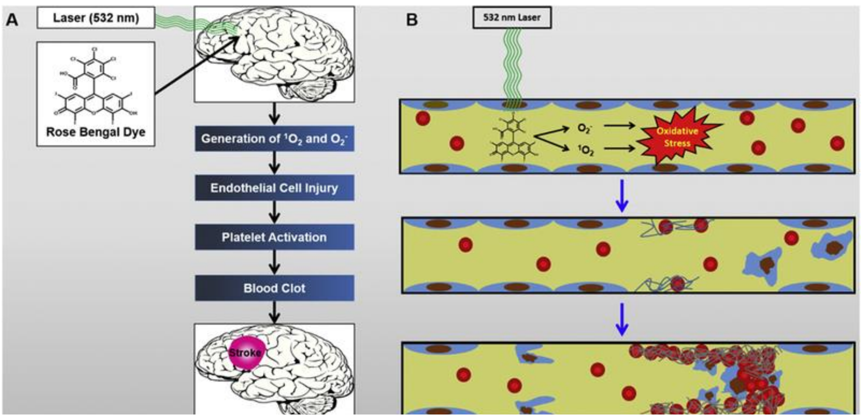

Figure 2.3 : A. Summary of stroke generation using Rose Bengal Dye. B. Stepwise depiction of stroke generation at molecular and cellular levels. [7]

One of the consequences is that it will adversely [8]:

- affect kinematics and kinetics in all paretic lower limb joints,
- disrupt stance and swing phases,
- create an inter-limb asymmetry.

- **Multiple sclerosis:** autoimmune disease that affects the central nervous system. A dysfunction of the immune system leads to lesions which cause motor, sensory, cognitive, visual, or even sphincter disturbances. Early active white matter demyelination falls into three major categories [9]. As shown in Figure 2.4, the most common types of lesions (Patterns I and II) involve mononuclear phagocytes with T-cell infiltration around blood vessels and within the tissue; Pattern II also shows immunoglobulin and complement deposition. In about 25% of active lesions (Pattern III), oligodendrocyte apoptosis occurs along with oligodendrogliopathy, resembling viral, toxic, and ischemic processes, which can be destructive. After the acute phase, the surviving axons can experience different outcomes: they may develop a thin myelin sheath through remyelination, remain without myelin with resolved inflammation, or suffer from persistent inflammation leading to slow myelin degeneration, known as smoldering [10].

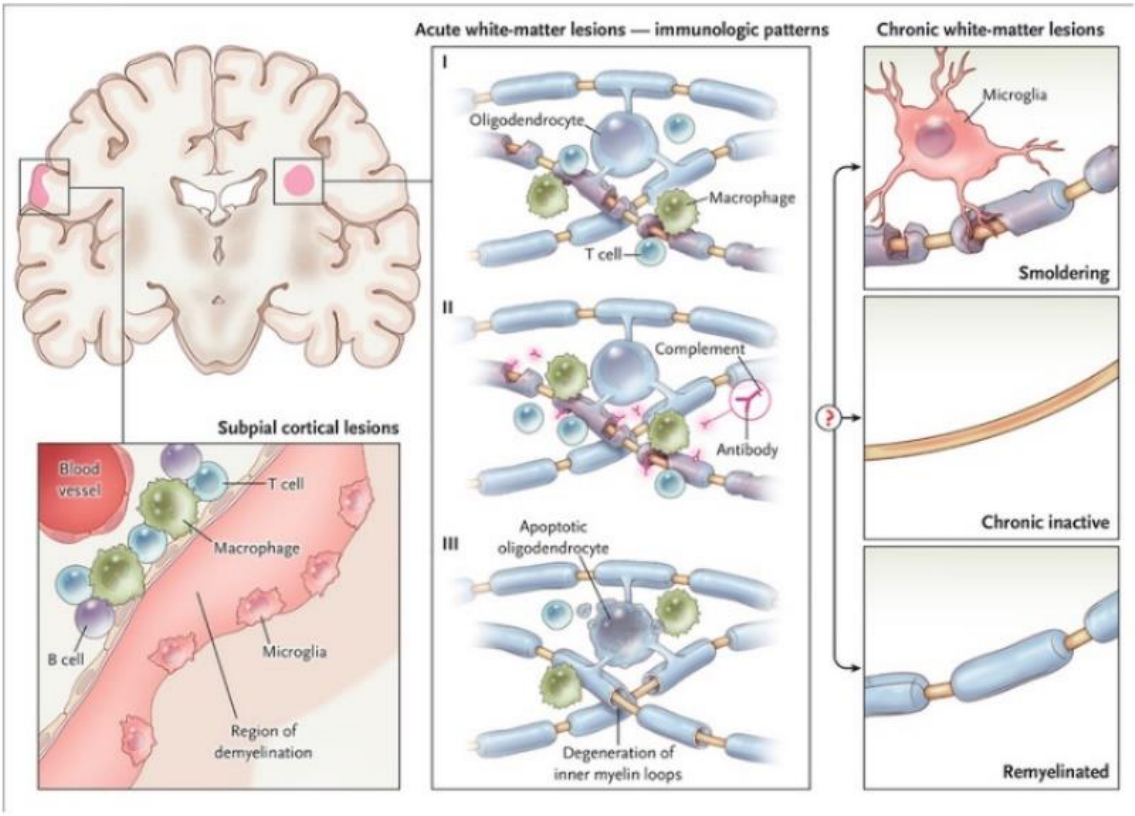

Figure 2.4 : White and grey matter lesions [11]

- **Parkinson:** brain disease that causes motor problems, mental health and sleep problems, as well as pain and other health problems. Additionally, these patients suffer motor fluctuations which are variations in movement ability, also known as “on-off” times.[12] As shown in Figure 2.6, when Parkinson's medications start working, you have periods of well-controlled symptoms, called "active periods," when you can move and function normally. As the effect of a phenomenon known as “fading,” you may enter phases where symptoms return suddenly and movement becomes more difficult, these phases being called “off periods.”. Additionally, involuntary movements (dyskinesia) may occur when drug levels are at their peak.

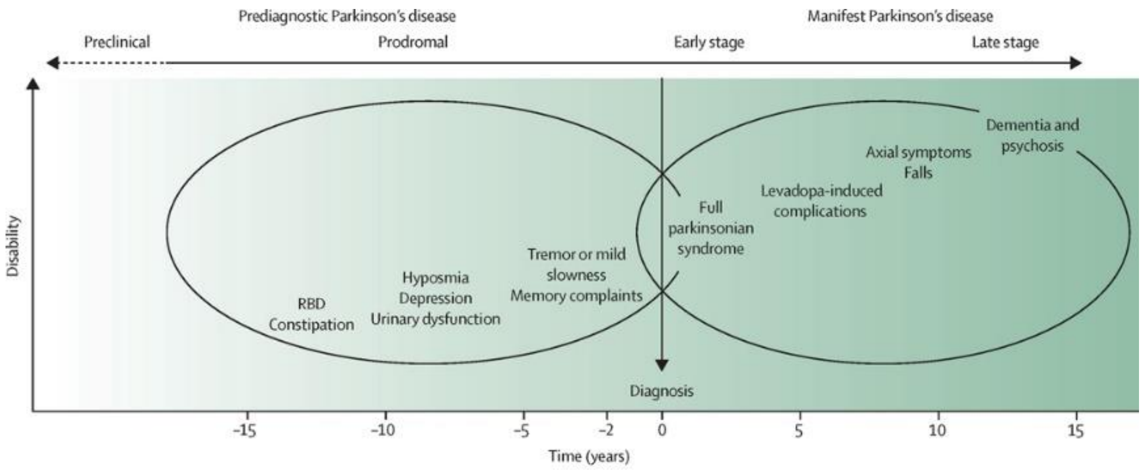

Figure 2.6 : The natural history of Parkinson's disease stages [13]

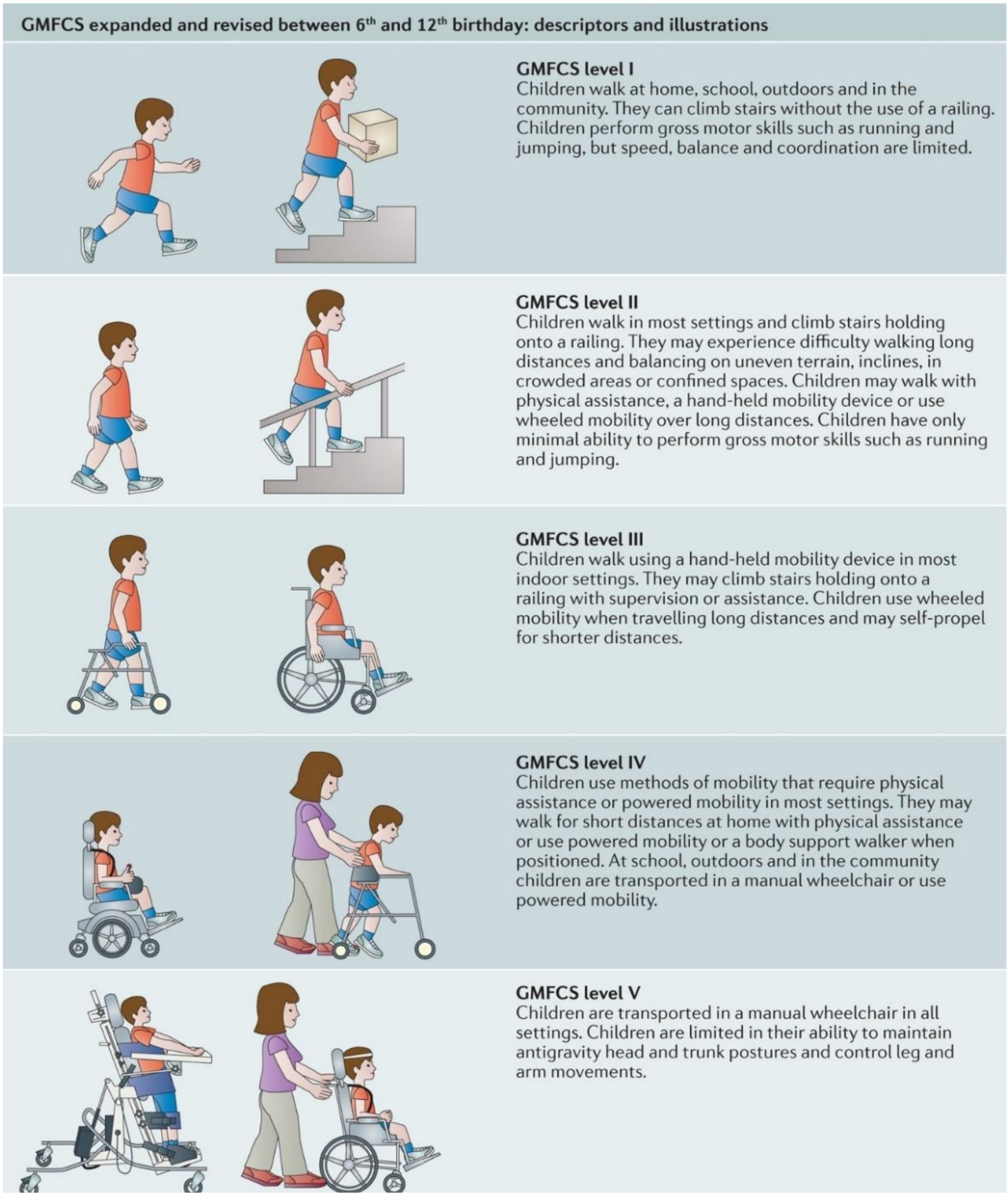

Figure 2.5 : Gross motor function classification system expanded and revised for children with Cerebral Palsy, 6-12 years of age. [17]

- **Cerebral palsy**: The Figure 2.5 refers to a group of disorders affecting a person's movements from birth. It is a permanent disability that generally does not get worse over time [14]. It is caused by damage to the baby's developing brain, either during pregnancy or around birth. The overall prevalence is approximately 2 per 1,000 live births, with a higher rate among low-income populations. It is the most common cause of physical impairment in children with low birth weight [15]. In terms of impairments, all patients have motor impairments, and 25-80% of them also have additional disorders such as cognitive, sensory, urogenital or endocrine impairments, as well as pathologies such as epilepsy [16].

To solve these locomotor problems, therapists offer rehabilitation sessions to allow the muscles regain their mobility and relearn to perform the correct movements. The objectives of these therapies are to prevent the kinetic deterioration of walking, or even to improve it, and to regain a certain autonomy in these movements.

To reach the previous objectives, different rehabilitation techniques are used. First, manual therapy performed by specialized therapists can help improve joint mobility. This treatment can also reduce pain and release muscle tension. The therapists can also make the patient perform some reinforcement exercises which:

- will target weakened muscles to improve strength and endurance,
- will develop the flexibility of muscles thanks to stretching exercises,
- will help them improve the range of motion and prevent contractures,
- will make them perform some balance and coordination training.

All these exercises are essential for improving stability and preventing falls, for example. Moreover, some therapies can use water or electric stimulation to:

- reduce pressure on joints and facilitate movement,
- stimulate paralyzed or weakened muscles with electrical impulses.

These techniques will be useful to provoke the muscle contraction. Finally, constraint-induced therapy is also popular. This method encourages neuroplasticity and functional recovery by constraining the unaffected limb, thereby forcing the use of the affected one [18].

However, all of these techniques have some advantages and disadvantages on the therapists' work. Indeed, manual rehabilitation sessions are often physically demanding for therapists, especially when handling patients. This can lead to muscle pain, strain and injury, especially in the back, shoulders and wrists. Moreover, the repetitive nature of manual exercises can be monotonous, which can reduce therapists' motivation and job satisfaction in the long term. Then, a therapist's physical ability to provide intensive, repetitive manual therapies is limited. After several sessions, the quality of therapy may decrease due to physical fatigue. And finally, manual techniques may vary between therapists, which can lead to variability in treatment results. It is difficult to guarantee perfectly homogeneous and repetitive therapy. That is why, the integration of robots into rehabilitation programs offers numerous advantages, both for patients and therapists. By reducing physical load and fatigue, increasing efficiency and improving the precision of therapies, robots allow therapists to focus more on complex and personalized tasks. This synergy between technology and human expertise promises faster and more effective rehabilitation results, while improving the quality of life of patients and healthcare professionals.

2.2. Robotics in gait rehabilitation

These past few years, an increase and a promotion in active therapy, which consists in the use of medical robots for gait rehabilitation, is visible. To improve gait rehabilitation, this active therapy includes [12]:

- intense training,
- repetitive training,
- specific training.

Conventional therapies have tried to achieve these goals without satisfactory results due to the complexity of the exercises, lack of patient engagement and physical fatigue of the therapists. However, the process of recovery and regaining function can be accelerated by using different robotic devices. Better results can be achieved when these robotic technologies are used in addition to traditional methods of physiotherapy and rehabilitation. [19]

Therapy in which a robot is used is called robot-assisted therapy. It can be defined as a form of physical therapy that uses a robotic device to help patients with impaired functional abilities recover their functions. As rehabilitation robots typically support the patients' weight and control their movements, the therapist can focus more easily on the patients, making more active, intense, and repetitive therapies possible.

Furthermore, rehabilitation robots generally introduce different types, modes, and levels of therapies, increasing patient-robot interaction, their participation in therapies and therefore their motivation during sessions, which leads to an increase in duration and frequency of these.

In recent years, the use of robotics has offered promising recovery results for stroke victims, spinal cord injury, multiple sclerosis, Parkinson's, and cerebral palsy patients, providing an alternative to traditional physiotherapy. Rehabilitation robots are interactive mechanical devices that facilitate limb movement for sensorimotor and, potentially, cognitive recovery. These robots can operate in two or three dimensions depending on their design and are built using various operating mechanisms, such as strength training, basic passive mobilization, and robot-assisted mobilization, which interact on different levels with the patient. The technical complexity of these systems varies considerably, indicating that these technologies are still in the development phase.

Three categories of rehabilitation robots have been developed to improve walking: Ground exoskeletons, end-effector devices, and wearable exoskeletons [20].

2.2.1. Ground exoskeletons

Ground exoskeletons, also called "body weight-supported treadmill (BWST) exoskeletons", involve a harness that supports an adjusted percentage of a patient's body weight, while robotic orthoses control hip, knee, and/or ankle movement patterns during gait. Initial stages of rehabilitation may require the manual assistance of two therapists. It is a class of gait rehabilitation devices that provide mechanical support to the patient's lower extremities while in direct contact with the ground.

- **Lokomat**

The Lokomat®, shown in Figure 2.7, developed by Hocoma AG, constitutes a robot-assisted gait therapy (RAGT) intended for adults and children with various movement pathologies. It is an electro mechanized lower limb exoskeleton which provides effective and motivating locomotor therapy for patients, whether they suffer from walking deficits following a stroke, spinal cord injuries or cerebral palsy. It represents the most widely used hospital rehabilitation robot.

The lokomat is composed of several modules, including a treadmill, a harness and an exoskeleton, it offers adaptability to meet the needs of patients of different sizes and to perform repetitive movements reproducing natural walking. In addition, it integrates different walking intensities and speeds so that the patient can progress throughout the sessions by adjusting them, making it an ideal approach to rehabilitation.

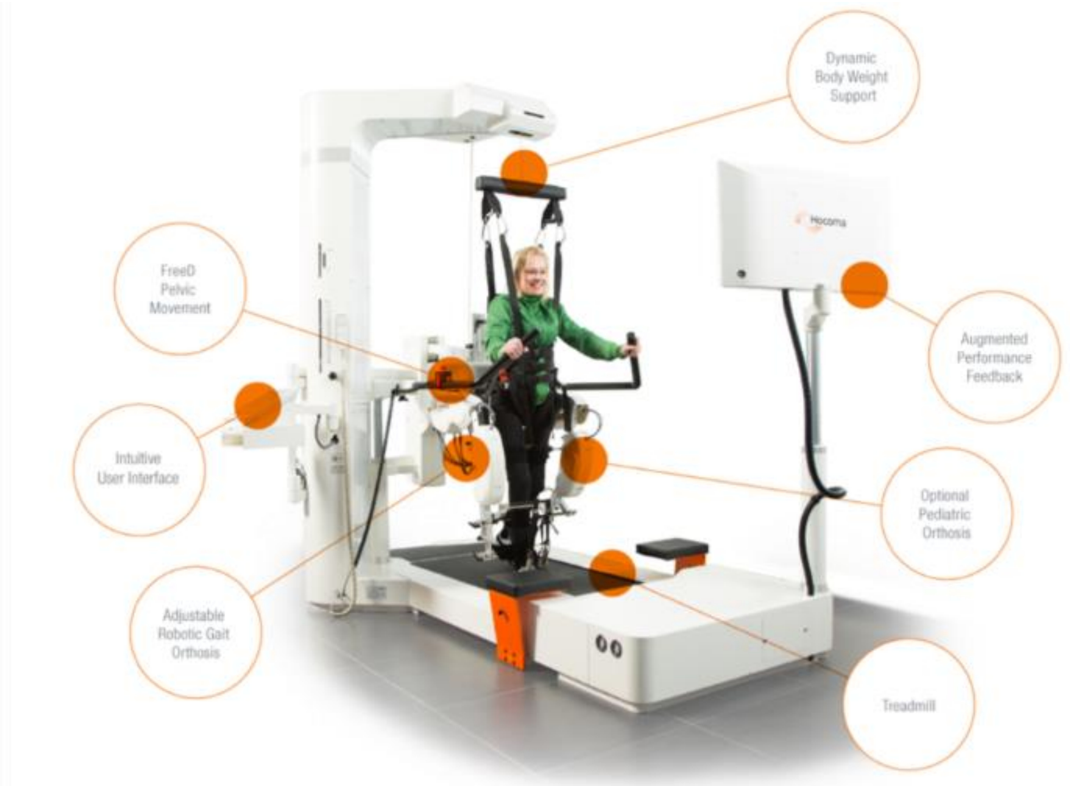

Figure 2.7: Lokomat [21]

- **LOPES (LOwer-extremity Powered ExoSkeleton)**

LOPES, shown in Figure 2.8, is an innovative device developed by the University of Twente in the Netherlands. It is a robotic system composed of motorized orthotics that are attached to the patient's legs. These orthoses provide mechanical support and guide leg movements during walking. It combines a two-dimensional mobile pelvis segment with a leg exoskeleton equipped with three rotating joints: two at the hip and one at the knee. These joints operate under impedance control, which promotes bidirectional mechanical interaction between the robot and the patient. LOPES is often used in conjunction with a treadmill, allowing patients to walk in place while receiving mechanical support and visual feedback on their performance [22].

Figure 2.8: LOPES (LOwer-extremity Powered ExoSkeleton) [23]

- **G-EO System**

The G-EO System™, shown in Figure 2.9, designed by the Swiss company Reha Robotics, represents a motorized exoskeleton intended for gait rehabilitation, equipped with a fixed frame. This wearable device does not only reproduce correct walking, but also allows you to climb stairs. The main objective of Reha Robotics is to improve the mobility of individuals until they can regain their autonomy of movement. [24]

The G-EO System is equipped with a walking platform on which the patient is positioned. This platform is mobile and can be tilted to simulate different types of terrain and inclination. The device is equipped with motorized orthotics that are attached to the patient's legs. These orthoses provide mechanical support and guide leg movements during walking. Additionally, the device is equipped with motion and force sensors that allow monitoring and analysis of the patient's movements during walking. This allows therapists to monitor the patient's progress and adapt treatment accordingly [25].

Figure 2.9: G-EO System [26]

2.2.2. End-effector devices

End-effector devices also provide some body weight support with the use of a harness, but instead of orthoses they generally strap the patient's feet and ankles onto footplates or moving platforms that mimic the trajectory of gait while providing mechanical support and sensory feedback. These devices often offer flexibility in movement, allowing rehabilitation exercises to be adapted to the patient's specific needs.

- **Gait Trainer GT I**

The Gait Trainer GT I, shown in Figure 2.10, was designed by the company Reha-Stim. This robot supports walking recovery by involving the weight supported by the patient and adjusting the pace according to their individual abilities. The Gait Trainer GT I uses pedals on which the patient's feet are placed. These pedals follow a predefined walking motion, simulating natural, repetitive walking. This method aims not only to improve the patient's walking abilities, but also to free up therapeutic resources for the nursing staff. Compared to traditional treadmill therapy, the Gait Trainer GT requires significantly less effort.

Figure 2.10: Gait Trainer GT I [27]

- **Haptic Walker**

A suspension system supports the patient on two platforms that move under their feet powered by electric motors, as shown in Figure 2.11. The software that controls the platforms makes the user perceive the ground as if they were really walking and even reproduces the sensation of climbing stairs. Designed as a modular and scalable system, this device offers unitary expandability allowing up to seven degrees of freedom (DOF) per foot. The basic configuration includes three DOFs per foot in the sagittal plane. The robot is based on a hybrid kinematic structure combining parallel and series elements, thus offering optimal rigidity. Featuring direct-drive electric motors, this device allows for extremely dynamic movements of the footrest. To measure contact force, each foot platform is equipped with six degrees of freedom (DOF) force/torque sensors [28].

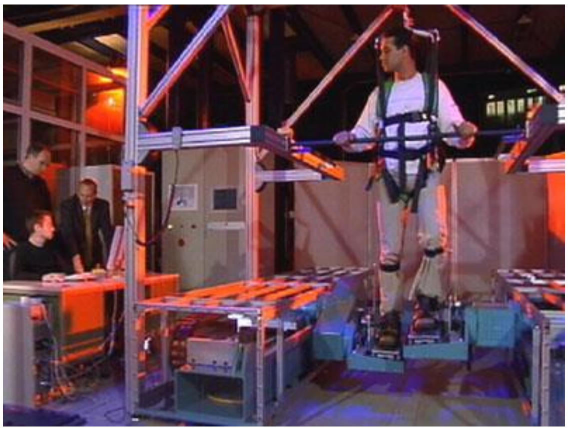

Figure 2.11: Haptic Walker [29]

- **LYRA**

THERA-Trainer Lyra, shown in Figure 2.12, is an end-effector gait rehabilitation robot for lower limb movement. The training device is intended for gait rehabilitation with weight reduction in patients with reduced mobility. It provides intensive locomotor therapy within the limits of the patient's capabilities during all phases of rehabilitation. Moreover, the patient achieves up to 20 times the number of repetitions compared to manual or treadmill locomotor therapy. LYRA uses a mobile platform on which the patient's feet are placed. This platform can move in different directions to simulate natural walking movements.

Figure 2.12 : THERA-Trainer LYRA [30]

2.2.3. Wearable exoskeletons

Wearable exoskeletons, also called "power overground exoskeleton devices," allow patients to ambulate without the need for an overhead support system. However, these devices generally require patients to have some upper extremity strength to use an assistive device in conjunction with the exoskeleton. This allows them to benefit from walking rehabilitation while maintaining a certain mobility and autonomy. Wearable exoskeletons are often used to provide intensive gait rehabilitation, allowing patients to practice walking for prolonged periods while receiving mechanical support. Moreover, these devices are often designed to be adjustable and adaptable to the specific needs of the patient, allowing precise customization of the mechanical assistance provided [31].

- **Ekso GT**

The Ekso GT, shown in Figure 2.13, is a wearable robotic exoskeleton designed to allow individuals to stand and facilitate them walking in a pattern similar to the physiological one and without the need for a treadmill. Backed by years of research and implemented in more than 270 rehabilitation centres, Ekso GT was designed to optimize the patient and therapist experience. Designed for rehabilitation facilities, the Ekso GT incorporates intelligent Variable Assist software, which adapts the power delivered to each side of the patient's body, ensuring active engagement throughout their care journey. This technology helps to engage patients in the early stages of their recovery, providing frequent sessions with many high-intensity steps [32].

Figure 2.13 : Ekso GT Exoskeleton [33]

- **ReWalk**

Rewalk Robotics, an innovative medical device company, has developed Rewalk, an exoskeleton that allows a person who is in a wheelchair to stand and walk again, shown in Figure 2.14. This device is put on like a wetsuit. It can adapt to the size of the person's body because certain parts are particularly adjustable at the legs and bust. The user can then move around using a motorization system. In addition, with the control and power device placed in a bag on the user's back, the user can move independently and control their movements. The ReWalk is made up of articulated metal structures that attach to the user’s legs and torso. It includes motors at the hip and knee joints to facilitate walking movements.

Figure 2.14: ReWalk Exoskeleton [34]

Each of this robot has its own specific characteristics which are adapted to different therapeutic needs and patients. However, they all have three common points which are:

- **High intensity**: Robot-assisted gait training enables repetitive task training, which can improve walking ability and distance.
- **High dose**: Patients using robot-assisted gait therapy practice two to three times longer than those with manual assistance for ground-based walking. By increasing the time spent on therapeutic exercises, patients may see improvements more quickly.
- **High motivation**: Robot-assisted gait training devices incorporate gamification elements to encourage patients to fully engage during each exercise session. By combining achievable goals and levels to overcome, rehabilitation becomes fun. Thanks to virtual environments projected on screens, patients can perform their exercises in varied settings, such as a snowy forest path or a sunny park.

Chapter 3

Mechanical model design

3.1. Exoleg CAD design

In this section, we will focus on the design of the ExoLeg. The design was created using Autodesk Inventor, a powerful software tool for 3D modeling, numerical prototyping, and simulation of various forces applied to the prototypes. Autodesk Inventor allowed engineers to create accurate and detailed models of parts and assemblies, facilitating the visualization, optimization, and validation of designs before production. With advanced features such as stress and motion simulation, automatic plan generation, and integration with other CAD and data management software, Autodesk Inventor proved to be an essential tool for improving the efficiency and precision of the ExoLeg design.

3.1.1. Original CAD

The original design of the ExoLeg is presented in the Figure 3.1. The medical robot will be placed behind the patient, and it will hold his leg by the calf thanks to the purple piece shown in Figure 3.1.

Figure 3.1: Position of the ExoLeg

The kinematic diagram shown in Figure 3.2. represents the relative movements between the different parts of a mechanism. This helps to understand how components interact and move relative to each other in the ExoLeg.

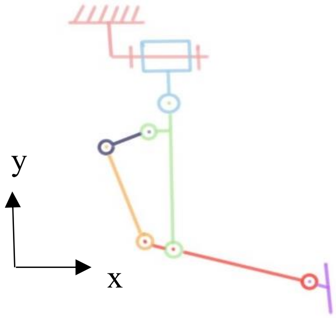

Figure 3.2: Kinematic diagram

Thanks to the kinematic diagram, it can be seen that the ExoLeg is composed of seven main subsystems, all linked to each other through joints. Moreover, two motors are integrated into the device to enable vertical and horizontal movements. The first motor is positioned on the light blue part, and, thanks to a pulleys/belt mechanism, it allows the rotation of the green part to create horizontal movement. Then, the second motor is located on the green part, and through two mechanisms: a pulley/belt system and a four-bar linkage, the rotation of the red part generates vertical movement of the ExoLeg.

The design is divided into seven subgroups:

1. First subgroup named “Subassembly 11”:

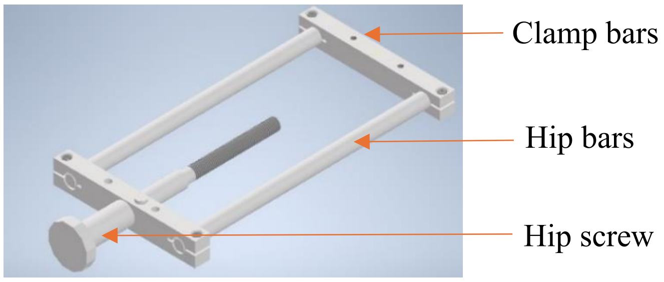

Figure 3.3: Subassembly 11

This first subgroup, shown in Figure 3.3, will be important when the exoskeleton is fixed to the test structure, but it has no effect on the mechanical properties of the prototype.

2. Second subgroup named “Subassembly 10”:

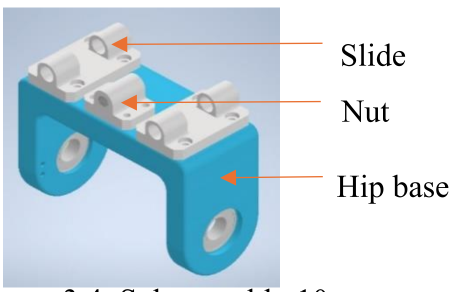

Figure 3.4: Subassembly 10

This second assembly, shown in Figure 3.4, is fixed to the previous one thanks mechanical components such as screws. This subgroup will constitute the ExoLeg's rigid frame which is therefore connected to the ground via a metal structure. Consequently, this part is fixed and will have no movement. It is composed of four parts:

- Two slides, where the two previous hip bars will be inserted with a sliding pivot connection.
- One nut, in which the previous hip screw can be inserted.
- One hip base, where two bearings are integrated to allow a pivot link with the next subgroup.

3. Third subgroup named "Subassembly 9":

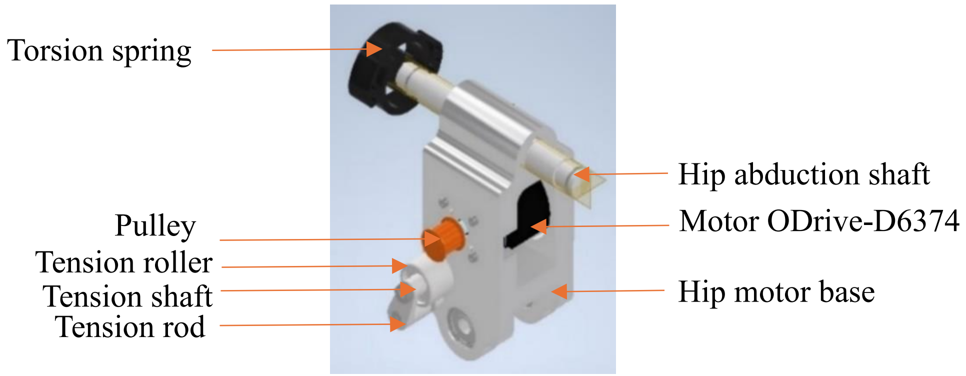

Figure 3.5: Subassembly 9

This assembly, shown in Figure 3.5, is connected via a pivot to the previous structure through the top axis called the "Hip abduction shaft". This subgroup is composed of height parts:

- Hip motor base which corresponds to the frame of this subassembly
- ODrive-D6374 is the motor which will transmit to the exoskeleton the horizontal movement thanks to the mechanism of two pulleys and a toothed belt
- Hip abduction axis, it is the main axis which allows the pivot link with the previous subassembly
- Torsion spring, it will limit the rotation between the subassembly 9 and 10.
- The tension roller, tension shaft and the tension rod, constitute the tensor which will allow the future toothed belt to be well stretched around the pulleys

4. Fourth subgroup named "Subassembly 8":

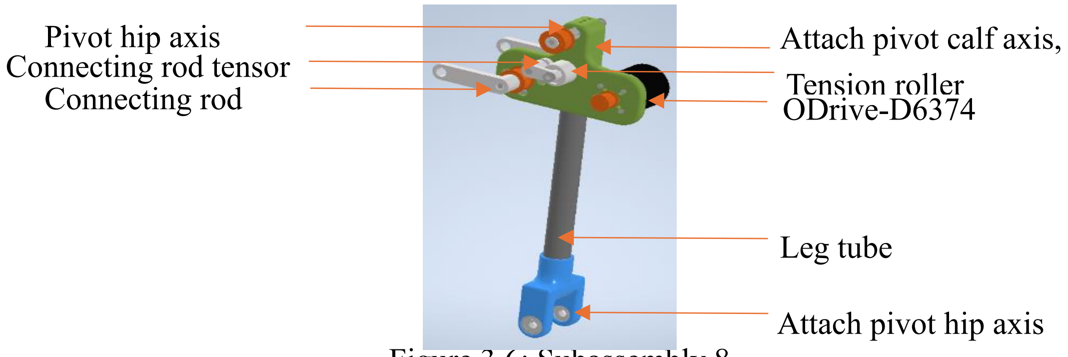

Figure 3.6: Subassembly 8

The top axis allows to create a pivot connexion with the third subgroup. The movement between these two subparts is possible thanks to the top pulley which transmits the torque of the previous motor. In this assembly we have fourteen pieces, but the more important ones are the:

- Attach pivot calf axis, has two bearing which will allow a pivot connexion with the second PVC bar.
- Attach pivot hip axis represents the frame of this subassembly where the second motor and connecting rods are located
- Pivot hip axis allows to have a pivot connection with the previous subassembly in order to obtain a horizontal movement of the ExoLeg

In this subassembly, shown in Figure 3.6, a second motor is included. It will allow the vertical movement of the lower grey bar. Initially, mechanical transmission will be achieved through two pulleys and a toothed belt tensioned by a tensioner. This is how the rotational movement will be transmitted to the two connecting rods.

5. Fifth subgroup named “Subassembly 7”:

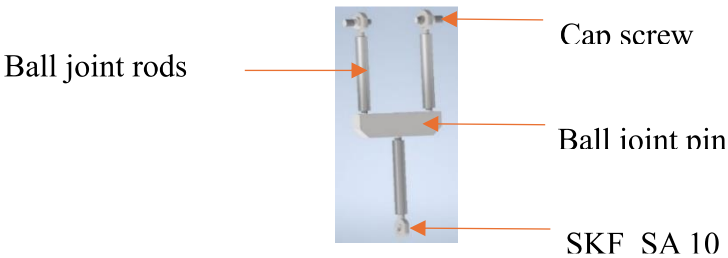

Figure 3.7: Subassembly 7

This mechanism of four bars, shown in Figure 3.7, will allow the transmission of the previous motor torque to the inferior bar of the exoskeleton. This subassembly is linked to the two previous connecting rods thanks to the mechanical parts named Cap screw. The main 3D components are the ball joint pins, these parts allow to transform the rotation of both of the previous connecting rods to only one bar.

The mechanical component named “SKF_SA 10” is a SKF joint head. It will allow a pivot connexion with the following subgroup.

6. Sixth subgroup named “Subassembly 6”:

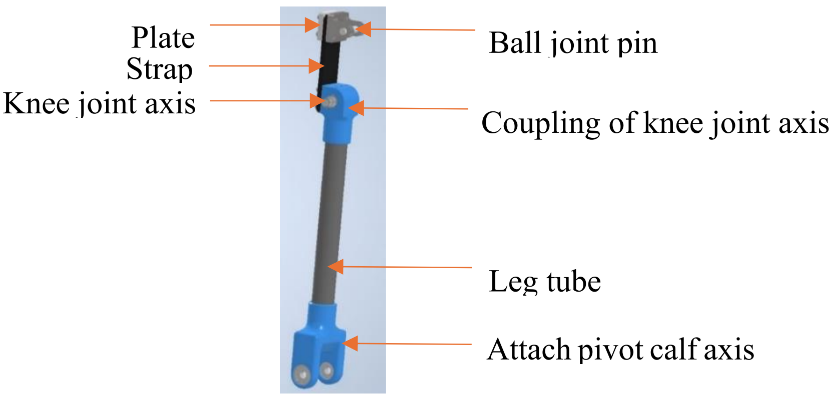

Figure 3.8: Subassembly 6

The first axis at the top of the Figure 3.8, is the one which will allow the pivot connexion with the previous subassembly. The eight different 3D part of this subgroup are:

- Attach pivot calf axis, this part has two bearing which will allow a pivot connexion with the second PVC bar.
- Attach pivot knee axis, it represents the frame of this subassembly where the torque of second motor will be transmitted
- Pivot knee axis, it allows to have a pivot connection with the previous subassembly in order to obtain a vertical movement of the ExoLeg
- Strip, it allows to have a certain flexibility and helps absorb the rotational force of the motor
- Ball joint pin, it is where the pivot connexion with the previous subassembly is done

7. Seventh subgroup named "ensamble_estructura5":

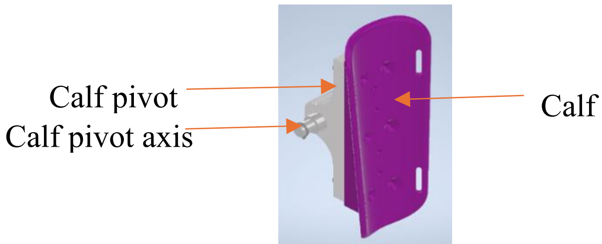

Figure 3.9: Subassembly 5

This last subassembly, shown in Figure 3.9, is in pivot connexion to the previous one thanks to the unique axis which is positioned into the attach pivot calf axis. The 3D parts in this assembly are:

- calf, it corresponds to the part which will be in contact with the patient
- calf pivot axis it is the axis in pivot connexion with the previous assembly.

Consequently, the first step of the project was to understand the previous cinematic and how was made the medical exoskeleton. This involved studying the previous design, analysing the mechanical components, and understanding the movements and functions they were intended to perform. It was also essential to review detailed documentation, including technical drawings (see Annexes).

3.1.2. CAD modifications

Taking into account the need to integrate the motors into the design, as shown in Figure 3.10, modifications were necessary. As originally planned, my teammate responsible for the electrical aspects requested adjustments to incorporate the two motors and their respective encoders.

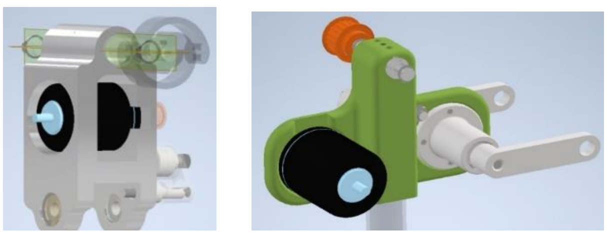

Figure 3.10: Motors integration to the design (motor 1 left, motor 2 right)

When motors are utilized within a mechanical system, it becomes essential for the electrical engineer to install encoders on the motor axes. These encoders enable precise control and determination of the motor positions, crucial for ensuring accurate exoskeleton trajectories and optimizing system performance by providing velocity data. Therefore, to fulfill this task, redesigning the two parts where the motors were initially integrated was required.

First, the second motor integrated into "Subassembly 8" was focused on. The sensor had to be positioned at the extremity of the motor axis. To secure it, a case around the motor had to be designed. However, the original green piece called " Attach pivot calf axis " does not provide enough space to create a case around the motor. Therefore, this part had to be redesigned, as shown in Figure 3.11.

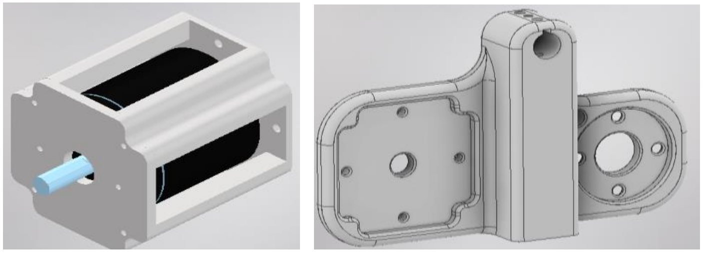

Figure 3.11 : Motor case (left) and the new “Attach pivot calf axis” (right)

The enclosure consists of two parts that are bolted together. The required mounting hardware is:

- 4x M4 8mm screws for the motor
- 4x M3 8mm screws for the encoder. These self-tap into the 3D printed plastic.
- 4x M3 10mm screws to hold the plate to the shell. These self-tap into plastic.

The appendix C “Modification of the attach pivot calf axis” presents the assembly of the motor case onto the “Attach pivot calf axis”. Moreover, all the details concerning the dimensions are available through design plans.

Regarding the second motor, fewer modifications were required. Indeed, there was no need to redesign the part called " Hip motor base"; instead, four holes were drilled, and the structure shown in Figure 3.12, was printed. Subsequently, the structure could be bolted to the part called " Hip motor base", and the sensor could be installed.

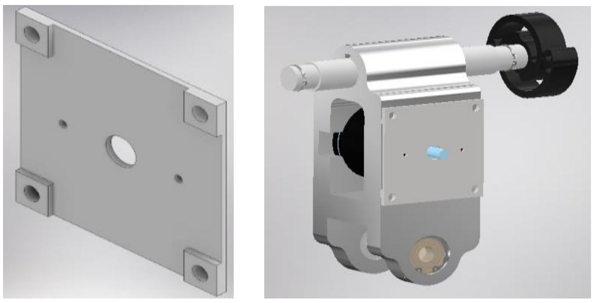

Figure 3.12 : Motor case (left) and the final assembly (right)

To fix the motor case, I used four screw M6 8mm.

3.2. Theoretical Study of ExoLeg Dynamics

In this section, the theoretical study of the ExoLeg will be focused on. This section is necessary to understand the underlying mechanical principles, optimize design, predict, and improve performances. Lagrange equations play a central role in these goals by providing a robust methodological approach for the analysis and modelling of complex mechanical systems such as exoskeletons.

3.2.1. Mathematical equations

In this section we derive a general set of differential equations that describe the time evolution of mechanical systems subjected to holonomic constraints, when the constraint forces satisfy the principle of virtual work. The principle of virtual work is a fundamental concept in structural mechanics and mechanics of continuous media. It makes it possible to analyse the balance and deformation of mechanical systems without the need to directly solve the associated complex differential equations. These are called the Euler-Lagrange equations of motion.

That is why, my second objective was to determine the mechanical equations of the exoskeleton. To do that, we first determine some data, shown in Figure 3.13, which are:

- **L_1**: dimension of the upper half bar
- **L_2**: dimension of the lower half bar
- **T_1**: top rotation
- **T_2**: lower rotation
- **Θ_1**: angle of rotation between the upper part of the robot and the upper bar
- **Θ_2**: angle of rotation between the upper bar and the upper bar
- **I_1**: moment of inertia of the upper bar
- **I_2**: moment of inertia of the lower bar
- **M_1**: mass of the upper bar
- **M_2**: mass of the lower bar

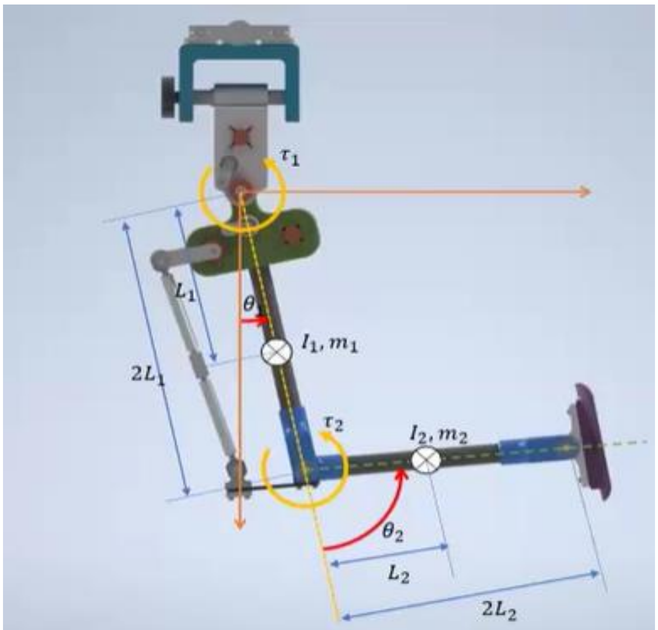

Figure 3.13: Cinematic Model

The model is defined as:

$$D(q).\ddot{q} + C(q,\dot{q}).\dot{q} + G(q) = \Gamma$$

With:

$$q = [\,\theta_1 \quad \theta_2\,]^T, \dot{q} = [\,\dot{\theta_1} \quad \dot{\theta_2}\,]^T, \ddot{q} = [\,\ddot{\theta_1} \quad \ddot{\theta_2}\,]^T$$

$$D(q)\ is\ the\ inertia\ matrix$$

$$C(q,\dot{q})\ is\ the\ matrix\ of\ centripetal\ and\ Coriolis\ effects$$

$$G(q)\ is\ a\ vector\ of\ the\ gravity\ effects$$

$$\Gamma = [\,\tau_1 \quad \tau_2\,]^T\ is\ a\ vector\ of\ generalized\ forces\ and\ torques$$

First, we determined the important points P_1 and P_2 which correspond to the extremities of the upper and lower bar.

$$P_1 = \begin{cases} x_{P1} = 2.L_1.\sin(\theta_1) \\ y_{P1} = -2.L_1.\cos(\theta_1) \end{cases}$$

$$P_2 = \begin{cases} x_{P2} = 2.L_1.\sin(\theta_1) + 2.L_2.\sin(\theta_1+\theta_2) \\ y_{P2} = -2.L_1.\cos(\theta_1) - 2.L_2.\cos\,(\theta_1+\theta_2) \end{cases}$$

Then the position of centre of masses

$$r_1 = \begin{cases} x_{r1} = L_1.\sin(\theta_1) \\ y_{r1} = -L_1.\cos(\theta_1) \end{cases}$$

$$r_2 = \begin{cases} x_{r2} = 2.L_1.\sin(\theta_1) + L_2.\sin(\theta_1+\theta_2) \\ y_{r2} = -2.L_1.\cos(\theta_1) - L_2.\cos\,(\theta_1+\theta_2) \end{cases}$$

Now, we can calculate the velocities of r_1 and r_2:

$$\dot{r_1} = \begin{cases} \dot{x_{r1}} = L_1.\dot{\theta_1}.\cos(\theta_1) \\ \dot{y_{r1}} = L_1.\dot{\theta_1}.\sin(\theta_1) \end{cases}$$

$$\dot{r_2} = \begin{cases} \dot{x_{r2}} = \dot{\theta_1}.(L_2\,.\cos(\theta_1+\theta_2) + 2.L_1.\cos(\theta_1)) + L_2.\dot{\theta}_2\,.\cos(\theta_1+\theta_2) \\ \dot{y_{r2}} = \dot{\theta_1}.(L_2\,.\sin(\theta_1+\theta_2) + 2.L_1.\sin(\theta_1)) + L_2.\dot{\theta}_2\,.\sin(\theta_1+\theta_2) \end{cases}$$

We can deduce:

$$v_1{}^2 = L_1{}^2.\dot{\theta}_1{}^2$$

$$v_2{}^2 = \left[2.L_1.\dot{\theta_1}.\cos(\theta_1) + L_2.\dot{\theta}_2\,.\cos(\theta_2)\right]^2 + \left[2.L_1.\dot{\theta_1}.\sin(\theta_1) + L_2.\dot{\theta}_2\,.\sin(\theta_2)\right]^2$$

The next step is to determine the kinetic energy:

$$T = \frac{1}{2}.m_1.v_1{}^2 + \frac{1}{2}.m_2.v_2{}^2 + \frac{1}{2}.\left(I_1.\dot{\theta}_1{}^2 + I_2.\dot{\theta}_2{}^2\right)$$

$$\begin{aligned} T = \frac{1}{2}.m_1.L_1{}^2.\dot{\theta}_1{}^2 \\ &+ \frac{1}{2}.m_2.\left(\left[2.L_1.\dot{\theta}_1.\cos(\theta_1) + L_2.\dot{\theta}_2\ .\cos(\theta_2)\right]^2\right. \\ &\left. + \left[2.L_1.\dot{\theta}_1.\sin(\theta_1) + L_2.\dot{\theta}_2\ .\sin(\theta_2)\right]^2\right) + \frac{1}{2}.\left(I_1.\dot{\theta}_1{}^2 + I_2.\dot{\theta}_2{}^2\right) \end{aligned}$$

Parallelly, we can also determine the potential energy:

$$V = V_1 + V_2 = m_1.g.y_{r1} + m_2.g.y_{r2}$$

$$V = g.m_1.(\,L_1 + L_1.\sin(\theta_1)) + g.m_2.(2.L_1 + L_2 + 2.L_1.\sin(\theta_1) + L_2.\sin(\theta_2))$$

Once we have the kinetic and the potential energies, we can calculate the lagrangian, which is:

$$L = T - V$$

$$\begin{aligned} L = \Bigg(\frac{1}{2}.m_1.L_1{}^2.\dot{\theta}_1{}^2 + \frac{1}{2}.m_2.(\left[2.L_1.\dot{\theta}_1.\cos(\theta_1) + L_2.\dot{\theta}_2\ .\cos(\theta_2)\right]^2 \\ &+ \left[2.L_1.\dot{\theta}_1.\sin(\theta_1) + L_2.\dot{\theta}_2\ .\sin(\theta_2)\right]^2) + \frac{1}{2}.\left(I_1.\dot{\theta}_1{}^2 + I_2.\dot{\theta}_2{}^2\right)\Bigg) \\ &- \left(g.m_1.(\,L_1 + L_1.\sin(\theta_1))\right. \\ &\left. + g.m_2.(2.L_1 + L_2 + 2.L_1.\sin(\theta_1) + L_2.\sin(\theta_2))\right) \end{aligned}$$

And finally obtain the Lagrange differential:

$$\frac{d}{dt}\frac{\partial L}{\partial \dot{\theta}_1} - \frac{\partial L}{\partial \theta_1} = Q_{\theta_1} \qquad and \qquad \frac{d}{dt}\frac{\partial L}{\partial \dot{\theta}_2} - \frac{\partial L}{\partial \theta_2} = Q_{\theta_2}$$

With:

$$\frac{\partial L}{\partial \dot{\theta}_1} = \left[(m_1 + 4.m_2).L_1{}^2 + I_1\right].\dot{\theta}_1 + 2.L_1.L_2.m_2.\dot{\theta}_2\ .\cos(\theta_1 - \theta_2)$$

$$\frac{\partial L}{\partial \dot{\theta}_2} = \left[m_2.L_2{}^2 + I_2\right].\dot{\theta}_2 + 2.L_1.L_2.m_2.\dot{\theta}_1\ .\cos(\theta_1 - \theta_2)$$

$$\begin{aligned} \frac{d}{dt}\frac{\partial L}{\partial \dot{\theta}_1} = [(m_1 + 4.m_2).L_1^2 + I_1].\ddot{\theta}_1 + 2.L_1.L_2.m_2.\ddot{\theta}_2.\cos(\theta_1 - \theta_2) \\ &- 2.L_1.L_2.m_2.\dot{\theta}_1.\dot{\theta}_2.\sin(\theta_1 - \theta_2) + 2.L_1.L_2.m_2.\dot{\theta}_1{}^2.\sin(\theta_1 - \theta_2) \end{aligned}$$

$$\frac{d}{dt}\frac{\partial L}{\partial \dot{\theta}_2} = [m_2.l_2{}^2 + \mathrm{I}_2].\ddot{\theta}_2 + 2.L_1.L_2.m_2.\ddot{\theta}_1.\cos(\theta_1 - \theta_2)$$
$$- 2.L_1.L_2.m_2.\dot{\theta}_1{}^2.\sin(\theta_1 - \theta_2) + 2.L_1.L_2.m_2.\dot{\theta}_1.\dot{\theta}_2.\sin(\theta_1 - \theta_2)$$

$$\frac{\partial L}{\partial \theta_1} = -2.L_1.L_2.m_2.\dot{\theta}_1.\dot{\theta}_2.\sin(\theta_1 - \theta_2) + g.L_1.(m_1 + 2.m_2).\cos(\theta_1)$$

$$\frac{\partial L}{\partial \theta_2} = 2.L_1.L_2.m_2.\dot{\theta}_1.\dot{\theta}_2.\sin(\theta_1 - \theta_2) + g.L_1.(m_1 + 2.m_2).\cos(\theta_2)$$

$$Q_{\theta_1} = \left[(m_1 + 4.m_2).L_1^2 + I_1\right].\ddot{\theta}_1 + 2.L_1.L_2.m_2.\ddot{\theta}_2.\cos(\theta_1 - \theta_2)$$
$$+ 2.L_1.L_2.m_2.\dot{\theta}_1{}^2.\sin(\theta_1 - \theta_2) - g.L_1.(m_1 + 2.m_2).\cos(\theta_1)$$

$$Q_{\theta_2} = \left(m_2.L_2^2 + I_2\right).\ddot{\theta}_2 + 2.L_1.L_2.m_2.\ddot{\theta}_1.\cos(\theta_1 - \theta_2)$$
$$- 2.L_1.L_2.m_2.\dot{\theta}_1{}^2.\sin(\theta_1 - \theta_2) - g.L_2.m_2.\cos(\theta_2)$$

The model was defined as:

$$D(q).\ddot{q} + C(q,\dot{q}).\dot{q} + G(q) = \Gamma$$

With:

$$\begin{bmatrix} D_{11} & D_{12} \\ D_{21} & D_{22} \end{bmatrix}.\begin{bmatrix} \ddot{\theta}_1 \\ \ddot{\theta}_2 \end{bmatrix} + \begin{bmatrix} C_{11} & C_{12} \\ C_{21} & C_{22} \end{bmatrix}.\begin{bmatrix} \dot{\theta}_1 \\ \dot{\theta}_2 \end{bmatrix}^2 + \begin{bmatrix} G_1 \\ G_2 \end{bmatrix} = \begin{bmatrix} \Gamma_1 \\ \Gamma_2 \end{bmatrix}$$

$$\begin{cases} D_{11}.\ddot{\theta}_1 + D_{12}.\ddot{\theta}_2 + C_{11}.\dot{\theta}_1{}^2 + C_{12}.\dot{\theta}_2{}^2 + G_1 = \Gamma_1 \\ D_{21}.\ddot{\theta}_1 + D_{22}.\ddot{\theta}_2 + C_{21}.\dot{\theta}_1{}^2 + C_{22}.\dot{\theta}_2{}^2 + G_2 = \Gamma_1 \end{cases}$$

To conclude, by identification, I deduced:

$$G = \begin{bmatrix} L_1.g.\cos(\theta_1).(m_1 + 2.m_2) \\ L_2.g.m_2.\cos(\theta_2) \end{bmatrix}$$

$$D = \begin{bmatrix} I_1 + L_1{}^2.m_1 + 4.L_1{}^2.m_2 & 2.L_1.L_2.m_2.\cos(\theta_1 - \theta_2) \\ 2.L_1.L_2.m_2.\cos(\theta_1 - \theta_2) & m_2.L_2{}^2 + I_2 \end{bmatrix}$$

$$C = \begin{bmatrix} 0 & 2.L_1.L_2.\dot{\theta}_2.m_2.\sin(\theta_1 - \theta_2) \\ -2.L_1.L_2.\dot{\theta}_1.m_2.\sin(\theta_1 - \theta_2) & 0 \end{bmatrix}$$

Equation 3.1: Model equations

3.2.2. Simulink implementation

Now that the theoretical equations have been obtained, they were simulated on Simulink using the model shown in Figure 3.14. Simulink is a graphic simulation software integrated at MATLAB. It is useful to model, simulate and analyse dynamic systems. Simulink uses a visual modelling with blocks to represent systems. Each block corresponds to a mathematical function, a physic component, or a part of the system to model. It allows to simulate different behaviours of the system in function of the input that the user chose.

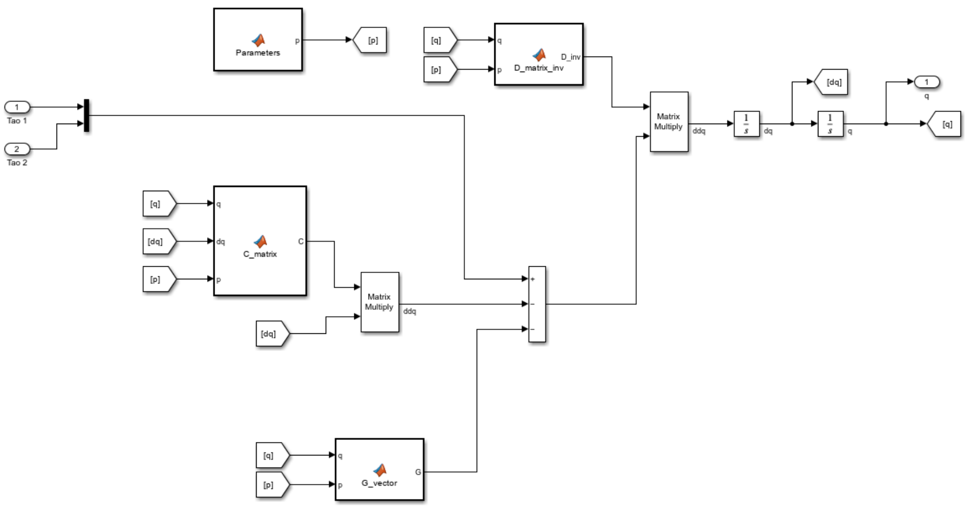

Figure 3.14: Simulink model allowing to determine angles q(θ_1, θ_2) thanks to the equation XX

In the case of the project, this Simulink model will be useful to determine the torques of both motors (3.3.4). For now, I concentred myself in modelling the Lagrange equations that I found in the previous section. This model simulates the different angles θ_1 and θ_2 of the ExoLeg. The mathematical equation is:

$$q = \iint \ddot{q} = \iint D(q)^{-1}.\left(\Gamma - C(q,\dot{q}).\dot{q} - G(q)\right)$$

The principal components are the blocks:

- **D_matrix_inv**: is the inverse inertia matrix,
- **C_matrix**: is the matrix of centripetal and Coriolis effects,
- **G_vector**: is the vector of the gravity effects,
- **Tau_1 and Tau_2**: are the generalized forces and torques,
- **Parameters**: is the variables storage,
- **Integrators**: they integrate, in function of time, the mathematical equation. They allow to determine the velocity and the position of the angles θ_1 and θ_2 of the ExoLeg.

3.3. Dynamic study and simulation

Dynamic studies and simulations are essential to the well development of the exoskeleton. They allow to understand the complex interactions between the different parts of the device and optimize the conception.

3.3.1. Reference trajectory

As previously stated, the objective of the exoskeleton is to apply a programmed trajectory to the patient's leg to aid in rehabilitation exercises. The first crucial step is to determine these specific trajectories. The objective is to implement different trajectories based on the patient's specific needs and medical decisions. This approach ensures that the exoskeleton can be tailored for optimal therapeutic outcomes. To demonstrate this capability, a test trajectory used to validate the mechanical design will be presented next. This trajectory serves as a preliminary validation step, ensuring that the design meets the necessary performance criteria before being customized for individual patient requirements. However, to progress with the mechanical development and test the basic functionality of the exoskeleton, it was necessary to have a reference trajectory. In the temporary absence of specific therapeutic trajectories, a simple test trajectory was defined. This trajectory is designed to allow testing and validation of the mechanical parameters of the exoskeleton without a therapeutic objective.

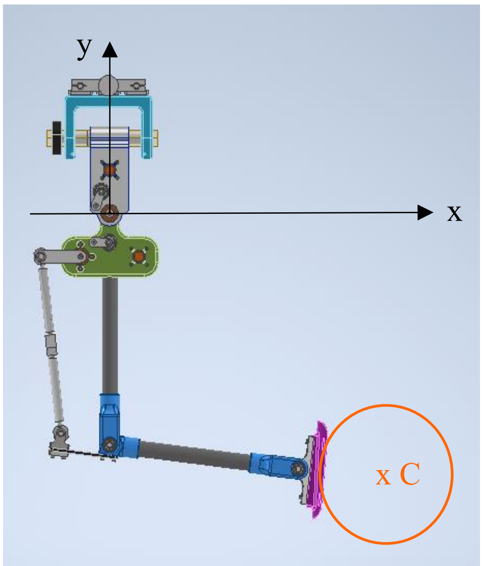

Figure 3.15 : Reference Trajectory

As shown in Figure 3.15, a circular trajectory with a radius of 100 mm around a reference point with specific coordinates was chosen for the design.

$$reference\ trajectory\ center\ C = \begin{cases} 150 & \vec{x}, \\ -250 & \vec{y}, \end{cases}$$

This trajectory is interesting because it allowed the mechanical and control aspects of the exoskeleton to be validated, including the precision of movements, the robustness of different components, and the reactivity of the control system. By using, a simple and well-controlled trajectory, the risks associated with testing are minimized, thus guaranteeing safety during the first test. Moreover, this approach allows for testing and refining of mechanical components, while remaining flexible to later integrate specific therapeutic trajectories as they become available.

3.3.2. Relation between the joint angles and the imposed trajectory

This section will develop the mathematical relationships between the two joint angles and the final trajectory of the robot. First, the direct model will be studied to determine these relationships, given the joint angles. Then, it will be compared to the inverse kinematics model, which will determine the joint angles based on the final robot trajectory.

- Direct Kinematic

First, it was mandatory to define the kinematic model beginning with the direct kinematics. This method consists of establishing algebraic equations that allowed me to determine the final position of the extremity of the exoskeleton given the joints variables. Consequently, in our case, presented in Figure 3.16, I calculated the extremity P of the robot as a function of θ_1 y θ_2.

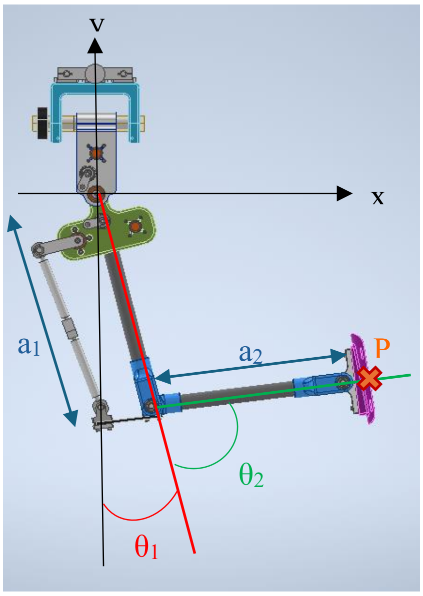

Figure 3.16 : Parameters setting

This is possible thanks to the Denavit – Hartenberg (DH) convention, which involves establishing reference frames for the robot joint and the final extremity. The DH convention standardizes the way the spatial relationships between adjacent links of a robot are described, making the process of defining and solving the kinematics more systematic and efficient.

Then, the interpretation of each parameter was performed, and the homogeneous transformation matrices for each robotic arm were deduced. To define the global homogeneous transformation in terms of the original frame, the two individual homogeneous transformation matrices were multiplied. Each matrix represents the transformation between adjacent links, and their multiplication provides the overall transformation from the base to the end-effector.

$$^{0}A_2 = {}^{0}A_1 . {}^{1}A_2$$

With:

$$
{}^{0}A_1 = \begin{bmatrix} \cos(\theta_1) & -\sin(\theta_1) & 0 & a_1.\cos(\theta_1) \\ \sin(\theta_1) & \cos(\theta_1) & 0 & a_1.\sin(\theta_1) \\ 0 & 0 & 1 & 0 \\ 0 & 0 & 0 & 1 \end{bmatrix}
$$

$$
{}^{1}A_2 = \begin{bmatrix} \cos(\theta_2) & -\sin(\theta_2) & 0 & a_2.\cos(\theta_2) \\ \sin(\theta_2) & \cos(\theta_2) & 0 & a_2.\sin(\theta_2) \\ 0 & 0 & 1 & 0 \\ 0 & 0 & 0 & 1 \end{bmatrix}
$$

Consequently, I obtained the global homogeneous transformation matrix:

$$
{}^{0}A_2 = \begin{bmatrix} \cos(\theta_{12}) & -\sin(\theta_{12}) & 0 & a_2.\cos(\theta_{12}) + a_1.\cos(\theta_1) \\ \sin(\theta_{12}) & \cos(\theta_{12}) & 0 & a_2.\cos(\theta_{12}) + a_1.\sin(\theta_1) \\ 0 & 0 & 1 & 0 \\ 0 & 0 & 0 & 1 \end{bmatrix}
$$

Where:

$$
\cos(\theta_{12}) = \cos(\theta_1 + \theta_2) = \cos(\theta_1).\cos(\theta_2) + \sin(\theta_2).\sin(\theta_1)
$$

$$
\sin(\theta_{12}) = \sin(\theta_1 + \theta_2) = \sin(\theta_1).\cos(\theta_2) + \sin(\theta_2).\cos(\theta_1)
$$

Consequently, with this method, it was possible to determine the direct kinematic.

- Inverse Kinematic

Inverse kinematics will be used to calculate θ_1 and θ_2 to allow the extremity of the robot to be placed at the positions $P(P_x, P_y)$, as shown in Figure 3.17. This involves establishing the algebraic equations needed to determine θ_1 and θ_2 corresponding to the position P.

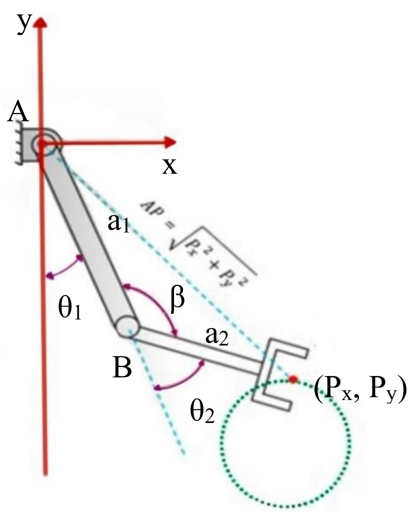

Figure 3.17 : Trigonometric relationships

To do this, the geometric method was used, which consists of defining triangles based on the known information and then using trigonometric relationships to solve for the joint angles. This method is particularly useful because it provides a clear visual and intuitive approach to solving the inverse kinematics problem.

$$\theta_2 = \cos^{-1}\left(\frac{{P_x}^2 + {P_y}^2 - {a_1}^2 - {a_2}^2}{2.\,a_1.\,a_2}\right)$$

$$\theta_1 = \gamma - \alpha$$

$$\gamma = \tan^{-1}\left(\frac{P_y}{P_x}\right)$$

$$\alpha = \tan^{-1}\left(\frac{a_2.\sin(\theta_2)}{a_1 + a_2.\cos(\theta_2)}\right)$$

$$\theta_1 = \tan^{-1}\left(\frac{P_y}{P_x}\right) - \tan^{-1}\left(\frac{a_2.\sin(\theta_2)}{a_1 + a_2.\cos(\theta_2)}\right)$$

In summary, understanding both direct and inverse kinematics is essential for the effective design and operation of the ExoLeg. This method provides a solid foundation but combining it with the advances computational tools and techniques will help to simulate the mechanical movement of the robot.

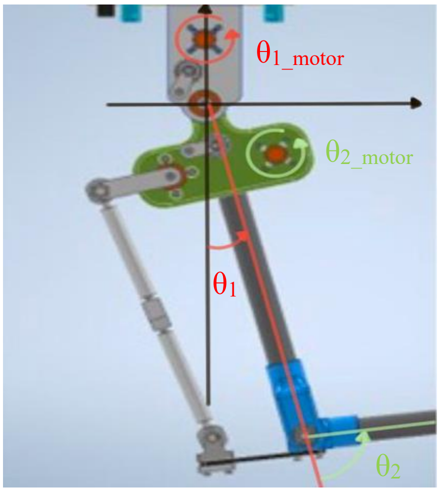

Figure 3.18 : Angle variation between θ_1 and θ_2 and the corresponding motors angles

However, as can be seen on the previous Figure 3.18, the angles θ_1 and θ_2 that were determined, do not correspond to the actual angles that need to be applied by the two motors to the device. Indeed, the angles are not located at the joints but at the upper part of the exoskeleton.

That is why the next step consisted in determining the mathematical relationships between the angles θ_1/ θ_{1_motor} and θ_2/ θ_{2_motor}.

- Relationship between θ_1 and θ_{1_motor}:

As seen in Figure 3.19, a mechanism consisting of two pulleys of different diameters linked by a toothed belt is presented. As a result, the rotation angles of the two pulleys are not equal. The relationship between the rotation angles of the pulleys depends on the ratio of the pulley diameters.

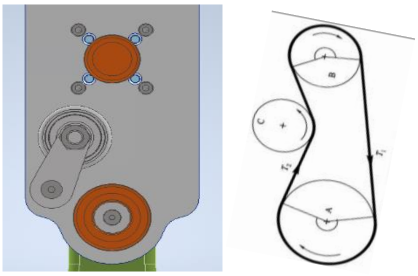

Figure 3.19 : Upper pulley system.

The transmission ratio R is given by:

$$R = \frac{D_1}{D_{1\_motor}}$$

Being D_{1_motor} the diameter of the driving pulley, corresponding at the axis of the motor (see Figure 33.19, part B), and D_1 the diameter of the driven pulley (see Figure 3.19, part A). The pulley C in the Figure 3.19 is an idler pulley which is neither powered nor driven. It is used to redirect the belt or to maintain tension without adding power to the belt.

If a pulley with diameter D_{1_motor} turns an angle θ_{1_motor}, the other pulley of diameter D_1 will turn with an angle θ_1 such as:

$$\theta_1 = \frac{D_{1\_motor}}{D_1} . \theta_{1\_motor}$$

- Relationship between θ_2 and θ_{2_motor}: The four-bar linkage mechanism

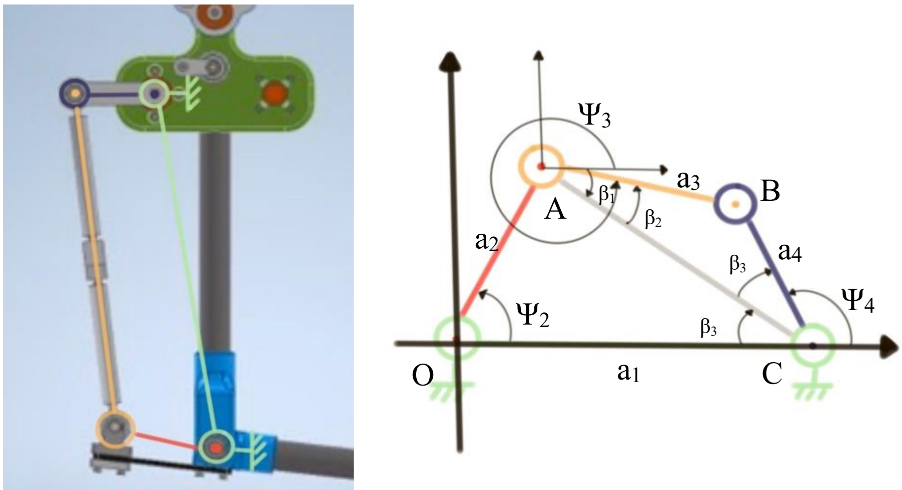

Figure 3.20 : Four-bar mechanism (left) and parameters (right)

The transmission of motor torque is done through a pulley/belt system as well as through a four-bar mechanism. In this situation, the pulley/belt system does not have an impact here. Indeed, because the two pulleys have the same external diameter, there is not an angle variation.

However, the four-bar linkage induces an angle variation. This mechanical system consists of four bodies, called bars or links, connected in a loop by four joints. Generally, the joints are configured so the links move in parallel planes, and the assembly is called a planar four-bar linkage.

The Figure 3.20, shows the four bodies of this mechanism:

- Ground link a_1: fixed to anchor pivots O and C.
- Input link a_2: driven by input angle Ψ_2.
- Output link a_4: gives output angle Ψ_4.
- Floating link a_3: connects the two moving pins A and B.

The angle Ψ_2 is the one which drive our four-bar linkage, resulting in the output Ψ_4 which will be equal to our θ_{2_motor} that we want to determine.

As we can see in the angle diagram, Ψ_2 is equal to the addition of θ_1 and θ_2. From there, we can use the trigonometric relations to deduce the output angle Ψ_4.

First, we can determine the β_1 angle:

$$\frac{OA}{\sin(\beta_1)} = \frac{AC}{\sin(\Psi_2)}$$

$$\Leftrightarrow \quad \sin(\beta_1) = \frac{OA.\sin(\Psi_2)}{AC}$$

$$\Leftrightarrow \quad \beta_1 = \sin^{-1}\left(\frac{OA.\sin(\Psi_2)}{AC}\right)$$

With:

$$AC = \sqrt{OA^2 + OC^2 - 2.OA.OC.\cos(\Psi_2)}$$

Then, we can calculate the β_2 angle:

$$BC^2 = AB^2 + AC^2 - 2.AB.AC.\cos(\beta_2)$$

$$\Leftrightarrow \quad \beta_2 = \cos^{-1}\left(\frac{-BC^2 + AB^2 + AC^2}{2.AB.AC}\right)$$

Finally, to deduce Ψ_3 and Ψ_4 we need to determine one last angle, β_3:

$$\frac{BC}{\sin(\beta_2)} = \frac{AB}{\sin(\beta_3)}$$

$$\Leftrightarrow \quad \beta_3 = \sin^{-1}\left(\frac{AB.\sin(\beta_2)}{BC}\right)$$

Consequently, we have:

$$\boxed{\begin{gathered}\Psi_3 = \beta_2 - \beta_1 \\ \Psi_4 = 180 - \beta_1 - \beta_3 = \theta_{2\_motor}\end{gathered}}$$

Equation 3.2: Angles in the four bars linkage

3.3.3. Trajectories simulation on MATLAB

Now that the theoretical angle equations have been determined, the simulation was initiated. For this purpose, MATLAB was used. It is a powerful and versatile numerical computing environment known for its efficiency in matrix manipulation, data visualization, and algorithm development. MATLAB was consequently chosen as the best software for determining and simulating the mechanism of the exoskeleton.

As explained in the 3.3.1, a circular trajectory with a radius of 100 mm was simulated (see Figure 3.15). The objective of this section is to elucidate the results obtained.

The Figure 3.21 is the final representation of the graphic animation of the Exoleg for the reference circular trajectory of radius equal to 100mm.

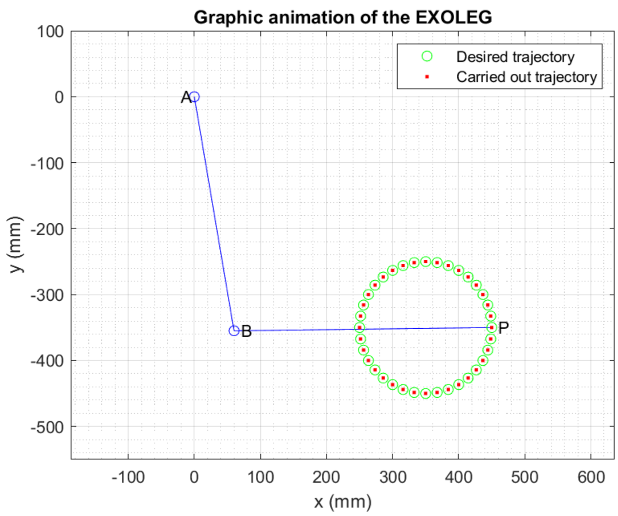

Figure 3.21: Graphic result of the ExoLeg's animation.

This simulation determines the angle's variation of the two joints articulations θ_1 and θ_2. Then, thanks to the mathematical equations found in the previous section, the motors angle variation (θ_{1_motor} and θ_{2_motor}) were deduced.

The following equation corresponds to the polynomial approximation of the angles variation that the upper motor must follow.

$$p(x) = p_1x^{10} + p_2x^9 + p_3x^8 + p_4x^7 + p_5x^6 + p_6x^5 + p_7x^4 + p_8x^3 + p_9x^2 + p_{10}x + p_{11}$$

Equation 3.3: Polynomial approximation for the first motor

With:

P_1	**P_2**	**P_3**	**P_4**	**P_5**	**P_6**	**P_7**	**P_8**	**P_9**	**P_{10}**	**P_{11}**
0.14	-2.49	18.67	74.35	167.36	-210.21	140.29	-43.39	-18.78	13.80	12.29

Table 3.1: Coefficients of the upper motor

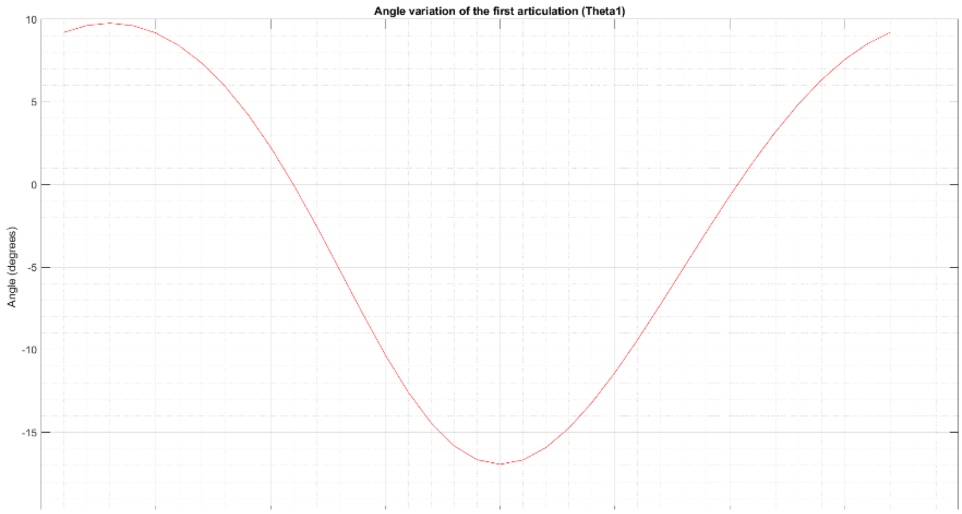

Figure 3.23: Graphic representation of the angle variation of the first articulation joint

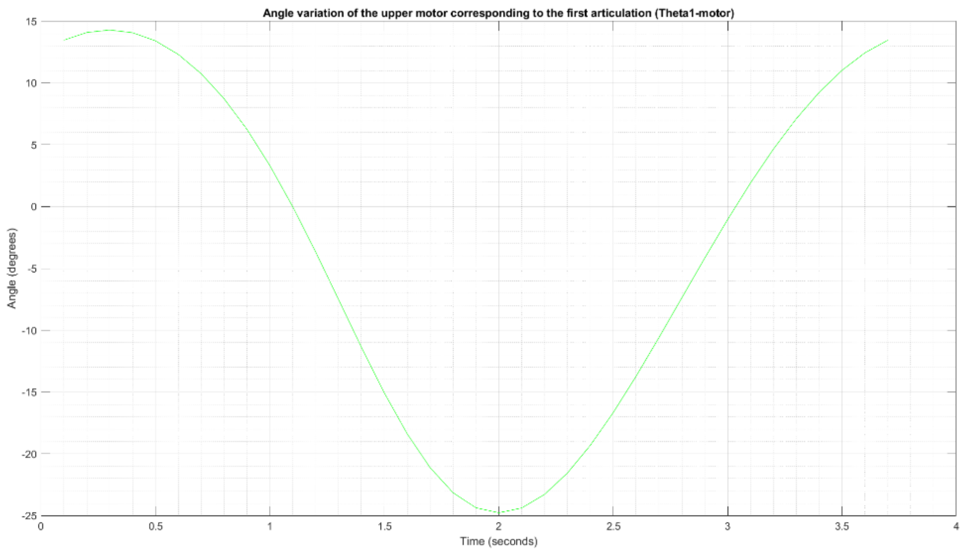

Figure 3.22: Graphic representation of the angle variation of the upper motor corresponding to the first joint

The following equation corresponds to the polynomial approximation of the angles variation that the lower motor must follow.

$$p(x) = p_1x^{10} + p_2x^9 + p_3x^8 + p_4x^7 + p_5x^6 + p_6x^5 + p_7x^4 + p_8x^3 + p_9x^2 + p_{10}x + p_{11}$$

Equation 3.4: Polynomial approximation for the second motor

With:

P_1	P_2	P_3	P_4	P_5	P_6	P_7	P_8	P_9	P_{10}	P_{11}
1.21	-24.31	208.10	-991.08	2863.95	-5139.98	5652.65	-3666.92	1319.75	-193.83	122.71

Table 3.2: Coefficients of the lower motor

The Equation 3.3 and Equation 3.4, will be send to the motors in order to generate the desired trajectory. In the 5.2. Test results, the theorical trajectory found with MATLAB will be compared to the real final trajectory.

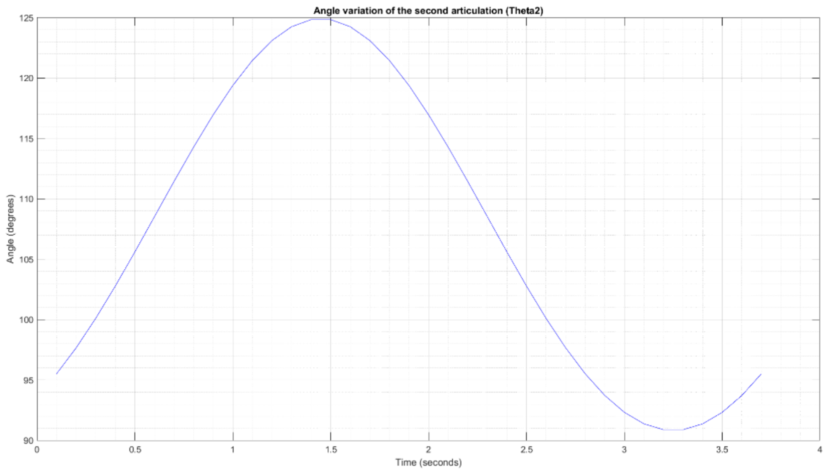

Figure 3.24: Graphic representation of the angle variation of the second articulation joint

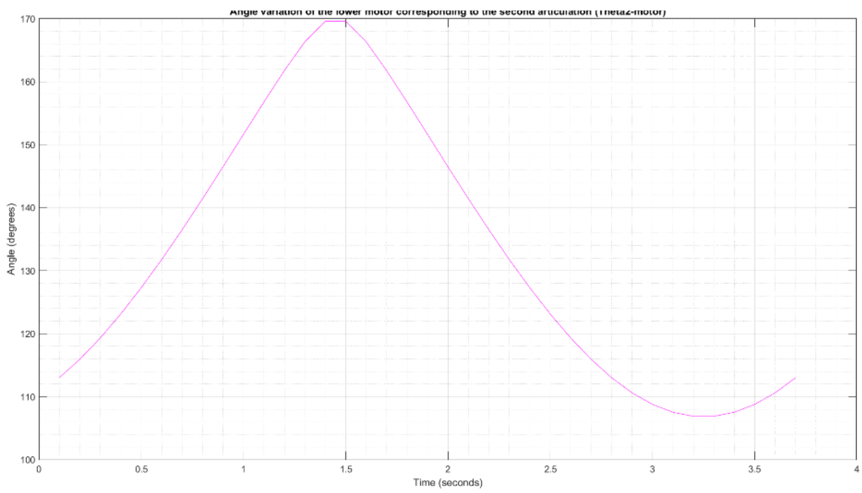

Figure 3.25: Graphic representation of the angle variation of the lower motor corresponding to the second joint

3.3.4. Joints and motors torque determination

In the previous section, θ_1, θ_2, θ_{1_motor}, and θ_{2_motor} were determined. The feedback linearization control can be performed. To recap, the following equation corresponds to the real system:

$$\ddot{q} = D(q)^{-1}.(-C(q,\dot{q}).\dot{q} - G(q) + \Gamma)$$

Then, the following equation corresponds to the control law:

$$\Gamma := \left(+\hat{C}(q,\dot{q}).\dot{q} + \hat{G}(q) + \hat{D}(q)\mu\right)$$

It was assumed that a great estimation is available, allowing us to state $C = \hat{C}$, $G = \hat{G}$ and $D = \hat{D}$. Consequently, an auxiliary control law was obtained:

$$\ddot{q} = \mu$$

With

$$\mu := \ddot{q}^* - K_p.(q - q^*) - K_d(\dot{q} - \dot{q}^*)$$

With q^* corresponding to the desired angles and q corresponding to the actual angles used by the system, the following mathematical relation was obtaines:

$$(\ddot{q} - \ddot{q}^*) + K_d(\dot{q} - \dot{q}^*) + K_p.(q - q^*) = 0$$

If $e = q - q^*$ is posed, the following equation is finally obtained:

$$\ddot{e} + K_d.\dot{e} + K_p.e = 0$$

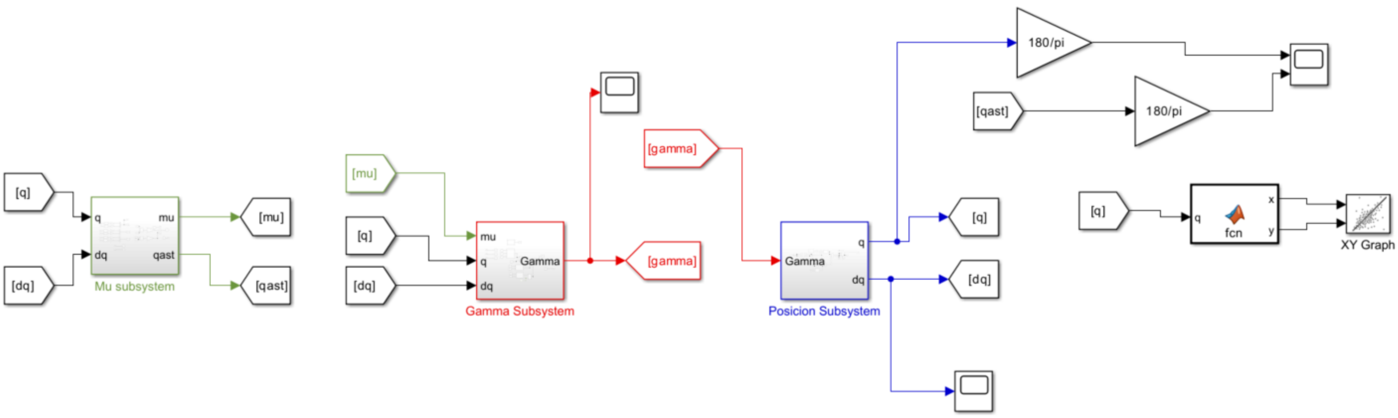

Figure 3.26: Simulink model (torques determination)

Figure 3.26 simulates all the equations previously shown.

- The "Position Subsystem" (of colour blue) corresponds to the following equation: $\ddot{q} = D(q)^{-1}.(-C(q,\dot{q}).\dot{q} - G(q) + \Gamma)$

Which was already modelled in the Figure 3.14.

- The "Gamma Subsystem" (of colour red) corresponds to the following equation: $\Gamma := \left(+\hat{C}(q,\dot{q}).\dot{q} + \hat{G}(q) + \hat{D}(q)\mu\right)$

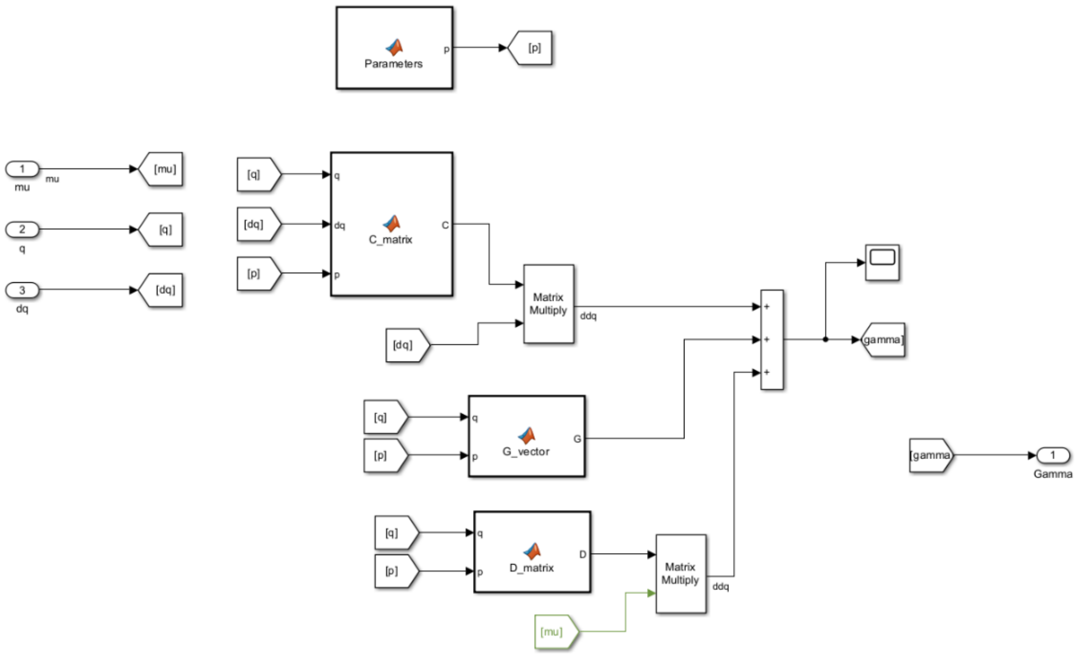

Figure 3.27 : Simulink Model (Gamma determination)

- The "Mu Subsystem" (of green colour) corresponds to the following equation: $\mu := \ddot{q}^* - K_p.(q - q^*) - K_d(\dot{q} - \dot{q}^*)$

This subsystem is receiving the previous values of θ1 and θ2 find previously with MATLAB.

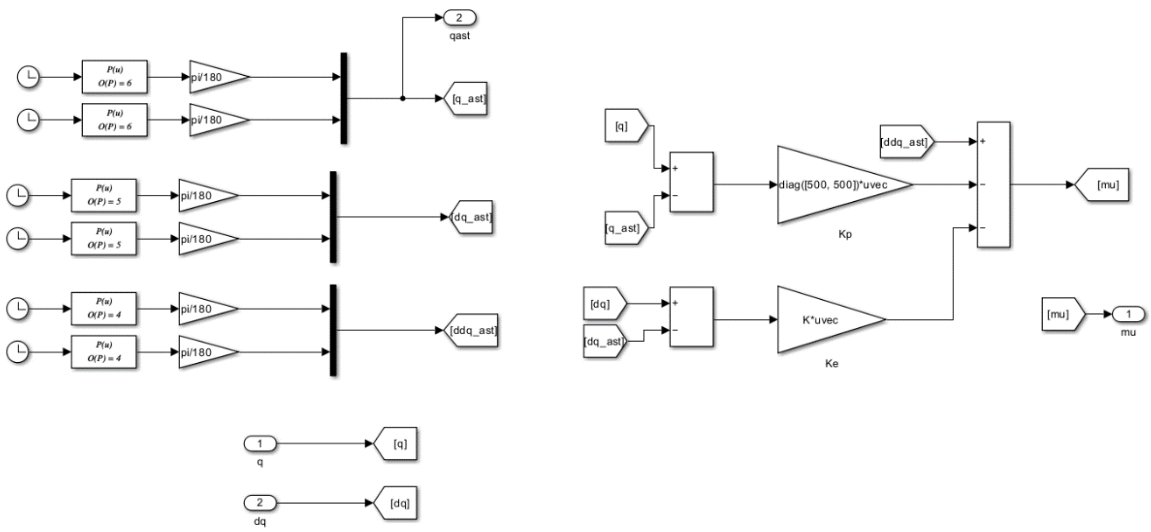

Figure 3.28 : Simulink Model (Mu determination)

Thanks to this control law Simulink model, the following results were obtained (Figure 3.29: Torques (Nm) for the joint 1 and joint 2 in function of time (s)).

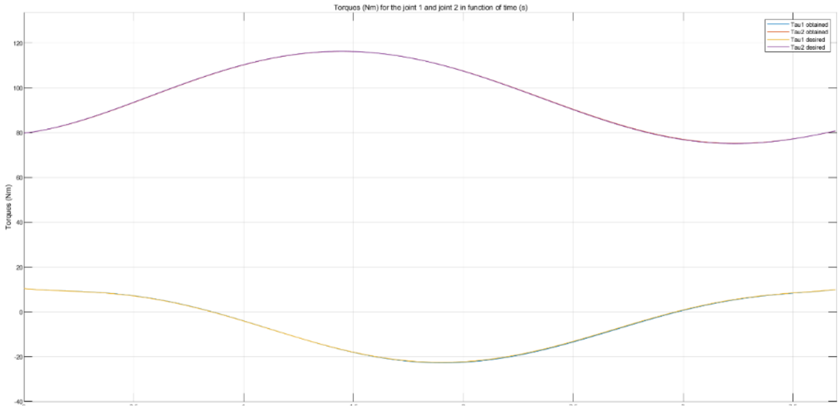

Figure 3.29: Torques (Nm) for the joint 1 and joint 2 in function of time (s)

First, it can be seen that the control system is great because the real torque is really closed to the desired one. For the first joint corresponding to Γ_1, the maximal torque is around 10 Nm. For the second joint corresponding to Γ_2, the maximal torque is around 115 Nm.

In order to verified that these torques are correct, the direct kinematic with these results was simulated (Figure 3.31: Direct kinematic):

Figure 3.31 : Direct kinematic

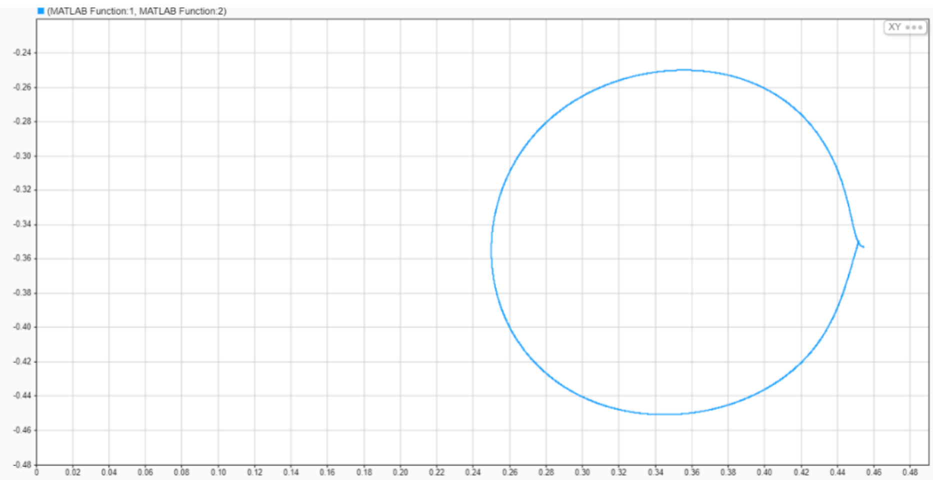

Figure 3.30 : Direct kinematic verification

Because the desired trajectory was obtained exactly, it can be concluded that the simulation is correct.

Now that the articulation torques have been determined, the motor torques can be deduced. To achieve this, some mechanical equations needed to be determined. First, the focus was on the second motor torque conversion.

- Torque of the second motor

To develop all the calculations necessary to determine the output torque in C, it is mandatory to know:

- the input torque in O: T_{input},
- the angles: Ψ_2, Ψ_3, and Ψ_4,
- the length of: OC, OA, AB, and BC
- the angular velocity of the segment OA,
- the angular acceleration of the segment OA.

In the Figure 3.26, a T_{input} torque is applied on the crank clockwise direction, so there will be a resisting torque T_{output} that is in the counterclockwise direction. The mechanical advantage is:

$$Mechanical\ Advantage = \frac{T_{output}}{T_{input}}$$

Since there is a torque T_{input} acting towards the clockwise direction and there is resisting torque acting in counterclockwise direction, this coupler link will undergo compression. Consequently, the compression force of the AB bar is f_{23} and f_{32}.

It is known that:

$$f_{23} = f_{32}$$

Then thanks to the Figure XX, it can be deduced:

$$T_{input} = f_{23} \times OA \times \sin(180 - \beta)$$

$$T_{input} = f_{23} \times OA \times \sin(\beta)$$

$$T_{output} = f_{32} \times BC \times \sin\,(\alpha)$$

Consequently, re following relation is obtain:

$$T_{output} = \frac{T_{input}}{OA \times \sin(\beta)} \times BC \times \sin\,(\alpha)$$

Once the relation between the input torque and the output torque has been determined, the Simulink model could be completed. It was necessary to add a subsystem which will calculate the results of this previous relation to determine the motor torques.

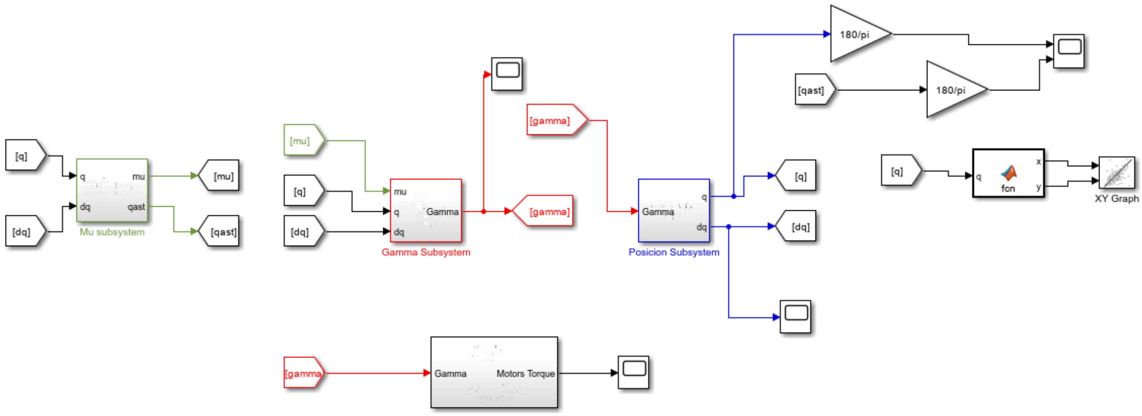

Figure 3.33 : Complete Simulink model

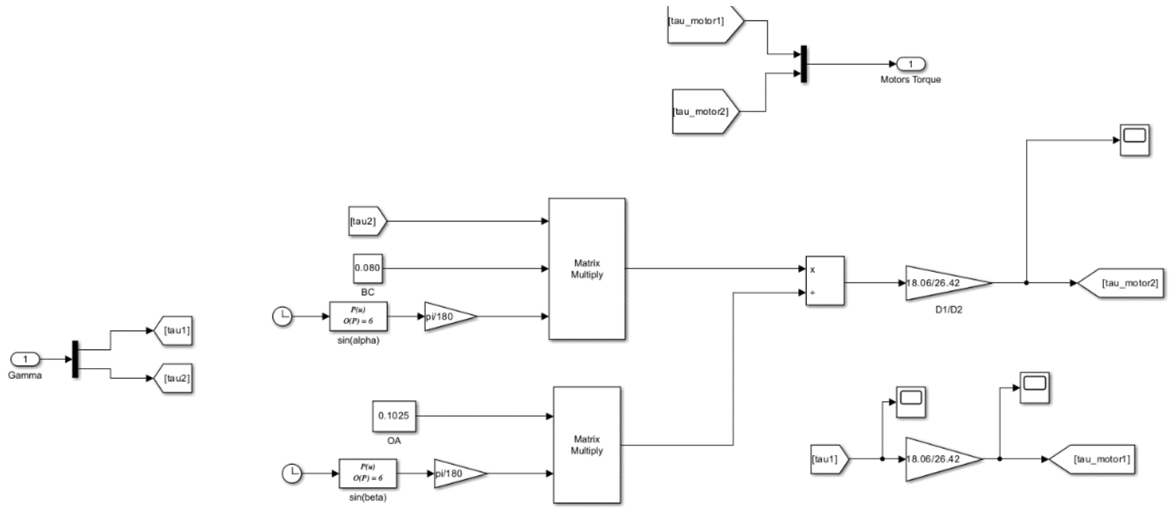

Figure 3.34 : Torques Subsystem

The Figure 3.34, corresponds to the torques subsystem which takes in entry, the two joints torques found before and will give in outup the motors torques results.

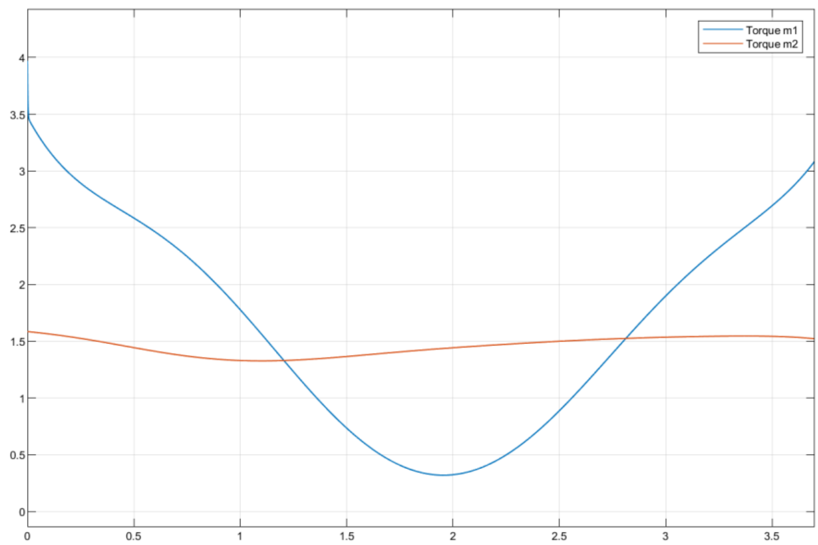

Figure 3.32 : Results of torques of motor 1 and 2

The Figure 3.32 represents the results of the motors torques. The blue curve corresponds to the second motor and the red curve corresponds to the first motor. Thanks to this graph, it is possible to conclude that the motors torque are much less important than the joint torques. Indeed, for the second motor, the maximum is 3.5 Nm and for the first motor 1.5 Nm approximately.

3.4. Dynamic and static studies with Autodesk Inventor

Dynamic analysis considers time-dependent forces and how they affect the movement and performance of the exoskeleton. It provides a comprehensive understanding of how the ExoLeg responds to varying conditions, such as walking or lifting. Static analysis, on the other hand, focuses on the system's response to constant loads, enabling a detailed examination of the stresses and strains in specific parts.

By combining both dynamic and static analyses, a thorough validation of the ExoLeg's design can be achieved. The dynamic simulation identifies critical load conditions, while the static simulation ensures that the key components can withstand these loads, highlighting any potential weaknesses and guiding necessary design improvements. This approach makes it possible to determine the distribution of stresses and strains, check the resistance of the materials used, and identify possible areas of weakness before validating the ExoLeg.

3.4.1. External forces simulation

The first step involved simplifying the ExoLeg design. Certain parts of the mechanism do not have a direct impact on the simulation, allowing the removal of these mechanical components. Figure 3.35 shows the resulting simplified model.

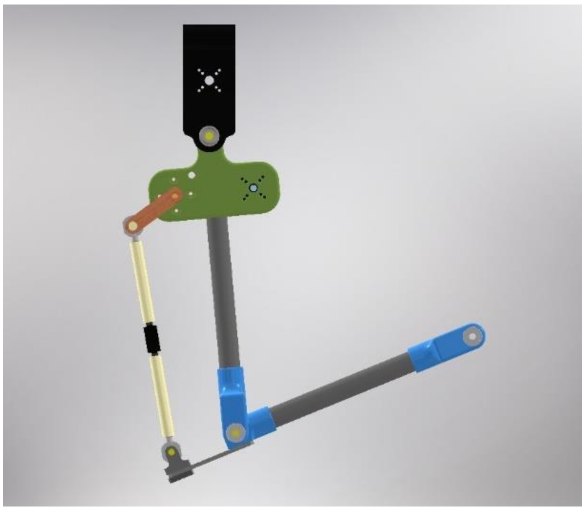

Figure 3.35: Simplified model for the dynamic simulation.

Next, to determine the forces applied to the model, a forced movement was applied to the ExoLeg. The motor movement equations (Equation 1 and Equation 2) were injected into the simulation for this purpose.

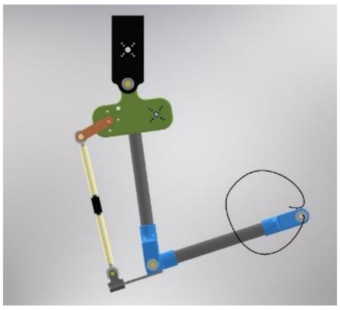

Figure 3.36: Dynamic trajectory of the ExoLeg on Inventor

As seen in Figure 3.36, the circular trajectory introduced in Inventor is not perfect. This is due to the fact that the original equations are polynomials with ten coefficients. However, in Inventor, it was only possible to introduce a polynomial with a maximum of five coefficients. As a result, the trajectory in Inventor is less precise. Nevertheless, this approximated trajectory will not have consequences on the forces applied to the mechanism.

The results of the simulation provide a comprehensive understanding of the ExoLeg's structural performance under various conditions. Four results will be studied here:

- **Loads determined from dynamic simulation:** The dynamic simulation provided insights into the forces and moments acting on the ExoLeg during typical operational scenarios. These forces were applied to the model to simulate real-world conditions and assess the mechanical performance of the design. The loads determined from this simulation serve as the basis for evaluating how well the ExoLeg can withstand operational stresses.
- **Von Mises Stress**: Von Mises stress is used to assess the material's ability to withstand applied loads. It is a critical measure in identifying whether the material will yield or fail under the given loads. In the simulation, von Mises stress values were calculated to determine the distribution of stress across the ExoLeg. High stress concentrations indicate potential areas of failure or where design modifications may be needed.
- **Displacements**: The simulation also provided data on the displacements of various components under applied loads. Displacement results help to understand how much the components move or deform when subjected to the forces. These results are essential for evaluating the performance and functionality of the ExoLeg, ensuring that the movements are within acceptable limits and do not affect the overall performance.
- **Safety coefficients**: Safety coefficients were calculated to assess the safety and reliability of the design. These coefficients compare the material's strength to the applied stresses, providing an indication of how much load the components can handle before reaching failure. A higher safety coefficient indicates a greater margin of safety, ensuring that the design can withstand unexpected loads or variations in operating conditions.

These results will be studied in relation to three main parts of the ExoLeg design. The first part is the four-bar linkage mechanism where the torque from the lower motor is applied. The second part is the hip axis, where the torque from the upper motor is applied. Finally, the third part is the strip that provides cushioning between the four-bar linkage mechanism and the lower bar.

Figure 3.37 presents the results obtained from the static analysis of the axis used in the four-bar linkage. First, the initial image (Figure 3.37a)), shows the load applied to this axis. The loads are primarily torques, represented by circular arrows, while the vertical and horizontal arrows indicate the gravitational force and compression forces applied to the axis.

Next, the von Mises stresses analysis (Figure 3.37b)), reveals a maximum value of 12.16 MPa. This result is reasonable, considering that PETG material can withstand between 50 and 70 MPa before breaking. Consequently, this indicates that the axis will not break during the operation of the ExoLeg.

Furthermore, the displacement (Figure 3.37c)), is not alarming, with a maximum of around 0.26 mm. This means that during the simulation, the axis will practically not deform.

Lastly, the safety coefficient (Figure 3.37d)) ranges between 4.47 and 15. A result of 15 indicates that the axis is very robust and has a significant margin of safety. This means that it is unlikely to fail under normal operating conditions and even under unexpected or extreme loads. This is particularly reassuring in ExoLeg applications because failure could have severe consequences for the patient. However, PETG is not a very strong material, so after several repetitions, this axis may suffer from fatigue and eventually break.

Consequently, this axis will not break during the operation of the ExoLeg. However, PETG isn't a very strong material, so after several repetitions, this axis may suffer from fatigue and eventually break.

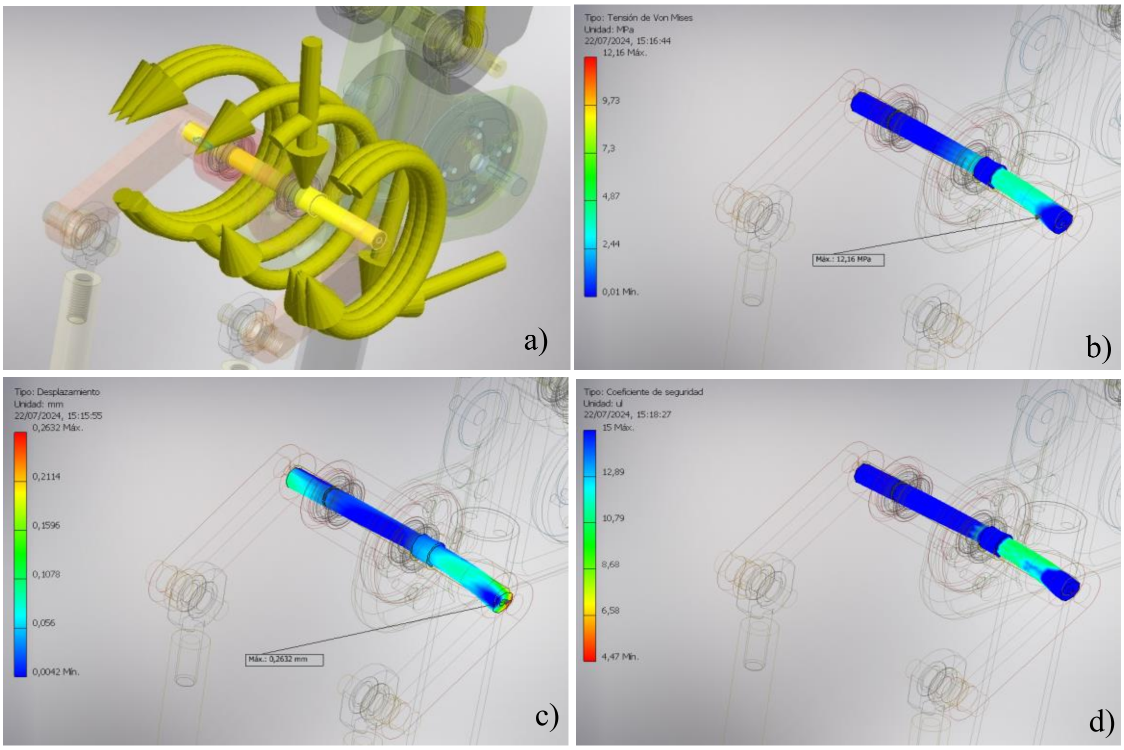

Figure 3.37: a) Loads applied to the four bars axis, b) Von Mises stress, c) Displacements, d) Security coefficients

Similarly, the first image of Figure 3.38 shows the load applied to the hip axis. This axis experiences more compression forces than torque.

Moreover, the maximum Von Mises stress (Figure 3.38b)) is 19.95 MPa, located where the pulley is fixed, which will impart the rotation movement created by the lower motor. This torsion torque is logical given the location. While this result is a bit high, it is still acceptable.

In addition, the displacement (Figure 3.38c)) is approximately 0.37 mm, similar to the axis of the four-bar linkage.

Furthermore, the safety coefficients (Figure 3.38d)) range between 2.73 and 15. This wide range indicates that the part has both very strong and very weak areas, making optimization difficult. While the axis will not break during the simulation, it can become fragile and, after several repetitions, may eventually break.

Consequently, like the previous axis, this one will not break during the simulation, but it can be fragilized and after several repetitions it can finally break.

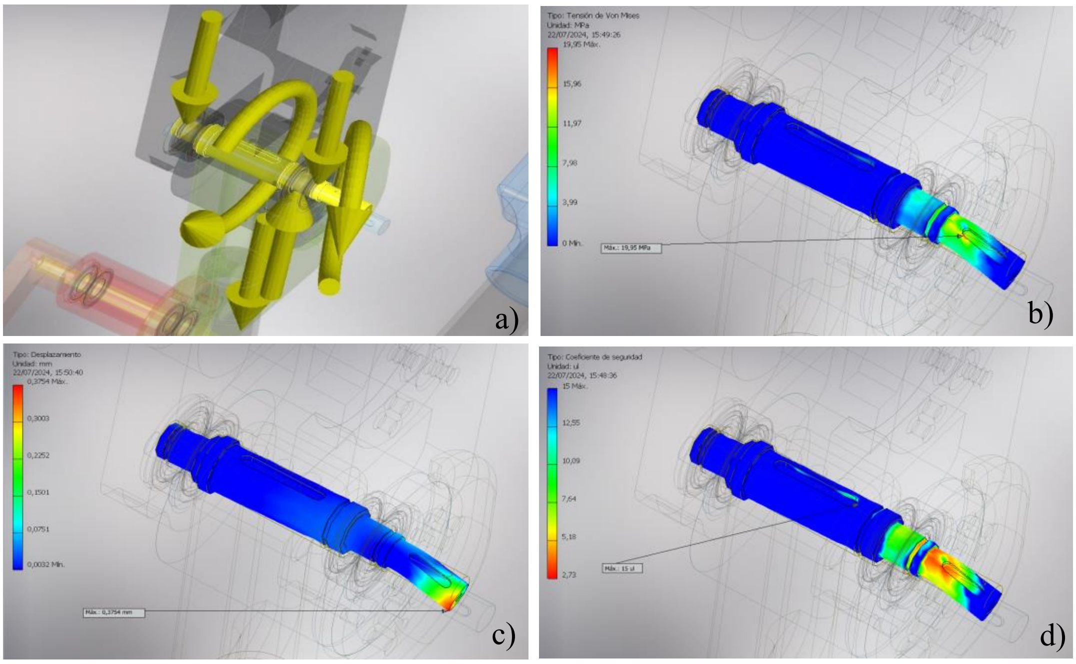

Figure 3.38: a) Loads applied to the hip axis, b) Von Mises stress, c) Displacements, d) Security coefficients

Finally, the last part that needed to be studied is the string allowing the mechanical transmission of movement between the four-bar linkage and the lower bar (Figure 3.39). This part experiences significant torsion loads. Consequently, these loads will cause a more substantial displacement than in the previous parts. As seen in Figure 3.39c), the maximum displacement is around 0.42 mm.

However, the Von Mises stresses (Figure 3.39b)) are much less important, around 7.74 MPa. Thus, this part is not at high risk of breaking. Moreover, the safety coefficients (Figure 3.39d)) are also better, ranging between 7 and 15. This indicates that the string is strong and will not break easily.

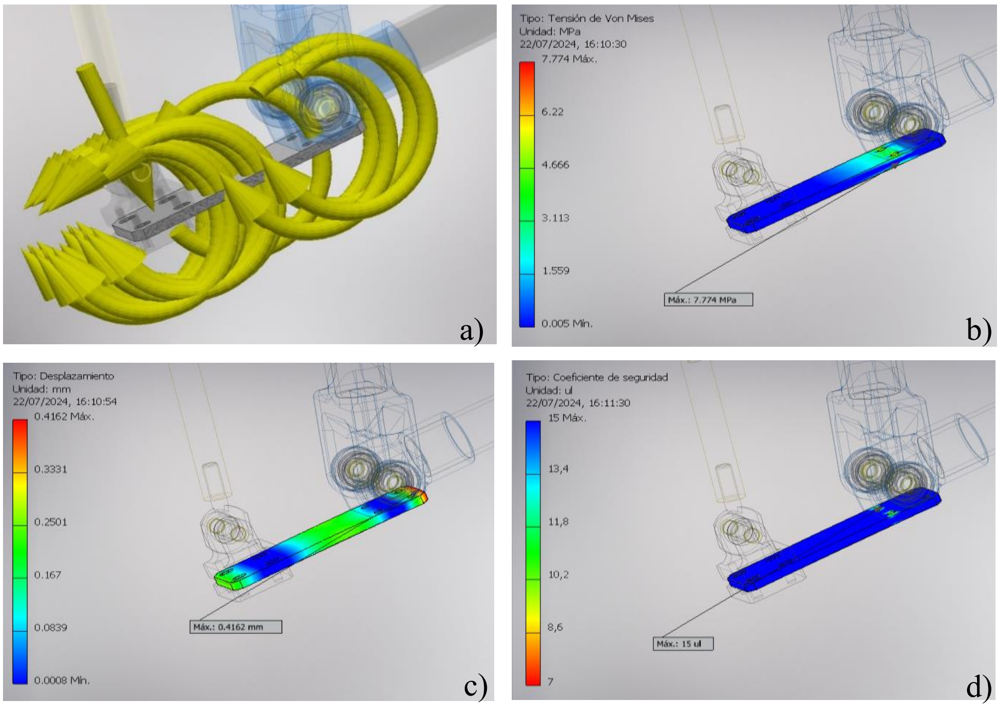

Figure 3.39: a) Loads applied to the strip, b) Von Mises stress, c) Displacements, d) Security coefficients

In summary, these simulation results offer a detailed view of the ExoLeg's structural integrity and performance. These results are crucial for verifying the design's robustness and guiding any necessary improvements to ensure reliability and safety in real-world applications.

3.4.2. Optimisation

The primary goal of this section is to enhance the performance, efficiency, and durability of the ExoLeg through systematic optimization. After conducting thorough static and dynamic simulations, it is evident that certain components of the ExoLeg can be further improved to ensure optimal functionality and user safety.

Optimization is a crucial step in the design process as it allows for the refinement of various parameters to achieve the best possible performance. The initial design and simulations provided valuable insights into the mechanical behavior of the ExoLeg under different conditions. However, there are several aspects that can still be improved, including:

- **Weight Reduction**: Minimizing the weight of the exoskeleton to improve user comfort and reduce energy consumption.
- **Material Efficiency**: Ensuring that the materials used provide sufficient strength while reducing costs and potential fatigue issues.
- **Performance enhancement**: Fine-tuning the mechanical components to achieve smoother and more precise movements.
- **Safety Margins**: Increasing the safety factors in critical areas to prevent failures during prolonged use.

To achieve these goals, it will be interesting to adjust key design parameters such as dimensions, shapes, and material properties to find the optimal configuration. In the following sections, each optimization objective will be addressed in detail, showcasing the methods used, the iterations performed, and the results obtained. This comprehensive approach will ensure that the ExoLeg design is not only functional but also optimized for real-world application.

First, it was necessary to properly dimension the string component. This part is critical to the overall functionality of the ExoLeg. The string needs to possess a specific level of flexibility to effectively dampen the mechanical forces and motions, thereby minimizing the impact on the patient. Proper dimensioning ensures that the string can absorb shocks and vibrations, providing a smoother and safer experience for the user. Despite its need for flexibility, the string must also be strong enough to bear the loads imposed by the exoskeleton's movements. This balance between flexibility and strength is essential for the reliable operation of the ExoLeg.

To better optimize the thickness of the string, it was mandatory to use the previous results from the static and dynamic simulations. The maximum loads that the string will experience were identified. This data helps in determining the required thickness of the string to ensure it can handle the stresses without failure.

To do that, a study was made with different string's thickness of material PETG. The Figure 3.40 graphs the results of this experiment.

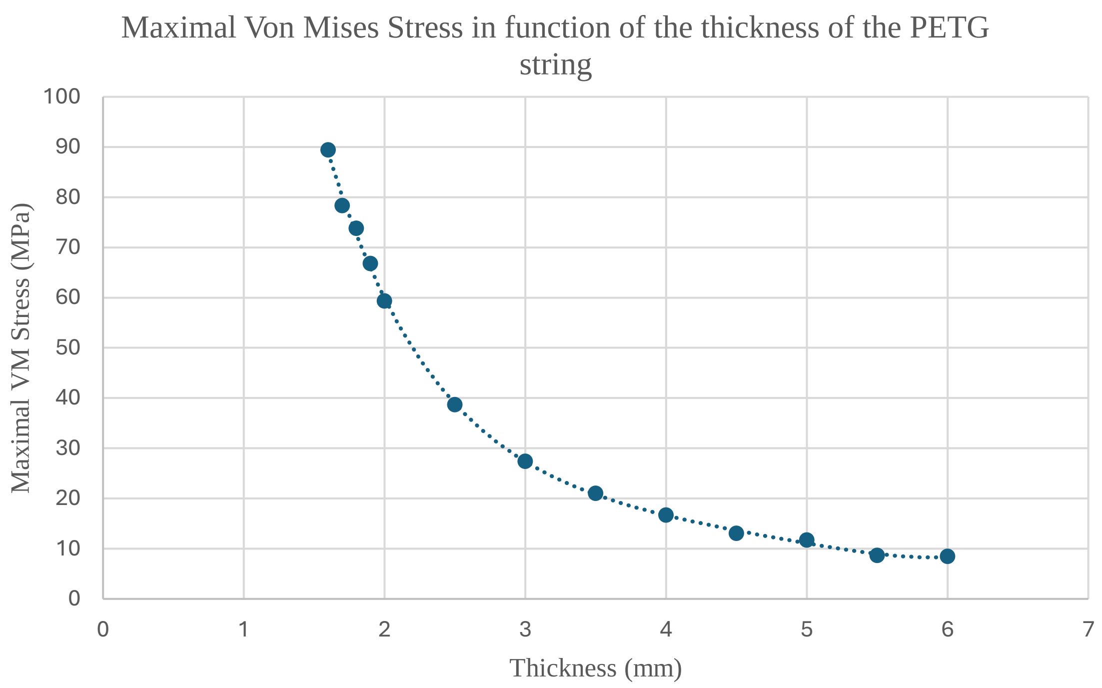

Figure 3.40: Maximal Von Mises Stress in function of the thickness of the PETG string

As it is known, the ultimate tensile strength (or breaking limit) of PETG is generally in the range of 50 to 70 MPa. That is why all the thickness that have a maximal VM stress above 50 MPa were directly rejected. It was decided to keep the optimize thickness of 3 mm. Indeed, it's maximal VM stress is around 30 MPa which is safe.

The Figure 3.41 presents the results of the static analysis of a string plate of 3mm of PETG.

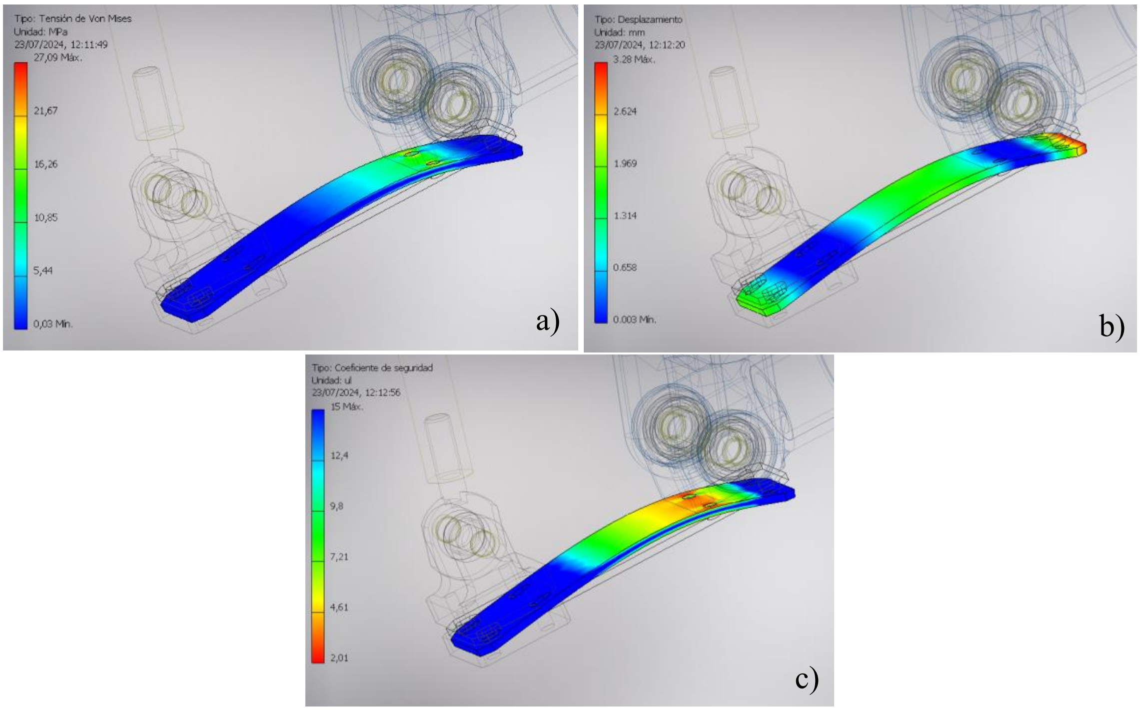

Figure 3.41: a) Von Mises stress applied to the strip plate of 3mm of PETG, b) Displacements, c) Security coefficients

Thanks to this study, it is evident that this plate has a certain flexibility. However, the safety coefficient is somewhat low (around 2, particularly near the drilled holes). It would be beneficial to explore alternative materials that are more flexible and have a higher safety coefficient.

One of the materials that can be tried is Nylon. It offers a good combination of flexibility, strength and durability. The Figure 3.42 presents the obtained results. It is seen that for a same thickness of 3 mm, the displacement (3,4 mm) and the security coefficient (around 3 ul) are better than for the string plate of PETG. Consequently, Nylon offers superior properties compared to PETG for the application in the ExoLeg. The enhanced mechanical strength, make Nylon, a more suitable material for the components subjected to significant loads and movements.

However, it is important to note that further studies on other materials could provide additional insights and potentially better alternatives. Unfortunately, due to the limitations of our study, only the materials that were readily accessible were tested. A broader range of materials could be explored in future research to optimize the performance and durability of the ExoLeg even further.

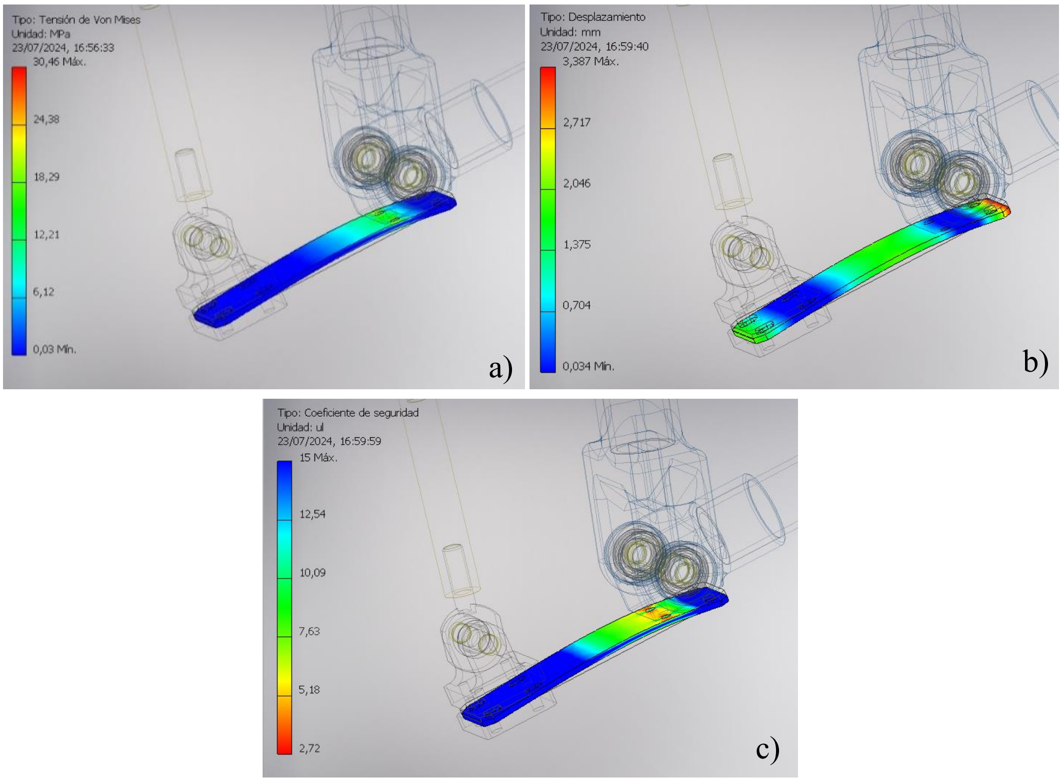

Figure 3.42: a) Von Mises stress applied to the strip plate of 3mm of Nylon, b) Displacements, c) Security coefficients

Two other optimizations were made onto the previous axis. In order to obtain a better safety coefficient, the material was changed from PETG to steel. The Figure 3.43 and 3.44 presents the results. It is notable that the safety coefficients are much better going from 2,73 ul to 8,25 ul for the hip axis and from 4,47 to 15 ul for the four bars axis.

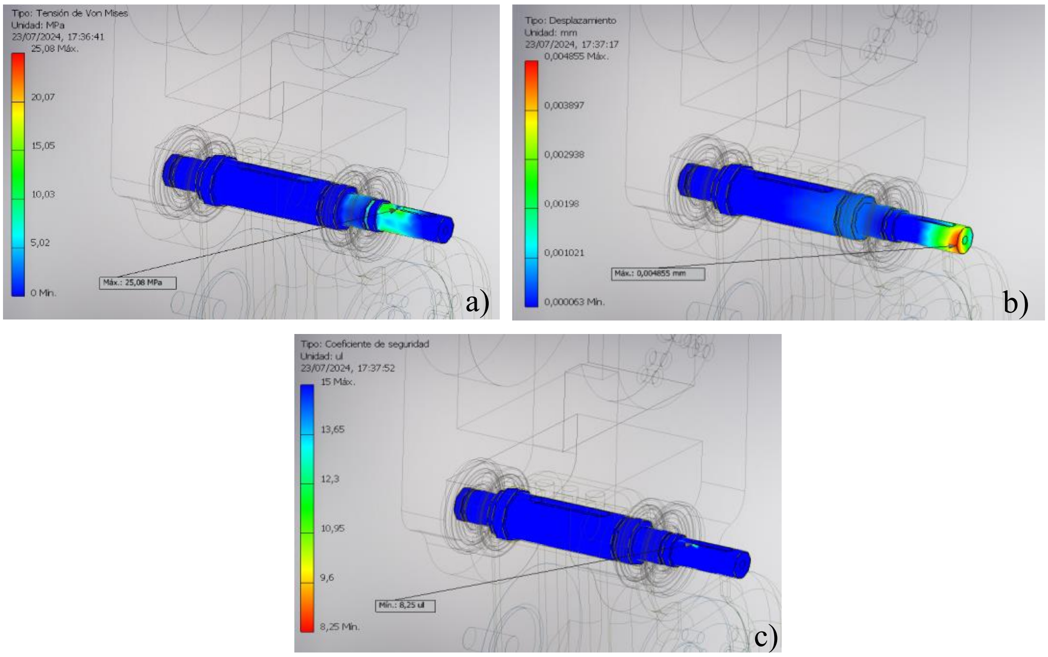

Figure 3.43: a) Von Mises stress applied to the hip axis, b) Displacements, c) Security coefficients

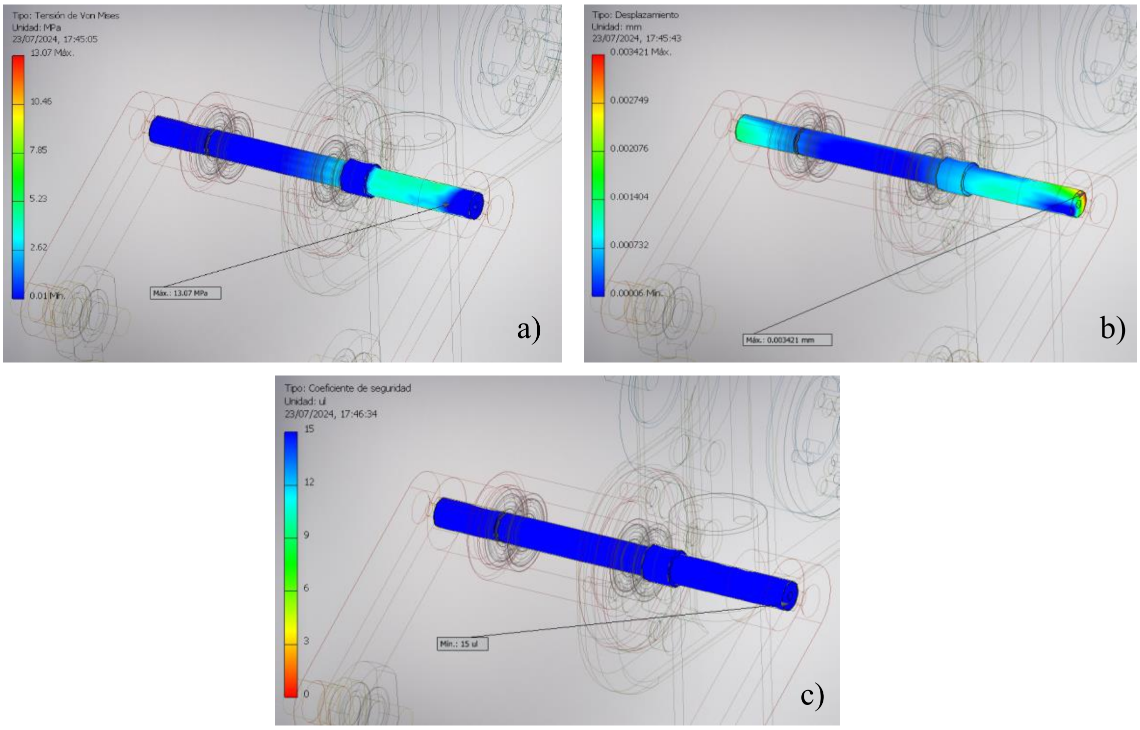

Figure 3.44: a) Von Mises stress applied to the four bars axis, b) Displacements, c) Security coefficients

In summary, these optimizations have significantly improved the structural integrity and performance of the ExoLeg. Future research should continue to explore other materials and design modifications to further enhance the exoskeleton's capabilities and ensure its long-term effectiveness and safety for patients.

Chapter 4

Mechanical assembly

After mechanical analyses were conducted, the next crucial step involved the physical construction of the ExoLeg through the assembly of all its components. The aim of this process was to validate the design, performance, and efficiency of the medical robot. In the following Section, the assembly process is detailed from three perspectives: the 3D printing of parts, the integration of mechanical components, and the final assembly of the ExoLeg. This comprehensive approach ensured that each component was accurately constructed and properly integrated into the overall design, thus facilitating the final testing phase.

4.1. 3D printing

When the project was undertaken, some parts of the robot had already been printed, including the "Hip base" (Figure 3.4), "Hip base motor" (Figure 3.5), "attach pivot calf axis" (Figure 3.6), "Attach pivot hip axis" (Figure 3.7), and the "Calf" (Figure 3.9). However, many parts were still missing, and new modified parts needed to be printed, as described in the section 3.1.2 to accommodate the motor's sensors.

Consequently, the first step involved conducting an inventory to determine which 3D parts were still needed for the assembly. Referring to the ExoLeg design shown in Figure 3.3, Figure 3.4, Figure 3.5, Figure 3.6, Figure 3.7, Figure 3.8 and Figure 3.9, the device comprises several key components, each requiring a specific number of pieces. The parts needed for the assembly include:

- barra_cadera x2
- barra_rotulas x3
- eje_cadera_abduction x1
- eje_cuatro_barras x1
- eje_tensor x2
- pasador_rotula x1
- pasador_rotula_2 x1
- pasador_tornillo_fino x1
- perno x2
- perno_tensor x2
- pivote_cadera_eje x1
- pivote_pantorrilla_eje x2
- tornillo_cadera x1

Then, it was important to decide in which order these 3D parts will be printed to assemble the robot as quickly as possible. In total, thirty pieces were printed. To simplify the assembly process, the robot was divided into two subsystems.

Two 3D Prusa Slicer were used. These 3D printers are low cost and ease of construction and modification made it very popular.

Figure 4.1: Original Prusa i3 MK3 [37]

This printer has some advantages like removable printing sheets which are easy to maintain and make it easy to remove the printed object from the printing surface. Moreover, it is fully compatible with a wide range of different types of materials. Some of the key features of the Original Prusa i3 MK3 are:

- Build volume: 250 x 210 x 210 mm,
- Layer resolution: from 50 to 350 microns,
- Z-axis accuracy: 0.01 mm,
- Filament compatibility: many types of filaments, including PLA, ABS, PETG, ASA, Polycarbonate, Nylon, and various composites such as wood or metal filaments,
- Printing speed: Up to 200 mm/s, although 60-80 mm/s is recommended for optimal quality,
- User-friendly design: Friendly user interface and clear instructions for assembly and use.

Overall, the Original Prusa i3 MK3 is a reliable and affordable 3D printer that is suitable for both, beginners and experienced users. It offers a good balance of features, performance, and ease of use, making it a popular choice among 3D printing.

The pieces were printed using PLA, PETG or Nylon. Table 4.1 shows all the materials used for each 3D printed parts, as well as their advantages and disadvantages.

Materials	Advantages	Drawbacks	Printing temperature (°C)	Plateau temperature (°C)	3D Parts
PLA	- Easy to print - Rigid - Biodegradable	- Can be brittle	190 – 220	50 – 60	Non-functional parts.
PETG	Easy to print - Combines some of the best features of PLA and ABS - More flexible - Less brittle - Impacts resistant	- Poor water resistance	220 – 250	70 – 90	Functional parts requiring mechanical strength.
NYLON	- Very resistant to wear - Impacts resistant - flexible - Sustainable	- Difficult to print - Absorbs a lot of moisture	240 – 270	70 – 90	Mechanical parts and gears requiring high strength and durability

Table 4.1 : Materials' characteristics

Once the best materials were chosen, the impression with the software PrusaSlicer 2.7.4 could be done. PrusaSlicer is a cutting software also created by Prusa Research, to prepare 3D printing files. It is an essential tool for converting 3D models, which are in .STL into understandable instructions for the 3D printer in .G-CODE. The interface is easy to use and proposes different complexity levels to adapt to every user skill. One of the advantages is that it generates automatically supports with the possibility to customize them manually. Moreover, it allows a visualization of the print path, to check trajectories and potentially problematic areas before printing. Finally, before printing, it calculates the printing time and the quantity of filament required.

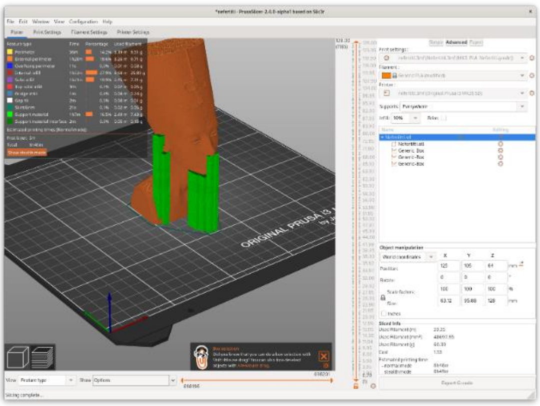

Figure 4.2 : PrusaSlicer software [38]

4.2. Mechanical components

While the 3D parts were being printed, the various mechanical components required for assembling the ExoLeg were simultaneously acquired. This included bearings, screws, pulleys, and toothed chains. Indeed, mechanical components play a crucial role in the performance and efficiency of the ExoLeg. These components are responsible for enabling movement and facilitating the transmission of forces throughout the device.

In this subsection, the different types of mechanical components used in the construction of the exoskeleton will be examined, as well as the design and integration criteria of these components.

- **Joints**: They are crucial components in the construction of exoskeletons, enabling the movements necessary to mimic human actions. They can be classified into several types according to their function and mode of movement: rotary joints, linear joints, ball joints and flexible joints. In the case of the ExoLeg, only rotary joints (bearing) and ball joints (rod end bearing) are used:
  - **Bearing**: A ball bearing is in the form of two coaxial rings between which balls are placed, lightly lubricated, and kept spaced apart by a cage, as shown in Figure 4.3. The materials used depend on the application for which the bearing is designed, but generally it must be resistant to compression. In the case of the ExoLeg, all the bearings have the same functions and have the same material characteristics. The differences will be in their bore diameter, external diameter, and width. The characteristics of the ball bearing used are presented in Table 4.2 : Ball bearings characteristics.

Figure 4.3 : Ball bearing [39]

Reference	Bore diameter (mm)	Outside diameter (mm)	Width (mm)	Basic dynamic load (kN)	Speed limit (r/min)	Quantity
SKF_6004-2RSH	20	42	12	9.95	11000	2
SKF_6201-2RSH	12	32	10	7.28	15000	2
SKF_6200-2RSH	10	30	9	5.4	17000	4
SKF_6000-2RSH	10	26	8	4.75	19000	2
SKF_6001-2RSH	12	28	8	5.4	17000	2

Table 4.2 : Ball bearings characteristics

- **Rod end bearing**: It consists of a spherical bearing mounted in a housing, with an external thread, as shown in Figure 4.4. This type of joint allows angular movements in multiple directions, and it is designed to support radial and axial loads. Rod end bearings are often used in applications where it is necessary to allow joint movement while maintaining a solid connection between components. In the case of the ExoLeg design, this type of joints is located into the four-bars linkage mechanism. The characteristics of the spherical joint used are presented in Table 4.3.

Figure 4.4: Rod end bearing [40]

Reference	Bore diameter (mm)	Width (mm)	Thread	Bearing length (mm)	Basic dynamic load (kN)	Quantity
SA 10 C	10	9	M10	65	8.65	3

Table 4.3 : Rod end bearing characteristics

- **Actuators**: They are key elements in mechanical systems. They enable the movement and feedback necessary to control the ExoLeg accurately and efficiently. In the case of this project, electrical actuators and sensors were used.
  - **Electric motor**: The ODrive-6374 is a brushless DC Motor (BLDC) which offers high efficiency, long life, and quiet operation, as shown in Figure 4.5. The characteristics of this motors are presented into the Table 4.4.

Figure 4.5 : Motor ODrive-6374 [41]

Reference	Speed constant (Kv)	Max current (A)	Max voltage (V)	Phase resistance (mOhm)	Mass (g)	Torque (Nm)	Quantity
ODrive-6374	150	70	48	39	890	3.86	2

Table 4.4 : Motors characteristics

- **Encoder**: It is a high resolution absolute rotary encoder, designed to provide precise information on the angular position of a rotating shaft. To do that, the encoder shown in Figure 4.6 is positioned onto the motor axe. The characteristics of this encoder are presented in the Table 4.5.

Figure 4.6 : Encoder [42]

Reference	Output type	Pulses per revolution	Supply voltage (V)	Quantity
AMT212B-V	RS-485	16384	3.8 ~ 5.5	2

Table 4.5 : Encoder characteristics

- **Transmission systems**: They are essential for transferring power and motion between different parts of a mechanical system. They convert and transit forces and movements efficiently and precisely. In the case of this exoskeleton, the important transmission mechanisms are composed of four pulleys and two toothed chains.
  - **Pulley**: It is used in a variety of mechanical transmission applications. Flat pulleys are often used in belt drive systems to transmit motion between two parallel shafts. In the ExoLeg device, two different types of pulleys were used. Their characteristics are presented in Table 4.6.

Figure 4.7 : Pulley [43]

Reference	Pitch (mm)	Number of teeth	Pilot bore (mm)	Width over hub (mm)	Compatible timing belt (mm)	Quantity
LS 28 AT5 / 20-2 hub 24x6	5	20	6	28	16	2
LS 28 AT5 / 14-2 hub 14x6	5	14	6	28	16	2

Table 4.6 : Pulleys characteristics

- **Toothed belt**: It is a power transmission element used in many mechanical systems. It is made from a synthetic rubber, polybutadiene, and has a V-shaped trapezoidal cross section, as shown in Figure 4.8. This shape allows the belt to fit the corresponding groove of the pulley. The advantages are that it provides durable, quiet and low maintenance power transmission. It is also effective for our project thanks to high efficiency. Moreover, this toothed belt is relatively easy to install. In the ExoLeg design, two different types of toothed belt are used, their characteristics are presented in Table 4.7.

Figure 4.8 : Toothed belt [44]

Reference	Belt width (mm)	Number of teeth	Pitch (mm)	Tooth style	Quantity
305-5M-15 Timing Belt	15	61	305	HTD 5mm	1
365-5M-16 Timing Belt	16	73	365	HTD 5mm	1

Table 4.7: Toothed belts characteristics

- **Fixings and supports**: They are essential elements in the design and assembly of mechanical systems. They ensure the stable and secure connection of components while allowing a certain modularity and flexibility in the construction and maintenance of the exoskeleton.
  - **Screw**: It is a mechanical part comprising a threaded rod and a head. Different types of head screws are presented in Figure 4.9. It is intended to secure one or more parts by pressure. Screw fixing creates a removal plan-to-plan connection, by pre-stressed plating of the two parts to be assembled. It exists a lot of different screw types. In the case of the ExoLeg, three of them were used as shown in Figure 4.9. The Table 4.8. shows the main characteristics of the screws used.

Figure 4.9 : Three different types of screws [45]

Reference	Type	Diameter (mm)	Threaded length (mm)	Quantity
DIN 933 M6x10	Hexagonal head	M6	10	4
AS 1420 M4x8	Pan head	M4	8	8
DIN 7991 M5x8	Triangular head	M5	8	2
DIN 7991 M4x8	Triangular head	M4	8	3
AS 1420 – M5x10	Pan head	M5	10	8
DIN 7984 M5x8	Pan head	M5	8	4
DIN 7984 M4x6	Pan head	M4	6	4

Table 4.8 : Screws characteristics

- **Nuts**: They are essential fasteners used in conjunction with screws or bolts to assemble mechanical components. They are designed to mate with the external threads of screws or bolts to create a secure connection. In the case of the ExoLeg, only nuts of diameter M8 were used as shown in Figure 4.10.

Figure 4.10 : Nuts [46]

- **Spring washer**: They are essential fasteners used to distribute loads, prevent movement and protect the surfaces of assembled components, shown in Figure 4.11. The spring washer provides spring force when compressed, creating additional tension on the assembly. It is used to prevent loosening due to vibration or load variations. The different types used for the ExoLeg are detailed in Table 4.9.

Reference	Type	Shaft/Bore diameter (mm)	External/Internal diameter (mm)	Thickness (mm)	Quantity
DIN 471 20x1.2	Extern	20	18.5	1.2	2
DIN 472 32x1.2	Intern	32	34.4	1	2
DIN 471 12x1	Extern	12	11	1	2
DIN 472 30x1.2	Intern	30	32.1	1.2	4
DIN 472 26x1.2	Intern	26	27.9	1.2	1
DIN 471 9x1	Extern	9	8.4	1	1
DIN 471 10x1	Extern	10	9.3	1	6
DIN 471 15x1	Extern	15	13.8	1	1
DIN 471 6x0.7	Extern	6	5.6	0.7	1

Table 4.9 : Spring washer characteristics

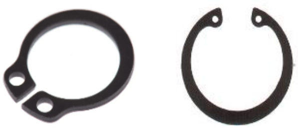

Figure 4.11 : Spring washer (External (left) and Internal (right)) [47]

4.3. Exoleg assembly

To assemble the ExoLeg, the CAD design was meticulously followed. The assembly process began with the independent assembly of each subassembly, which were later combined to build the complete robot.

The first component to be assembled was the extremity of the ExoLeg, where the patient's leg is positioned. This subassembly involved joining part 1 and part n°2 using screws. This step is crucial as it forms the foundational support structure for the patient's limb, ensuring stability and comfort. Figure 4.12 illustrates the assembly process, detailing how each component fits together and highlighting the secure attachment points used to maintain structural integrity.

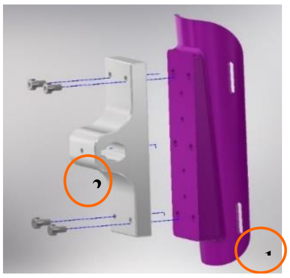

Figure 4.12: Subassembly of the extremity of the ExoLeg

To assemble the second part, the focus was on the inferior bar shown in Figure 4.13. The process began by securing piece 4 to piece 3 using four screws, ensuring a stable and secure connection. Similarly, parts 5 and 6 were attached to piece 4 using screws. This methodical assembly ensured that each component was firmly fixed in place, contributing to the overall stability and functionality of the ExoLeg.

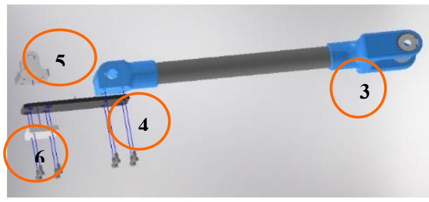

Figure 4.13: Subassembly inferior part

The third subassembly is the superior part, shown in Figure 4.14. This involves part 7, which consists of a green piece and a blue piece connected by two axes. On one side of the axis, piece 10 in Figure 4.14, a pulley and connecting rod piece 8a are inserted. On the opposite side of this axis, piece 9 and another connecting rod, piece 8b are attached. This careful assembly of components ensures the correct alignment and functioning of the superior part of the ExoLeg, contributing to its overall mechanical structure and performance.

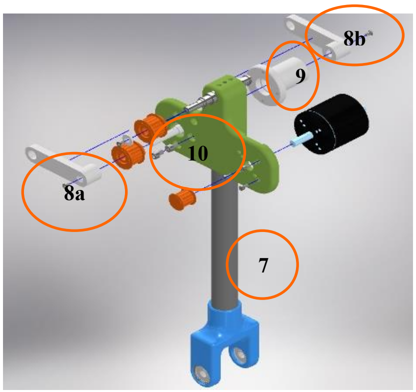

Figure 4.14: Subassembly superior part

The four-bar linkage, shown in Figure 4.15, consists of assembling three bars: 11a, 11b, and 11c, to piece 12 using a threaded connection. At each extremity of the bars, a rod end bearing is integrated to facilitate smooth motion. This setup is crucial for linking the subassembly of the inferior part, shown in Figure 4.13, with the superior part, shown in Figure 4.14, ensuring cohesive movement and stability in the ExoLeg structure. Indeed, the two top rod end bearing will be fixed to the connecting rod, piece 8.

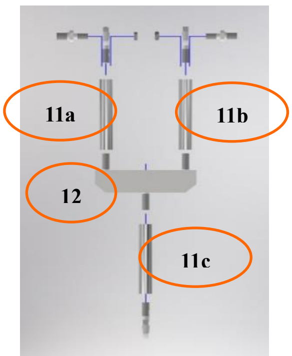

Figure 4.15: Subassembly four bars linkage

Finally, the last subassembly involves the section where the first motor is inserted. This subassembly includes a tensioner mounted into piece 17. The tensioner is assembled using pieces 13, 14, 15, and 16, which are secured together with screws and nuts. This arrangement ensures that the tensioner functions properly, maintaining the necessary tension for the motor's operation.

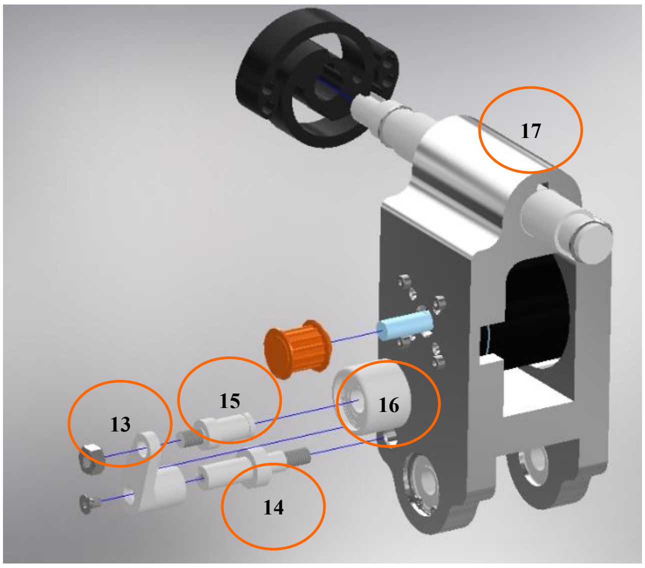

Figure 4.16: Subassembly first motor

Certain parts required modifications therefore, new pieces were designed and printted to fit all the pieces into the final structure. Furthermore, some components proved to be insufficiently durable in time, resulting in breakage, which required reprinting them using a stronger material. The final assembly is shown in Figure 4.17.

Figure 4.17: Final assembly.

Chapter 5

Tests

5.1. Conception of the test structure

Now that the ExoLeg was assembled, it was time to realize some tests. This phase was essential for the development of the ExoLeg. It is extremely useful to verify its performance, that's mean, verifying for example that the exoskeleton realises the desired trajectory. The ExoLeg must respect the medical standards and be safe for the patient. It must prevent every risk of injury to the user during operation. Moreover, the tests will allow us to measure the impact of the ExoLeg on the user's mobility.

Finally, the testing phase will be essential to confirm that the initial concepts and design choices are valid. This phase will also help us to identify potential weaknesses problems by providing us valuable data. Indeed, successive iterations based on test feedback make it possible to refine the device and adjust its functionalities for an optimal performance.

However, with a view to carrying out tests, the first step was to design a test structure made to hold the exoskeleton. Consequently, the test structure must be designed to evaluate all facets of the device, from its functionality and safety to its ergonomics and effectiveness. Has it been presented in the chapter 3 "Mechanical model design", the ExoLeg has a fixed part and can have movements only in the sagittal plane. Therefore, a structure was designed as shown in Figure 5.1.

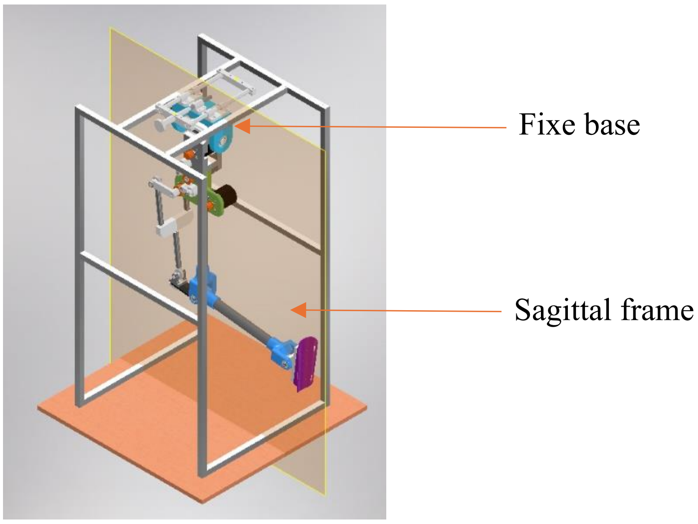

Figure 5.1 : Test Structure

This structure was designed with aluminium section of total length of one meter and one meter and half. In order to obtain the desired structure, it was necessary to saw the aluminium sections at the designed length (1.10 m) and width (0.5 m). Then to assemble the structure, we used the following mechanism (Figure 5.2), allowing me to create a bold system between each assembled section.

Figure 5.2 : Profile mounting bracket [48]

Moreover, in order to ensure stability, the structure was attached to a base using a rectangular piece of wood, which provided a surface for securely screwing the structure. Finally, the exoskeleton was fixed to the aluminium structure. New holes were drilled in the fixed top part of the ExoLeg, allowing metallic parts to be added and screwed into the aluminium structure.

Figure 5.3 : Final test structure

5.2. Tests results

During the test phase, it was first necessary to check if each mechanical system was functional independently.

- Pulley and toothed belt mechanism:

The first test consisted in programming the upper motor to allow the rotation of the first articulation of the ExoLeg. However, this rotation did not happen because the pulley/toothed belt mechanism wasn’t correctly designed. Three problems were identified:

- The pulley teeth were not large enough, so they could not grip correctly to the toothed belt and transmit the rotation to the driven pulley.
- The toothed belt length was a bit too important and was not perfectly corresponding to the separation distance between the two pulleys. That is why the pulley was skipping on the belt; it couldn't catch onto the belt's teeth, so the mechanical transmission was impossible.
- The fixation of the tensor was not optimal. Indeed, the tight compression of the tensioner by a nut was not strong enough. Consequently, the tensioner could not properly tighten the belt because it was loosening.

Each problem was addressed separately to resolve the issues effectively. Initially, attention was focused on the pulleys, specifically on the inadequacy of the teeth size. Since the decision was made early in the project to print the pulleys in PETG rather than purchasing them, access to the CAD files of the pulley components allowed for necessary modifications in Inventor. The modifications are illustrated in Figure 5.4.

The original teeth length for the 14 mm diameter pulley was 9.43 mm, which was reduced to 9.03 mm. This adjustment ensured that the pulley could properly engage with the toothed belt. Similarly, the teeth length of the 24 mm diameter pulley was adjusted from 14.21 mm to 13.21 mm to improve functionality. Additionally, a groove was added to the 14 mm diameter pulley, which enabled the installation of a shim between the motor shaft and the pulley to ensure smooth rotation.

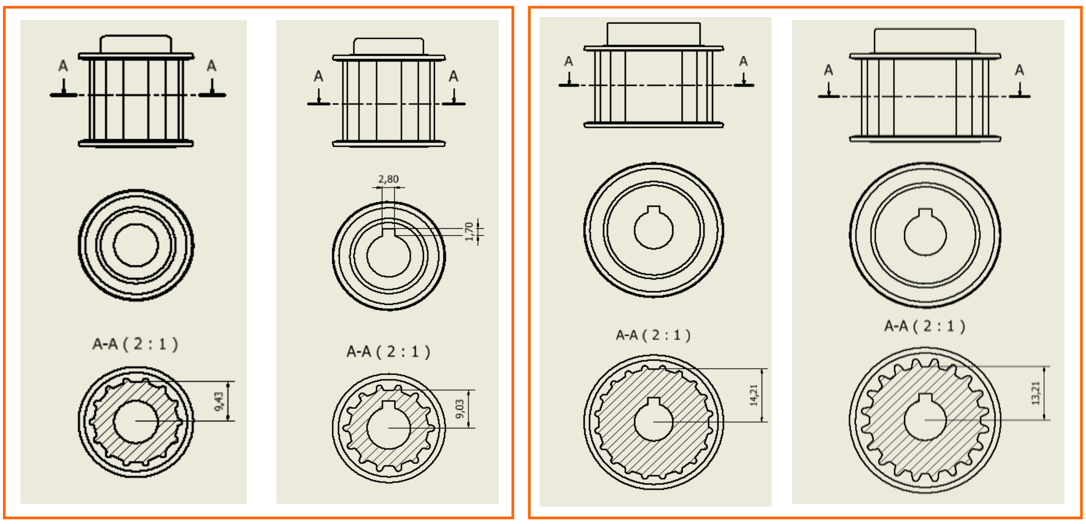

Figure 5.4 : Pulleys modifications

The length of the toothed belt was addressed by acquiring a new belt with the required total length. To achieve this, the exact distance between the two pulleys was determined, which in turn defined the characteristics of the toothed belt. Three toothed belts, each varying by approximately 5 mm in length, were ordered. This approach allowed for the evaluation of each belt, and the one that best matched the requirements was selected.

Finally, the issue with the pulleys/toothed belt mechanism related to the suboptimal fixation of the tensioner. The material originally used was not sufficiently strong to withstand significant compression forces. To address this, the PETG axis was replaced with a steel screw axis. This change allowed for the application of greater forces, ensuring a secure compression fit and proper fixation of the tensioner, thereby achieving optimal tension on the toothed belt (Figure 5.5).

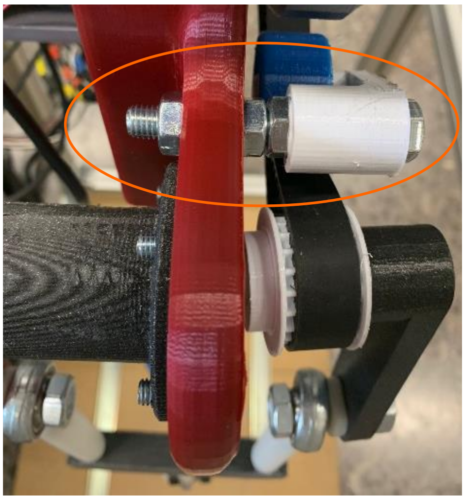

Figure 5.5 : Tensioner mechanism with a profile view (left) and front view (right)

- Four-bars linkage mechanism:

During the testing phase, another transmission mechanism was in trouble. That was the case of the four-bars linkage. Like it was detailed in the chapter 3 in the section of the mechanical design, the three nylon bars are fixed to the part called “pasador_rotula” thanks to a thread. However, a thread between two plastic parts is not optimal. That is why during the first trial, some of the bars detached themselves from the “pasador_rotula”. To resolve this problem some solutions can be imagined:

- Use a metallic mechanical component to secure the link between all the parts of the four-bars linkage.
- Use harder materials, like aluminium or steel in order to have a precise and solid thread which will allow a perfect maintain of contact.
- Use super glue to fix all these parts together and avoid a separation during trial.

The best solution for the future would be the second one, which is use harder materials like aluminium or steel. However, in the experimental condition, it was mandatory to find a quick and easy solution in order to continue the trials. Consequently, the best option was to use super glue to fix all the part together to be sure that no movement were possible.

- Global ExoLeg mechanism

Once all the previous mechanical problems were resolved, the overall functioning could be studied. The goal of the experiment is to verify if all the previous results found in the chapter 3, about the mechanical equations and the angles determination are correct. To achieve this, a test was conducted to ensure that the trajectory generated by the ExoLeg was as expected.

In this experiment, the theoretical trajectories calculated in Chapter 3 were compared with both the trajectories induced by the motor positions during testing and the actual trajectory traced by the ExoLeg's end effector.

First, the trajectories induced by the motor positions (blue curves) are compared in Figure 5.6 with the theoretical trajectories (green curves).

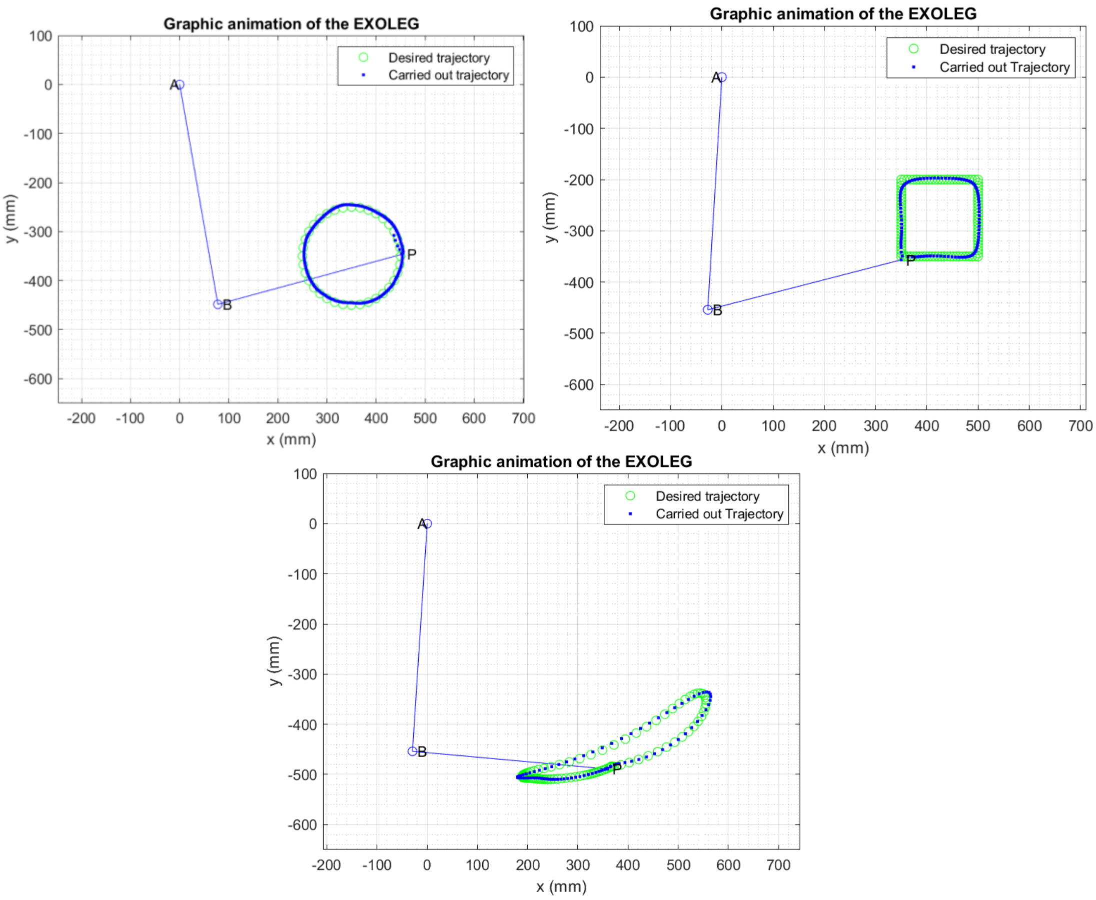

Figure 5.6: Comparation results

The results are very satisfying, as the executed trajectory closely follows the desired trajectory. However, some variations are observed along the curves, which can be attributed to motor vibrations. These slight deviations highlight the impact of real-world mechanical factors that were not fully accounted for in the theoretical model. Nonetheless, the close alignment between the observed and expected paths demonstrates the effectiveness of the system's design and control algorithms.

To observe the real trajectory produced at the end of the ExoLeg, a pen was mounted at its extremity. This setup allowed the ExoLeg to draw its trajectory on a piece of cardboard. By comparing the drawn trajectory with the theoretical trajectory, the accuracy of the mechanical model and control system could be assessed. Additionally, a video demonstrating this process is available via the following YouTube link *ExoLeg Gait Trajectory Demo*.

This practical validation was crucial for confirming that the theoretical calculations and simulations correctly represented the ExoLeg's real-world performance. However, the method used isn't highly precise because the pen wasn't securely fixed at the end of the robot, and the cardboard was held manually during the experiment. These factors could introduce inconsistencies in the results. This experiment serves more as an approximate indication of the trajectory rather than a definitive validation of the model. Further refinement in the setup and measurement techniques would be needed for more precise validation.

Chapter 6

Conclusion and future work

This Master Thesis encompassed the development of a lower limb exoskeleton intended to support rehabilitation therapies in patients suffering from various conditions, such as spinal cord injuries, strokes, neurological disorders, or motor impairments.

The first objective was to study the mechanical design of the robot and to develop an analysis to explain its functioning. This included the selection of appropriate materials in order to ensure both the solidity and lightness of the structure.

The second objective was to do a virtual representation of the ExoLeg using the software MATLAB and Simulink. This virtual model allowed to link different system components and the inclusion of the mathematical relationships necessary for optimal functioning of the device. This approach allowed the performance of the device to be evaluated and determine the relationship between the desired trajectory and motor equations.

As a result of this second objective, the forces exerted on each component were determined and analysed through a dynamic simulation. These simulation results enabled the evaluation of the device's stability, efficiency, and safety. Additionally, some design modifications were implemented, allowing the optimization of the robot.

Following these simulations and the assembly of the ExoLeg, extensive testing was conducted to validate its design and its functionality. The experiments, which involved comparing the theoretical and actual trajectories, confirmed that the ExoLeg closely follows the intended paths, with minor discrepancies due to mechanical limitations and motor vibrations. These findings not only validated the mechanical model and control algorithms but also provided insights into areas for further refinement.

In conclusion, the ExoLeg project successfully met its primary objectives: developing a robust mechanical structure, creating a comprehensive virtual model for dynamic analysis, and validating the design through practical testing. However, future research could explore the use of alternative materials to further enhance the device. Additionally, more precise testing could be conducted to verify the actual trajectory of the ExoLeg.

In future work, it could be beneficial to film the motion of the ExoLeg's extremity and use software like Kinovea to analyse the data. Kinovea allows for the import of video footage and the manual or automatic tracking of specific points, providing detailed information on the trajectory of those points.

This software is particularly useful for:

- Visualizing and analysing the motion of the ExoLeg's extremity,
- Comparing the actual trajectory with theoretical or expected paths,
- Measuring displacements, angles, and velocities.

Moreover, real-world testing with patients would be invaluable for assessing the ExoLeg's practical application in rehabilitation therapies. This project lays a strong foundation for the continued development and optimization of wearable exoskeleton technology, with the potential to significantly improve the quality of life for individuals with mobility impairments.

References

1. Laut, J., Porfiri, M., & Raghavan, P. (2016). The Present and Future of Robotic Technology in Rehabilitation. Current Physical Medicine and Rehabilitation Reports, 4(4), 312–319. https://doi.org/10.1007/s40141-016-0139-0

2. Cano-De-La-Cuerda, R., Blázquez-Fernández, A., Marcos-Antón, S., Sánchez-Herrera-Baeza, P., Fernández-González, P., Collado-Vázquez, S., Jiménez-Antona, C., & Laguarta-Val, S. (2024). Economic Cost of Rehabilitation with Robotic and Virtual Reality Systems in People with Neurological Disorders: A Systematic Review. Journal of Clinical Medicine, 13(6), 1531. https://doi.org/10.3390/jcm13061531

3. Types of paralysis- causes, symptoms, and treatment in Ayurveda. (n.d.). Lifehack. https://vocal.media/lifehack/types-of-paralysis-causes-symptoms-and-treatment-in-ayurveda

4. Pandey, S., Chouksey, A., Pitakpatapee, Y., & Srivanitchapoom, P. (2021). Movement disorders and musculoskeletal system: a reciprocal relationship. Movement Disorders Clinical Practice, 9(2), 156–169. https://doi.org/10.1002/mdc3.13390

5. Spinal cord injury: Anjum, A., Yazid, M. D., Daud, M. F., Idris, J., Ng, A. M. H., Naicker, A. S., Ismail, O. H. R., Kumar, R. K. A., & Lokanathan, Y. (2020). Spinal cord injury: pathophysiology, multimolecular interactions, and underlying recovery mechanisms. International Journal of Molecular Sciences, 21(20), 7533. https://doi.org/10.3390/ijms21207533

6. Vasudevan, E. V. L., Glass, R. N., & Packel, A. T. (2014). Effects of traumatic brain injury on locomotor adaptation. *Journal of Neurologic Physical Therapy*, *38*(3), 172–182. https://doi.org/10.1097/npt.0000000000000049

7. Barthels, D., & Das, H. (2020). Current advances in ischemic stroke research and therapies. Biochimica Et Biophysica Acta. Molecular Basis of Disease, 1866(4), 165260. https://doi.org/10.1016/j.bbadis.2018.09.012

8. Kesar, T. (2023). The Effects of Stroke and Stroke Gait Rehabilitation on Behavioral and Neurophysiological Outcomes: *Delaware Journal of Public Health*, *9*(3), 76–81. https://doi.org/10.32481/djph.2023.08.013

9. Cotsapas, C., Mitrovic, M., & Hafler, D. (2018). Multiple sclerosis. In *Handbook of clinical neurology* (pp. 723–730). https://doi.org/10.1016/b978-0-444-64076-5.00046-6

10. Reich, D. S., Lucchinetti, C. F., & Calabresi, P. A. (2018). Multiple sclerosis. *New England Journal of Medicine/ the New England Journal of Medicine*, *378*(2), 169–180. https://doi.org/10.1056/nejmra1401483

11. Europe PMC. (n.d.). Europe PMC. https://europepmc.org/article/MED/29320652

12. Tolosa, E., Garrido, A., Scholz, S. W., & Poewe, W. (2021). Challenges in the diagnosis of Parkinson's disease. Lancet Neurology, 20(5), 385–397. https://doi.org/10.1016/s1474-4422(21)00030-2

13. Freitas, M., Hess, C., & Fox, S. (2017). Motor complications of dopaminergic medications in Parkinson's disease. Seminars in Neurology, 37(02), 147–157. https://doi.org/10.1055/s-0037-1602423

14. Cerebral Palsy: Organisation mondiale de la sante, World Health Organization, and World Health Organization Sta . International classi cation of functioning, disability and health: ICF. World Health Organization, 2001.

15. Confederacion ASPACE. Descubriendo la paralisis cerebral. Confederacion Aspace, pages 169, 2014. (tetraplegia y types of paralysis)

16. Cerebral Palsy: Else Odding, Marij E. Roebroeck, and Hendrik J. Stam. The epidemiology of cerebral palsy: Incidence, impairments and risk factors. Disability and Rehabilitation, 28(4):183191, 2006. PMID: 16467053.

17. Vulpen, L. V. (2018). Functional power-training in young children with cerebral palsy. https://api.semanticscholar.org/CorpusID:81717801

18. Warutkar, V., Dadgal, R., & Mangulkar, U. R. (2022). Use of robotics in GAIT Rehabilitation following stroke: A review. *Curēus*. https://doi.org/10.7759/cureus.31075

19. Robot in rehab: Gait training after stroke with robot-assisted rehabilitation. (2023, February 27). Tyromotion. https://tyromotion.com/en/blog/robot-assisted-gait-training-improves-stroke-rehabilitation/

20. Robot in rehab: RedDot. (2023, January 11). *Robotic Assisted GAIT training*. Propel Physiotherapy. https://propelphysiotherapy.com/modalities/robotic-assisted-gait-training/

21. Ineuro. (2023, May 18). *Lokomat: órtesis de marcha robotizada*. Ineuro. https://ineuro.es/lokomat-ortesis-de-marcha-robotizada/

22. Veneman, J. F., Kruidhof, R., Hekman, E. E. G., Ekkelenkamp, R., Van Asseldonk, E. H. F., & Van Der Kooij, H. (2007). Design and Evaluation of the LOPES Exoskeleton Robot for Interactive Gait Rehabilitation. *IEEE Transactions on Neural Systems and Rehabilitation Engineering*, *15*(3), 379–386. https://doi.org/10.1109/tnsre.2007.903919

23. Ekkelenkamp, R., Veneman, J., & Kooij, H. (2007). *LOPES: a lower extremity powered exoskeleton*. https://www.semanticscholar.org/paper/LOPES%3A-a-lower-extremity-powered-exoskeleton-Ekkelenkamp-Veneman/b4c33e187fce9b6d186a47ea7abba438f16246d1

24. Riedo, J., & Hunt, K. J. (2016). Feedback control of heart rate during robotics-assisted end-effector-based stair climbing. *Systems Science & Control Engineering*, *4*(1), 223–234. https://doi.org/10.1080/21642583.2016.1228487

25. G-EO System - AAL Products. (n.d.). https://www.aal-products.com/index.php/frontend/product/Health-and-Care-1/G-EO-System-315?language_short=en

26. Exoskeleton Report. (2023, December 8). G-EO System - Exoskeleton Report. https://exoskeletonreport.com/product/g-eo-system/

27. *GAIT Trainer GT I - neurorehabdirectory.com*. (2019, December 10). Neurorehabdirectory.com. https://www.neurorehabdirectory.com/rehab-products/gait-trainer-gt-i/

28. Schmidt, H., Hesse, S., Bernhardt, R., & Krüger, J. (2005). HapticWalker---a novel haptic foot device. ACM Transactions on Applied Perception, 2(2), 166–180. https://doi.org/10.1145/1060581.1060589

29. Velsid. (2007, June 8). Haptic Walker, máquina para sostener y ayudar en la rehabilitación de las personas que han sufrido un ACV. Vitónica. https://www.vitonica.com/lesiones/haptic-walker-maquina-para-sostener-y-ayudar-en-la-rehabilitacion-de-las-personas-que-han-sufrido-una-apoplejia

30. Andador LYRA de Thera-Trainer. (n.d.). Orthexo.de - Guía De Neuroortopedia Y Exoesqueletos. https://orthexo.de/es/lyra-thera-trainer/

31. Molero, Luis. (2020). Sistema de reconocimiento de voz para personas en condición de discapacidad motriz. 10.47212/GamificaciónII2020.5

32. Ekso GT: EKSO GTTM robotic exoskeleton cleared by FDA for use with stroke and spinal cord injury patients. (n.d.). Ekso Bionics Holdings, Inc. https://ir.eksobionics.com/press-releases/detail/570/ekso-gt-robotic-exoskeletoncleared-by-fda-for-use-with

33. Lifeward Personal 6.0 exoskeleton for spinal cord injury. (2024, January 25). Lifeward. https://golifeward.com/products/rewalkpersonal-exoskeleton/

34. Wilmart, R., Garone, E., & Innocenti, B. (2019). The use of robotics devices in knee rehabilitation: a critical review. M.L.T.J. Muscles, Ligaments And Tendons Journal, 09(01), 21. https://doi.org/10.32098/mltj.01.2019.07

35. Zhao, G., Sharbafi, M. A., Vlutters, M., Van Asseldonk, E., & Seyfarth, A. (2019). Bio-Inspired balance control assistance can reduce metabolic energy consumption

in human walking. IEEE Transactions on Neural Systems and Rehabilitation Engineering, 27(9), 1760–1769. https://doi.org/10.1109/tnsre.2019.2929544

36. Enclosure motor: *NEMA Enclosures for D5065 and D6374 motors*. (2018, July 3). ODrive Community. https://discourse.odriverobotics.com/t/nema-enclosures-for-d5065-and-d6374-motors/830

37. Original Prusa i3 MK3S+ | Impresoras 3D Original Prusa vendidas directamente por Josef Prusa. (n.d.). Prusa3D by Josef Prusa. https://www.prusa3d.com/es/categoria/original-prusa-i3-mk3s/

38. Flathub. (2024, April 8). Instalar PrusaSlicer en Linux | Flathub. Flathub - Aplicaciones Para Linux. https://flathub.org/es/apps/com.prusa3d.PrusaSlicer

39. Amazon.es. (n.d.). https://www.amazon.es/Kugellager-6305-2RSC3-SKF-7424385/dp/B00652M3PW

40. Rotulas. (n.d.). https://www.rodamientosymas.com/es/6-rotulas

41. ODrive Europe. (n.d.). ODrive Europe. https://eu.odriverobotics.com/

42. IMB Electric Market. (n.d.). ENC-AMT11S Archives. https://imbelectric.com/tags/enc-amt11s/

43. Polea síncrona Aluminio 18 dientes , 5mm espaciado , 6mm calibre , para adaptar la anchura de la correa 16mm. (n.d.). RS Components Export. https://export.rsdelivers.com/es/product/rs-pro/polea-sincrona-aluminio-18-dientes-5mm-espaciado/0745680

44. Amazon.co.uk. (n.d.). https://www.amazon.co.uk/NEZIH-Synchronous-Timing-Length-Rubber/dp/B0C738T5KH

45. Tornillo m10x16 din-933 inox hexagonal jemi. (n.d.). Horeca Recambios Y Suministros S.L. https://efinox.com/tornillo-m10x16-din-933-inox-hexagonal-jemi

46. ALGI ECROU 6 Pans NYLSTOP-FREIN M4 (BOITE DE 100) (812000) : Amazon.es: Coche y moto. (n.d.). https://www.amazon.es/Tuerca-caras-NYLSTOP-FRENIN-caja-812000/dp/B07RDCC7YQ

47. Circlip de Seguridad Zapata de Embrague d.9mm Peugeot 103 | MAXISCOOT. (n.d.). https://www.maxiscoot.com/es/producto/circlip-de-seguridad-zapata-de-embrague-d.9mm-peugeot-103-81087

48. Ángulo 30 tipo I ranura 6 incluido kit de montaje, 2,65 €. (n.d.). Ángulo 30 Tipo I Ranura 6 Incluido Kit De Montaje, 2,65 €. https://www.dold-mechatronik.de/Angulo-30-tipo-I-ranura-6-incluido-kit-de-montaje

49. [17] Organisation mondiale de la sante, World Health Organization, and World Health Organization Sta . International classi cation of functioning, disability and health: ICF. World Health Organization, 2001.
50. [63] Marie Kruse, Susan Ishy Michelsen, Esben Meulengracht Flachs, HENRIK BR NNUM-HANSEN, Mette Madsen, and Peter Uldall. Lifetime costs of cerebral palsy. Developmental Medicine & Child Neurology, 51(8):622628, 2009. 66 5.

Appendix A

Ethical, economics, social and environmental aspects

A.1. Ethical aspects

The project of the ExoLeg is included into the framework of “Assistive Robotics”. It is a group of medical robots that assist people with physical disabilities through physical interactions. These devices enable repetitive task training, which can improve walking ability and distance. Moreover, patients using robot-assisted gait therapy practice two to three times longer than those with manual assistance for ground-based walking. By increasing the time spent on therapeutic exercises, patients may see improvements more quickly. Finally, the ExoLeg devices incorporate gamification elements to encourage patients to fully engage during each exercise session. By combining achievable goals and levels to overcome, rehabilitation becomes fun.

However, we can ask ourselves about the potential problems that we can face with a rehabilitation robot. This considers until what point the exoskeleton can replace the therapists. Maybe some patient will prefer being manipulated by a human which whom he can discuss whereas an impersonal machine. Moreover, if the robot has a defect or a bug, who will be responsible for the robot actions? Finally, how the data of the therapy are stored? In the case of medical robot, only engineers and healthcare professional can have access to them to analyse them.

A.2. Social impact

That is why we can say that this project has a positive powerful social impact. Indeed, it improve quality of life of patients by allowing them to regain a certain mobility and functionality of the lower limb which will contribute to a positive effect on their emotional, social and general well-being. Moreover, it can participate to the inclusion and participation of the patient into daily tasks. Like I said, the robot will allow a faster rehabilitation by improving their functional capacity and autonomy, which will contribute to their social integration.

A.3. Economical aspects

Cerebral palsy is the most common cause of physical disability in children, with an overall prevalence of approximately 2 per 1,000 live births [49]. For instance, the lifetime costs associated with cerebral palsy in the United States in the 2000s were approximately $11.5 billion, or $800,000 per patient [50]. This estimate highlights the need for effective primary and secondary prevention measures to prevent and reduce the impact of the disease.

A.4. Environmental aspects

The ExoLeg project has several environmental considerations. Choosing sustainable and recyclable materials, such as biodegradable plastics or recycled metals, can reduce its ecological footprint. Energy consumption is also crucial; optimizing the device's power efficiency, for example, by using low-energy motors, can minimize long-term environmental impact. Additionally, considering the entire product lifecycle, from manufacturing to end-of-life recycling, helps ensure an eco-friendlier approach. By addressing these factors, the ExoLeg can contribute to a more sustainable design in assistive robotics.

Appendix B

Economical budget

This project has been developed for four months at the Polytechnic University of Madrid, in collaboration with the "Consejo Superior de Investigaciones Cientificas" (CSIC), using some of their resources. An approximate budget is estimated considering human resources, software and technical equipment used during the Master Thesis.

- **Human Resources**: This table considers the salary of the engineering student, author of this Master Thesis, as well as the salary of the tutors. According to the Economic Research Institute (ERI), the salary of a junior biomedical engineer is 29000€ per year. However, since in this case the engineer is a student, he or she is not paid. Considering that the IRPF (Personal Income Tax) is approximately 30% and that the hours worked in year are 1800, the cost of people who participate in this project are calculated Table 10. Moreover, it has been considered that the tutors have contributed 20 hours of work at a salary of 60€ per hour.

	Cost per hour (€)	**Hours**	**Total (€)**
Engineer tutor 1	60	20	1 200
Engineer tutor 2	60	20	1 200
Engineer student	0	450	0
TOTAL			**2 400**

Table B.1 : Human resources costs

- **Materials**: In this section, we consider the cost of both mechanical components and forearm support platform used during the development of this Master Thesis. As me con observe, the most significant costs are attribute to both licence of MATLAB and Autodesk Inventor. The expenses are calculated taking account amortization in €/month, calculated as the cost of the product divided by the months of useful life as indicated by the Spanish Tax Agency.

	Lifetime (years)	Uds.	Cost (€)	Amortization (€/months)	Use (months)	Total (€)
Prusa Printer i3 MK3S	5	2	999	33.30	5	166.50
PLA Polymer	1	3	20	5	5	25
PETG Polymer	1	1	20	1.67	5	8.33
Nylon Polymer	1	1	50	4.17	5	20.83
Screws	-	150	0.10	-	-	1
Toothed belts	3	7	7.15	1.39	5	6.95
Rod End Bearing	-	3	6.67	-	-	1
Bearing	10	10	4	0.33	5	1.67
MATLAB	1	1	2 000	166.67	5	833.35
Inventor	1	1	2 862	238.50	5	1 192.50
Computer	5	1	1 200	20.00	5	100
Aluminium profile	10	8	12	0.80	5	4
TOTAL						**2 361.13**

Table B.2 : Costs derived from software and technical equipment.

Finally, the Table 12 indicates the total cost explained above. Moreover, it calculates the total cost of the project, considering a 21% VAT (Value Added Tax).

	Costs
Human Resources	2 400 €
Material Resources	2 361.13 €
Subtotal	4 761.13 €
VAT	952.23 €
TOTAL	**5 713.36 €**

Table B.3 : Total costs

Appendix C

Drawing of the 3D pieces

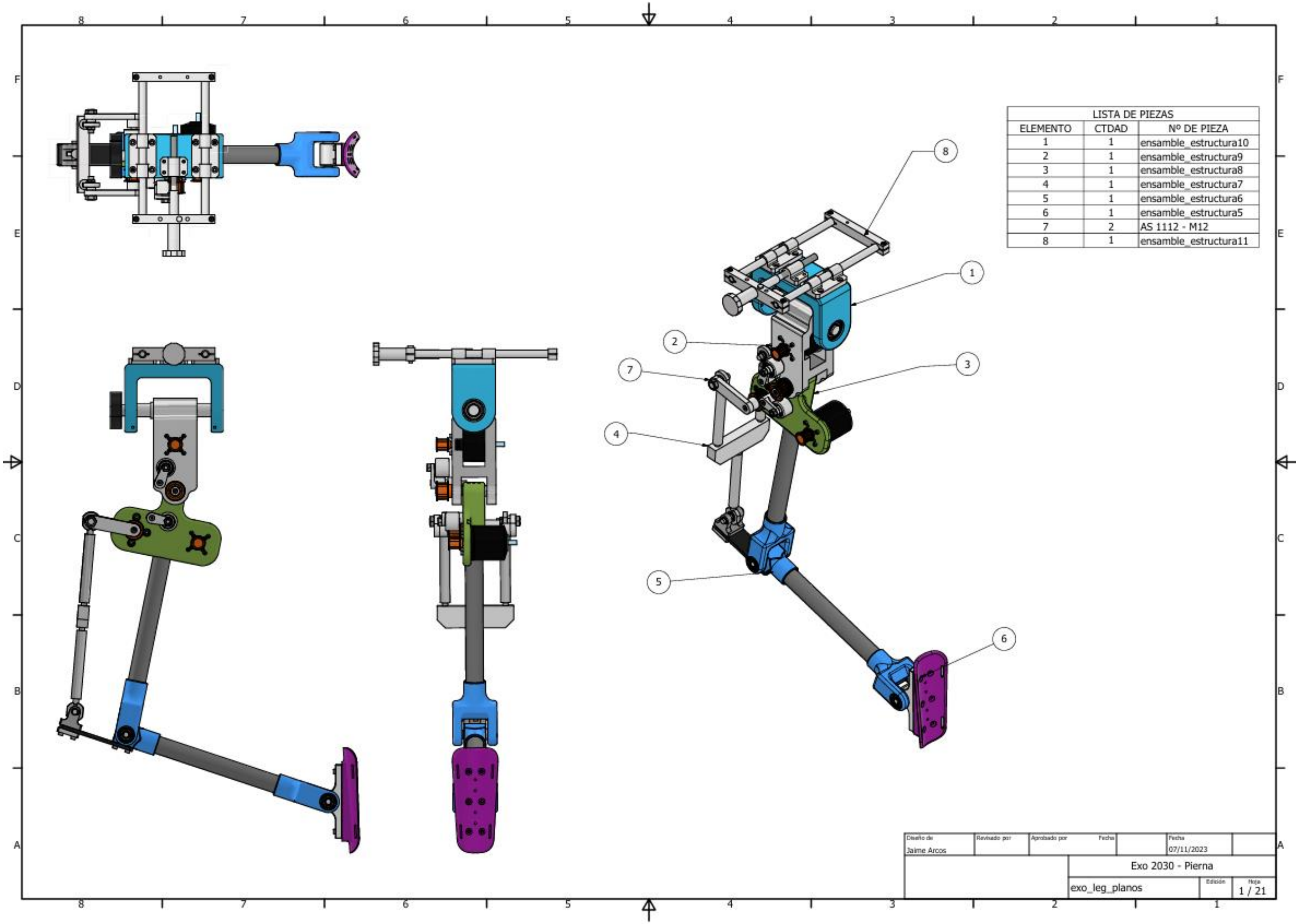

LISTA DE PIEZAS		
ELEMENTO	CTDAD	Nº DE PIEZA
1	1	ensamble_estructura10
2	1	ensamble_estructura9
3	1	ensamble_estructura8
4	1	ensamble_estructura7
5	1	ensamble_estructura6
6	1	ensamble_estructura5
7	2	AS 1112 - M12
8	1	ensamble_estructura11

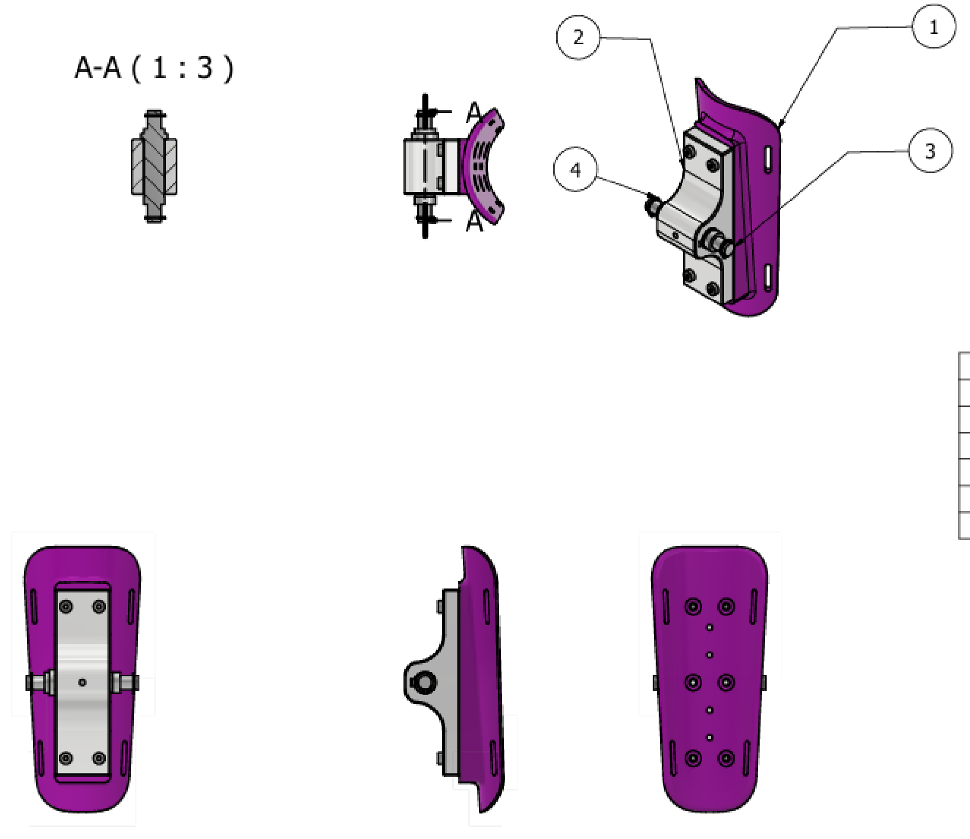

LISTA DE PIEZAS		
ELEMENTO	CTDAD	Nº DE PIEZA
1	1	pantorrilla
2	1	pivote-pantorrilla
3	1	pivote-pantorrilla-eje
4	2	DIN 471 - 10x1
5	4	DIN 7984 - M5 x 8

Diseño de	Revisado por	Aprobado por	Fecha	Fecha
Jaime Arcos				07/11/2023

Exo 2030 - Pierna

exo_leg_planos | Edición | Hoja 2 / 21

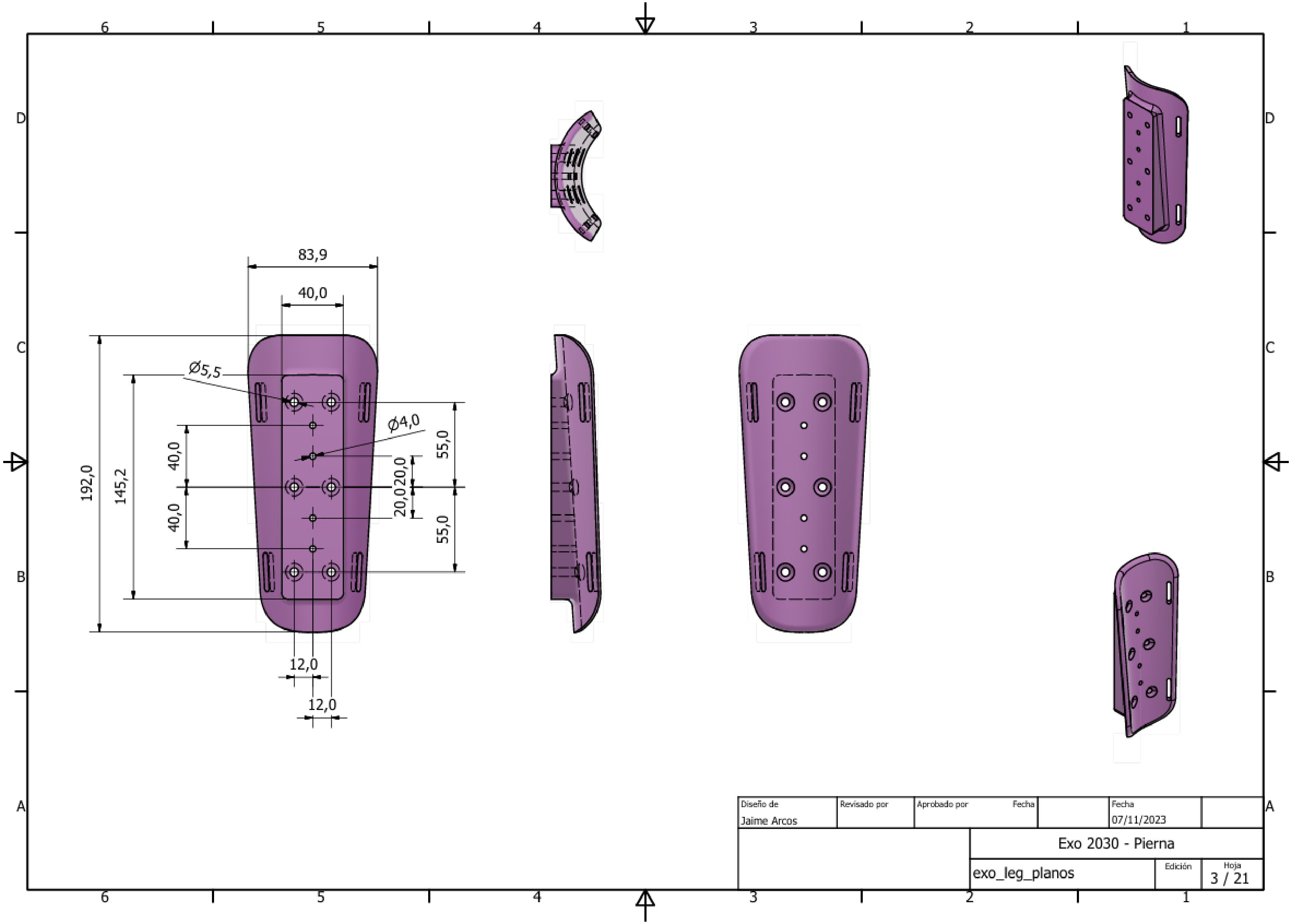
83,9
40,0
Ø5,5
Ø4,0
192,0
145,2
40,0
40,0
55,0
55,0
20,0
20,0
12,0
12,0
Diseño de
Jaime Arcos
Revisado por
Aprobado por
Fecha
Fecha
07/11/2023
Exo 2030 - Pierna
exo_leg_planos
Edición
Hoja
3 / 21

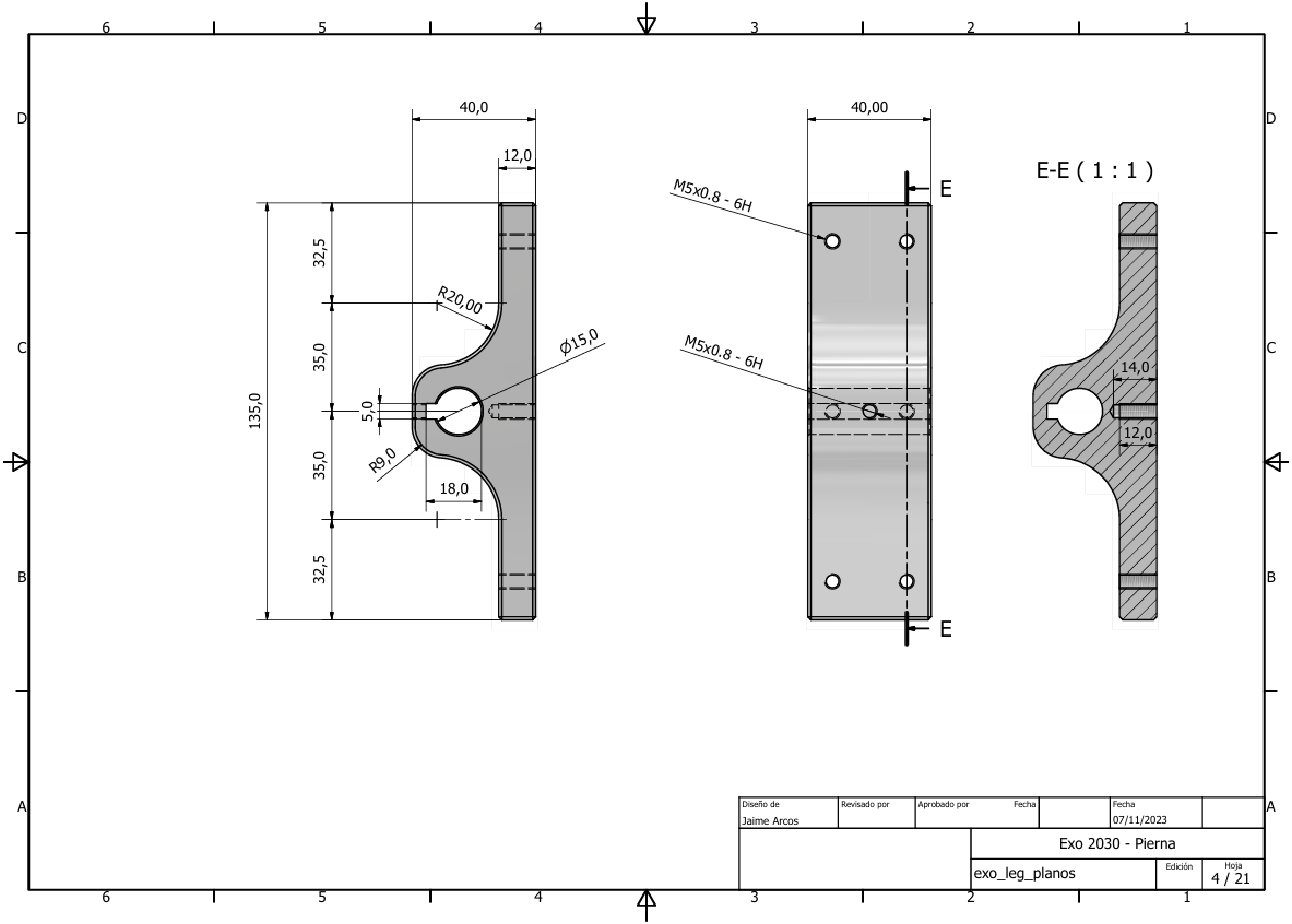
40,0
12,0
32,5
R20,00
35,0
Ø15,0
5,0
135,0
R9,0
35,0
18,0
32,5
40,00
M5x0.8 - 6H
M5x0.8 - 6H
E
E
E-E (1 : 1)
14,0
12,0
Diseño de
Jaime Arcos
Revisado por
Aprobado por
Fecha
Fecha
07/11/2023
Exo 2030 - Pierna
exo_leg_planos
Edición
Hoja
4 / 21

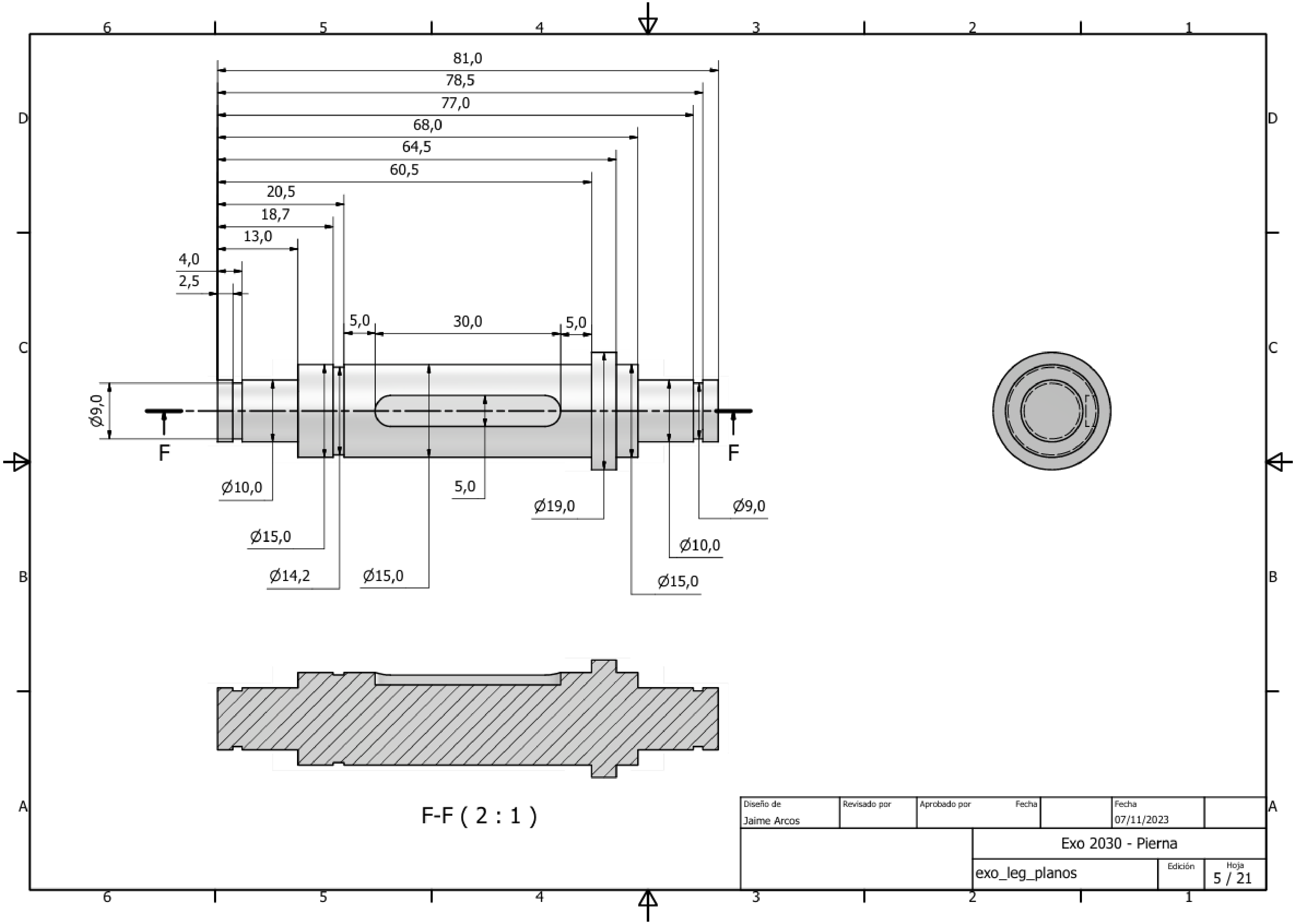
81,0
78,5
77,0
68,0
64,5
60,5
20,5
18,7
13,0
4,0
2,5
5,0
30,0
5,0
Ø9,0
F
F
Ø10,0
5,0
Ø19,0
Ø9,0
Ø15,0
Ø10,0
Ø14,2
Ø15,0
Ø15,0
F-F (2 : 1)
Diseño de
Jaime Arcos
Revisado por
Aprobado por
Fecha
Fecha
07/11/2023
Exo 2030 - Pierna
exo_leg_planos
Edición
Hoja
5 / 21

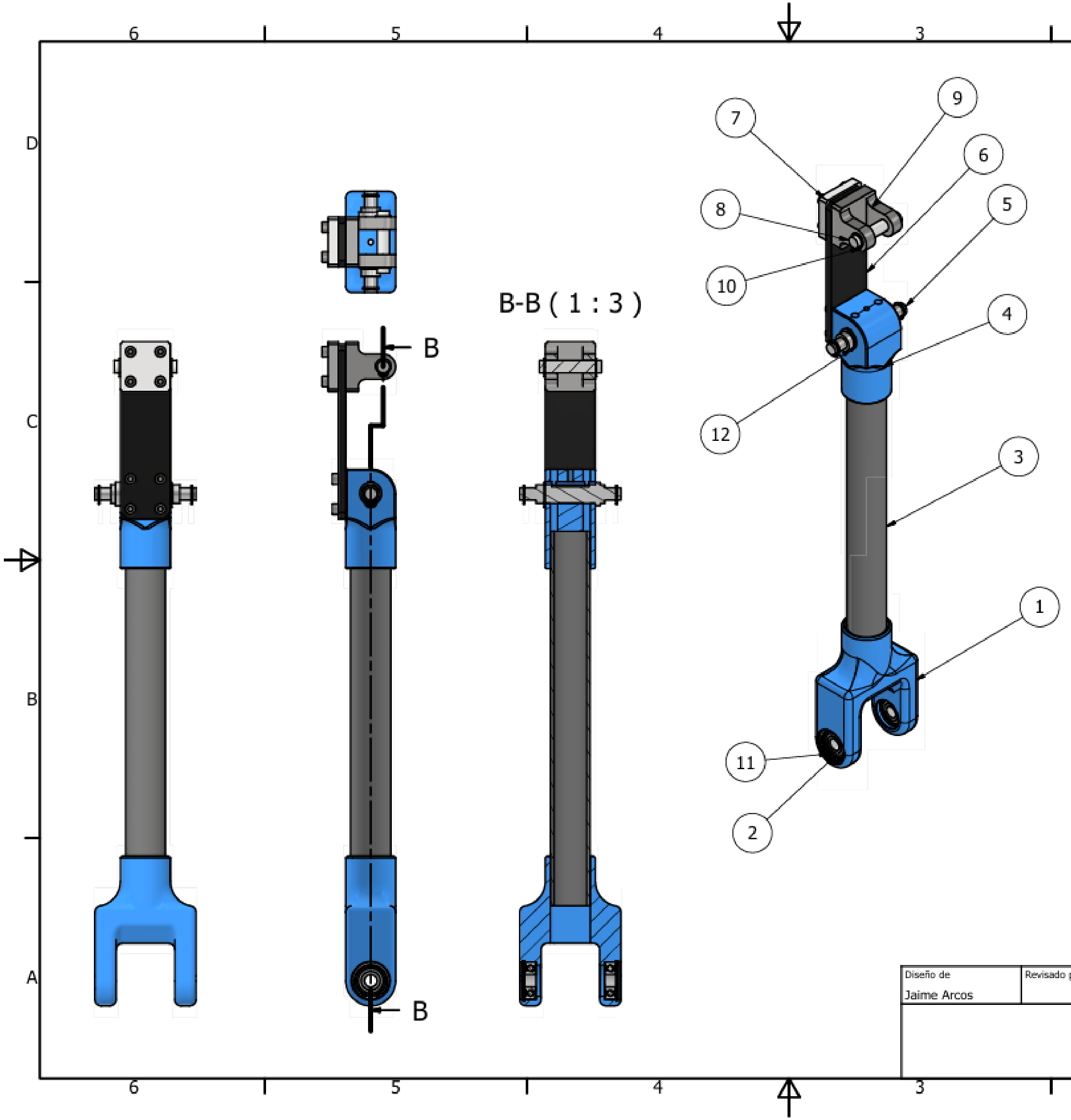

LISTA DE PIEZAS		
ELEMENTO	CTDAD	Nº DE PIEZA
1	1	acople-pivote-pantorrilla-eje
2	2	SKF_6200-2RSH
3	1	tubo_pierna
4	1	acople-pivote-rodilla-eje
5	1	pivote-pantorrilla-eje
6	1	fleje
7	1	platina
8	1	pasador_rotula
9	1	base_rotula_1
10	4	DIN 471 - 10x1
11	2	DIN 472 - 30 x 1.2
12	1	DIN 471 - 15x1
13	8	AS 1420 - 1973 - M5 x 10

Diseño de: Jaime Arcos | Revisado por | Aprobado por | Fecha | Fecha: 07/11/2023

Exo 2030 - Pierna

exo_leg_planos | Edición | Hoja 6 / 21

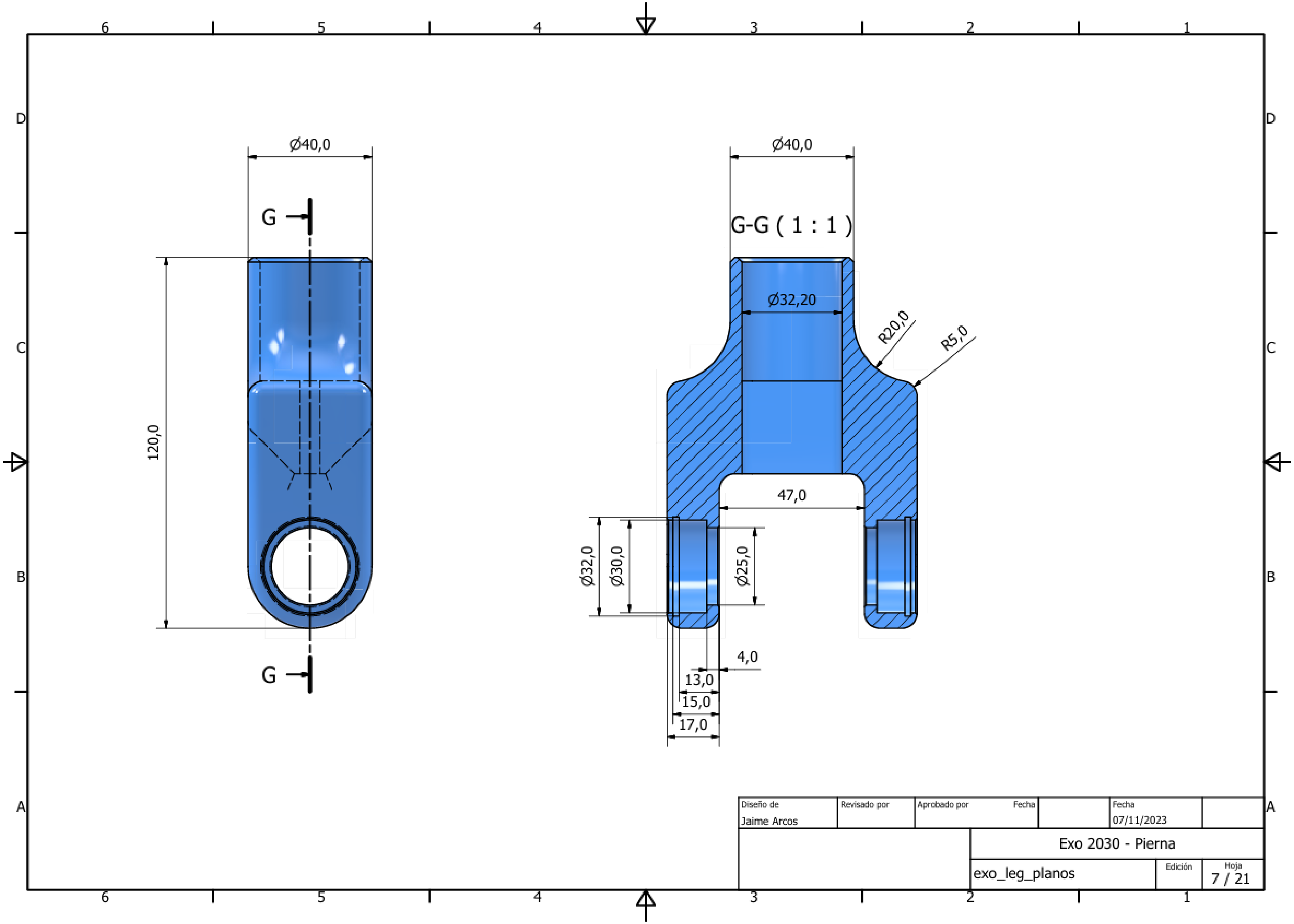

Ø40,0
G
120,0
Ø40,0
G-G (1 : 1)
Ø32,20
R20,0
R5,0
47,0
Ø32,0
Ø30,0
Ø25,0
4,0
13,0
15,0
17,0
Diseño de
Jaime Arcos
Revisado por
Aprobado por
Fecha
Fecha
07/11/2023
Exo 2030 - Pierna
exo_leg_planos
Edición
Hoja
7 / 21

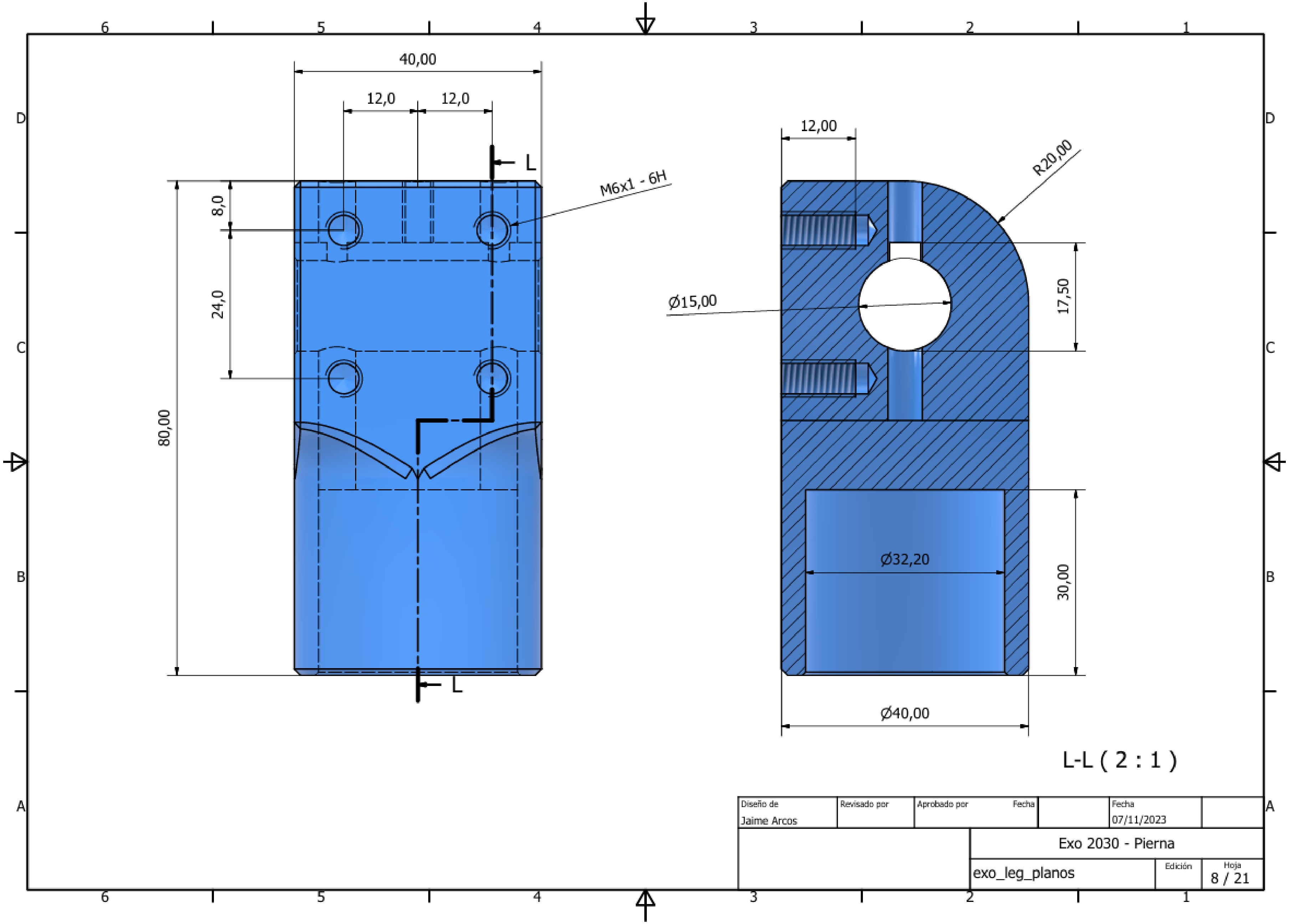
40,00
12,0
12,0
L
M6x1 - 6H
8,0
24,0
80,00
L
12,00
R20,00
Ø15,00
17,50
Ø32,20
30,00
Ø40,00
L-L (2 : 1)
Diseño de
Jaime Arcos
Revisado por
Aprobado por
Fecha
Fecha
07/11/2023
Exo 2030 - Pierna
exo_leg_planos
Edición
Hoja
8 / 21

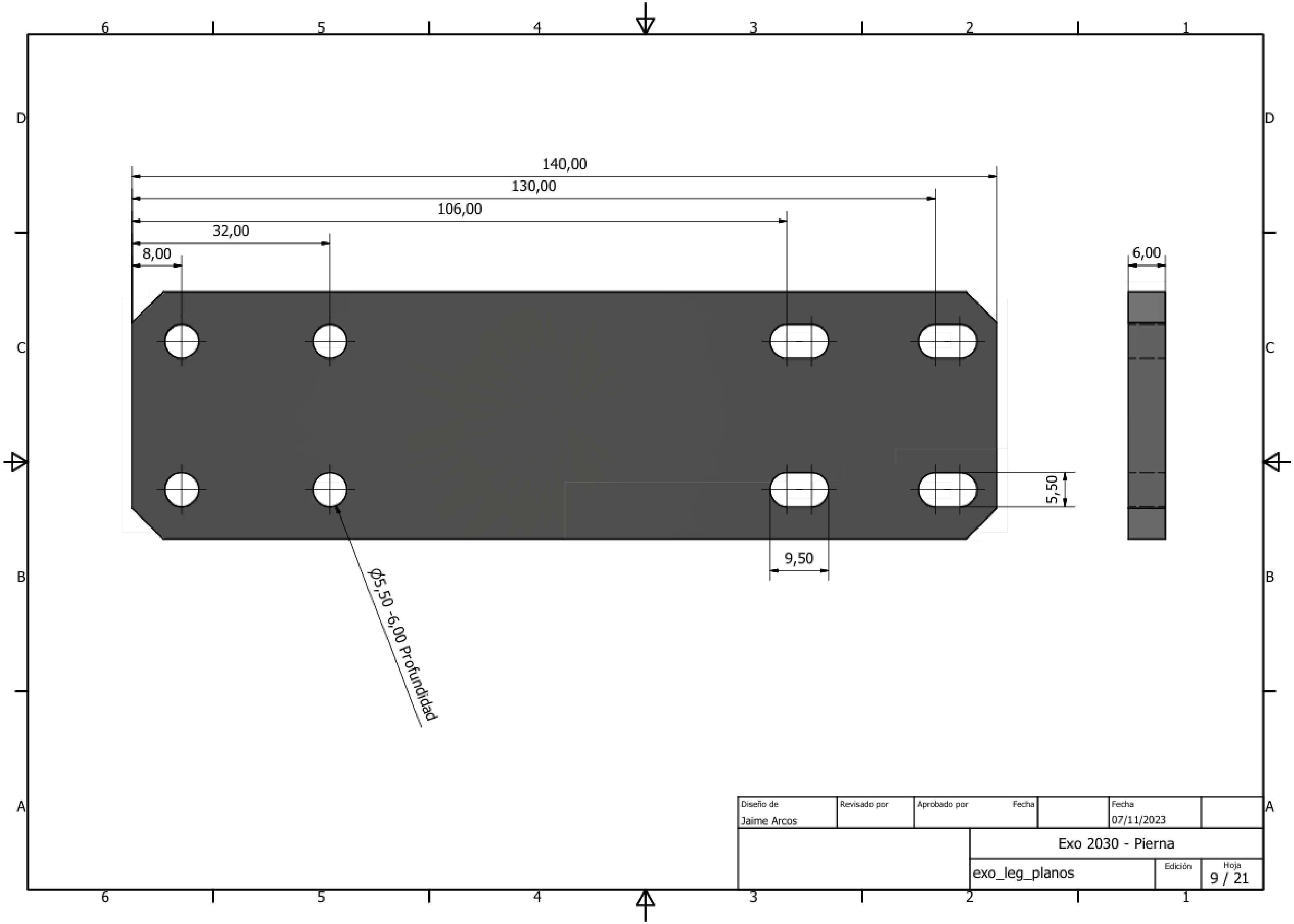
140,00
130,00
106,00
32,00
8,00
6,00
5,50
9,50
ϕ5,50 -6,00 Profundidad
Diseño de
Jaime Arcos
Revisado por
Aprobado por
Fecha
Fecha
07/11/2023
Exo 2030 - Pierna
exo_leg_planos
Edición
Hoja
9 / 21

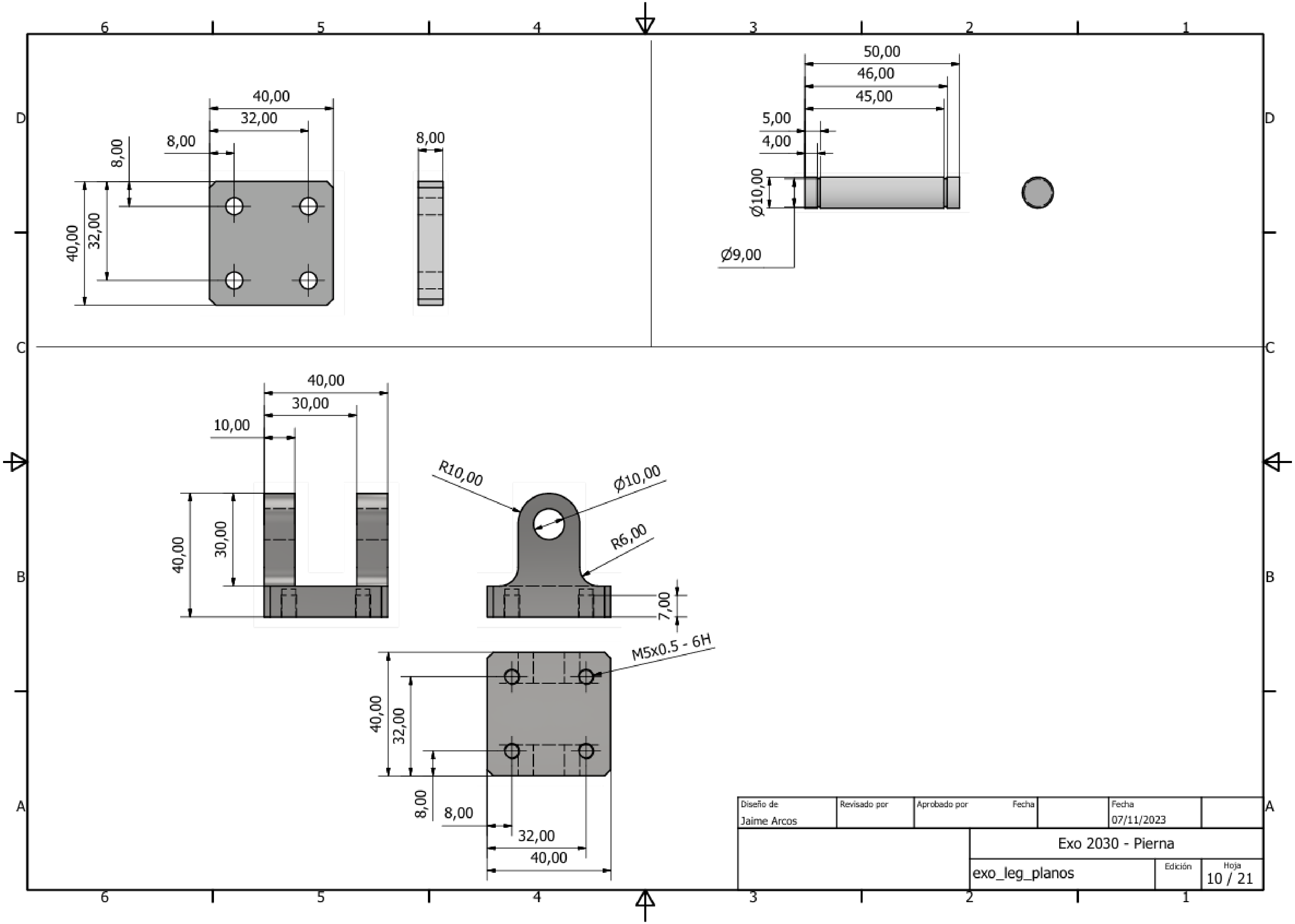
40,00
32,00
8,00
8,00
40,00
32,00
8,00
50,00
46,00
45,00
5,00
4,00
Ø10,00
Ø9,00
40,00
30,00
10,00
40,00
30,00
R10,00
Ø10,00
R6,00
7,00
M5x0.5 - 6H
40,00
32,00
8,00
8,00
32,00
40,00
Diseño de
Jaime Arcos
Revisado por
Aprobado por
Fecha
Fecha
07/11/2023
Exo 2030 - Pierna
exo_leg_planos
Edición
Hoja
10 / 21

LISTA DE PIEZAS		
ELEMENTO	CTDAD	Nº DE PIEZA
1	1	pasador_rotula_2
2	3	barra_rotulas
3	3	SKF_SA 10 C
4	2	Perno
5	2	AS 1112 - M8

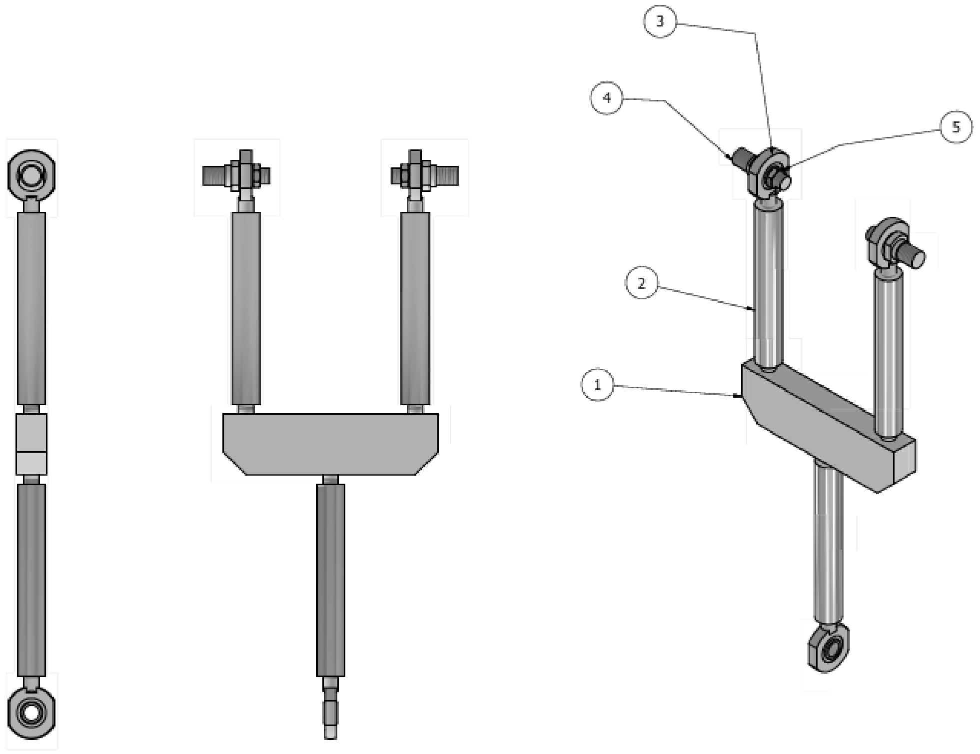

Diseño de	Revisado por	Aprobado por	Fecha	Fecha
Jaime Arcos				07/11/2023
	Exo 2030 - Pierna			
	exo_leg_planos		Edición	Hoja 11 / 21

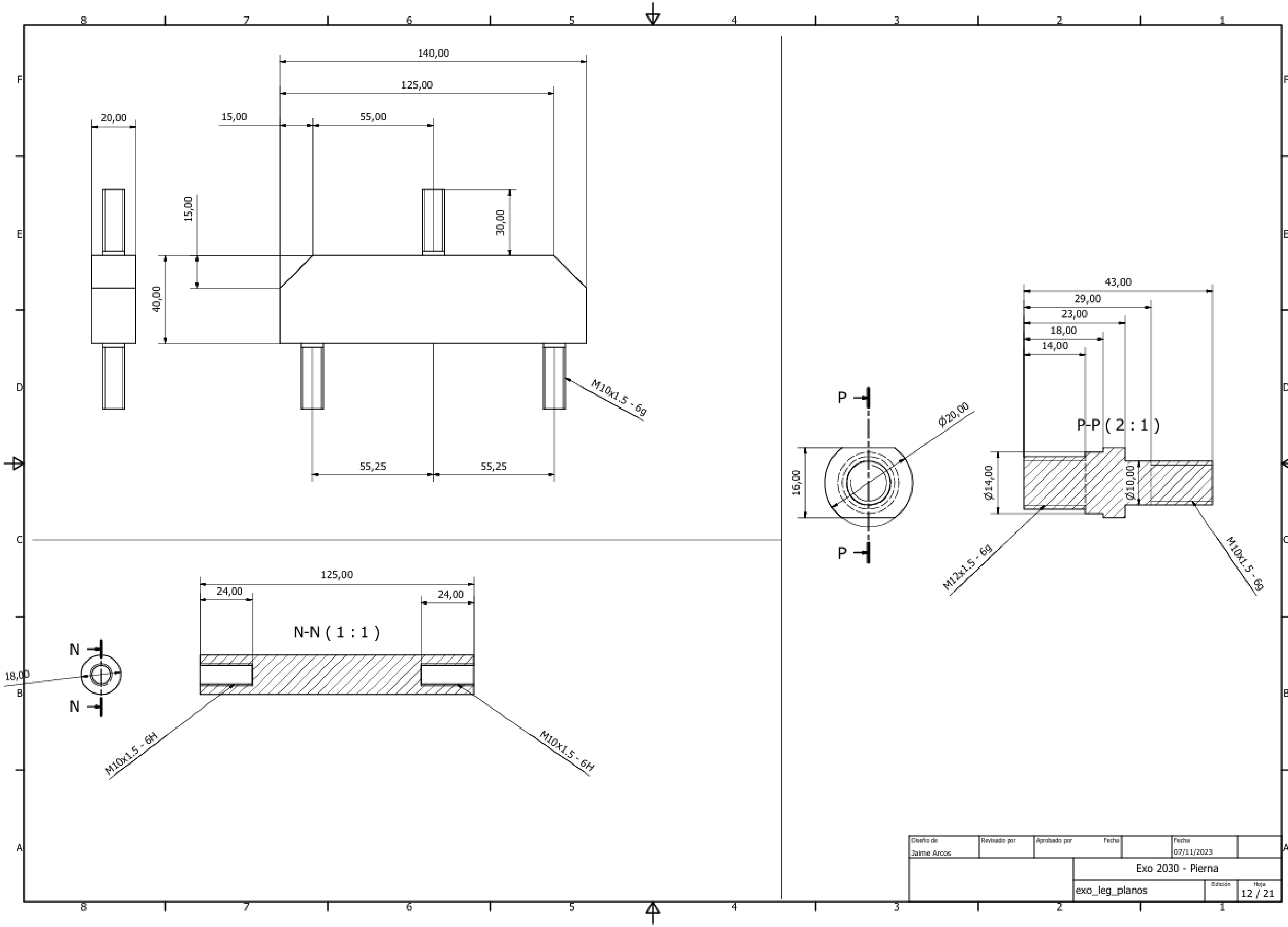
140,00
125,00
20,00
15,00
55,00
15,00
30,00
40,00
M10x1.5 - 6g
55,25
55,25
43,00
29,00
23,00
18,00
14,00
P
P-P (2 : 1)
Ø20,00
16,00
Ø14,00
Ø10,00
M12x1.5 - 6g
M10x1.5 - 6g
125,00
24,00
24,00
N-N (1 : 1)
N
18,00
M10x1.5 - 6H
M10x1.5 - 6H
Diseño de
Jaime Arcos
Revisado por
Aprobado por
Fecha
Fecha
07/11/2023
Exo 2030 - Pierna
exo_leg_planos
Edición
Hoja
12 / 21

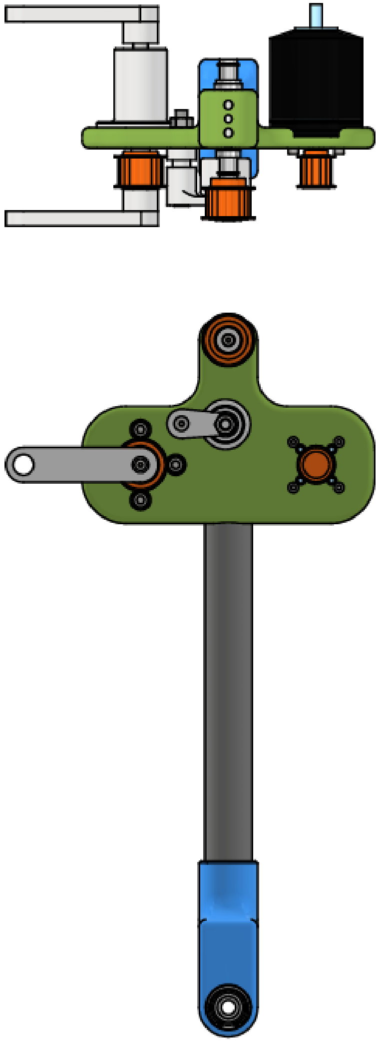

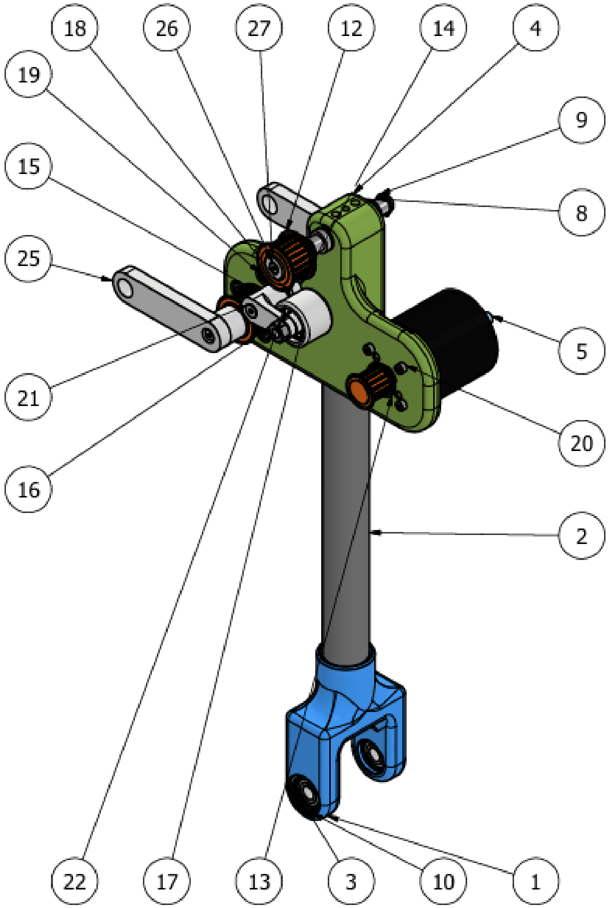

LISTA DE PIEZAS		
ELEMENTO	CTDAD	Nº DE PIEZA
1	1	acople-pivote-pantorrilla-eje
2	1	tubo_pierna
3	2	SKF_6200-2RSH
4	1	acople-pivote-rodilla-eje
5	1	Part 1
6	1	manzana_1
7	2	SKF_6000-2RSH
8	1	pivote-cadera-eje
9	2	DIN 471 - 12x1
10	2	DIN 472 - 30 x 1.2
11	1	DIN 472 - 26 x 1.2
12	2	LS 28 AT5_20-2 hub 24x6 dv=6
13	1	LS 28 AT5_14-2 hub 14x6 dv=6
14	1	Perno_tensor
15	1	biela_tensor
16	1	eje_tensor
17	2	skf_bearing_6001-2rsh_2
18	1	rodillo_tensor
19	4	AS 1420 - 1973 - M6 x 10
20	5	AS 1420 - 1973 - M4 x 8
21	1	DIN 7991 - M5x8
22	2	AS 1112 - M8 Tipo 5
23	1	eje_cuatro_barras
24	1	DIN 471 - 9x1
25	2	Biela
26	3	DIN 7991 - M4x8
27	1	arandela_pulley

Diseño de	Revisado por	Aprobado por	Fecha	Fecha
Jaime Arcos				07/11/2023

Exo 2030 - Pierna

	Edición	Hoja
exo_leg_planos		13 / 21

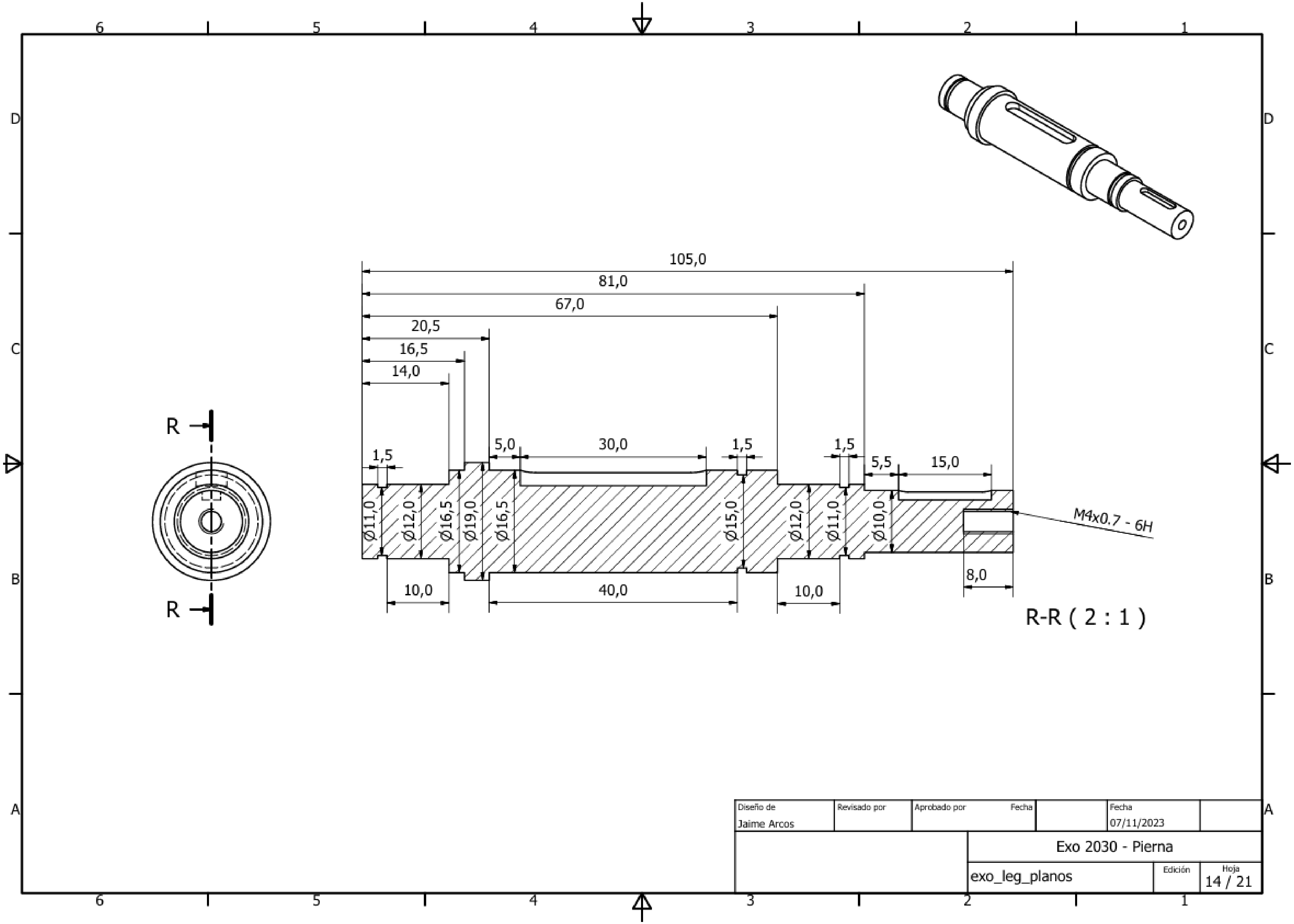

105,0
81,0
67,0
20,5
16,5
14,0
1,5
5,0
30,0
1,5
1,5
5,5
15,0
Ø11,0
Ø12,0
Ø16,5
Ø19,0
Ø16,5
Ø15,0
Ø12,0
Ø11,0
Ø10,0
M4x0.7 - 6H
10,0
40,0
10,0
8,0
R
R
R-R (2 : 1)
Diseño de
Jaime Arcos
Revisado por
Aprobado por
Fecha
Fecha
07/11/2023
Exo 2030 - Pierna
exo_leg_planos
Edición
Hoja
14 / 21

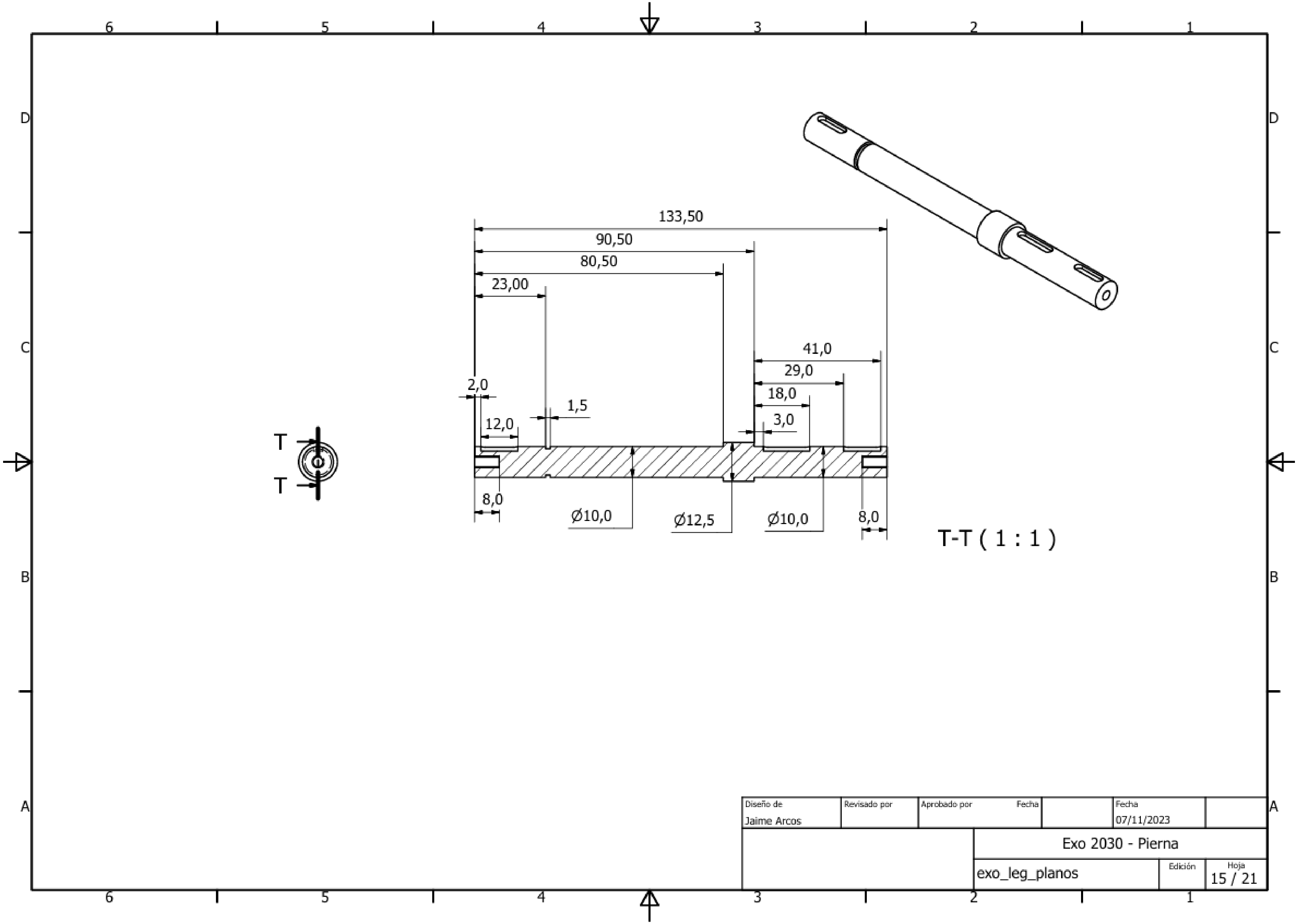
133,50
90,50
80,50
23,00
41,0
29,0
18,0
3,0
2,0
1,5
12,0
8,0
Ø10,0
Ø12,5
Ø10,0
8,0
T
T
T-T (1 : 1)
Diseño de
Jaime Arcos
Revisado por
Aprobado por
Fecha
Fecha
07/11/2023
Exo 2030 - Pierna
exo_leg_planos
Edición
Hoja
15 / 21

LISTA DE PIEZAS		
ELEMENTO	CTDAD	Nº DE PIEZA
1	1	Base_motor_cadera_2
2	1	Part 1
3	2	SKF_6201-2RSH
4	1	eje_cadera_abducion
5	1	resorte_torsion
6	2	DIN 472 - 32 x 1.2
7	2	DIN 471 - 19x1.2
8	1	LS 28 AT5_14-2 hub 14x6 dv=6
9	1	Perno_tensor
10	1	biela_tensor
11	1	eje_tensor
12	2	skf_bearing_6001-2rsh_2
13	1	rodillo_tensor
14	1	AS 1112 - M8 Tipo 5
15	1	DIN 7991 - M5x8
16	4	AS 1420 - 1973 - M4 x 8

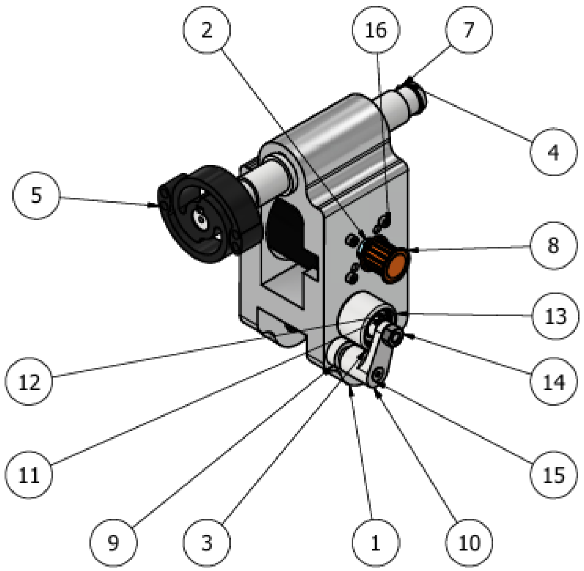

C-C (1 : 3)

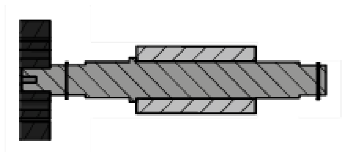

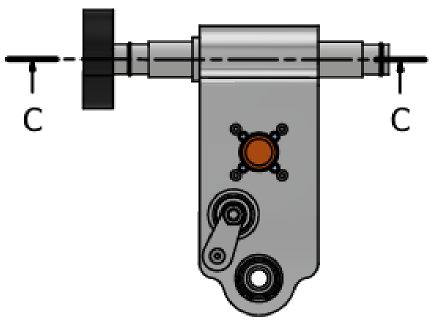

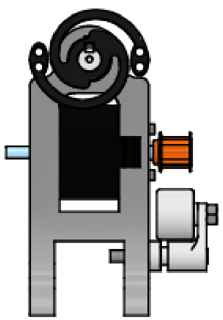

Diseño de	Revisado por	Aprobado por	Fecha		Fecha	
Jaime Arcos					07/11/2023	

	Exo 2030 - Pierna		
	exo_leg_planos	Edición	Hoja 16 / 21

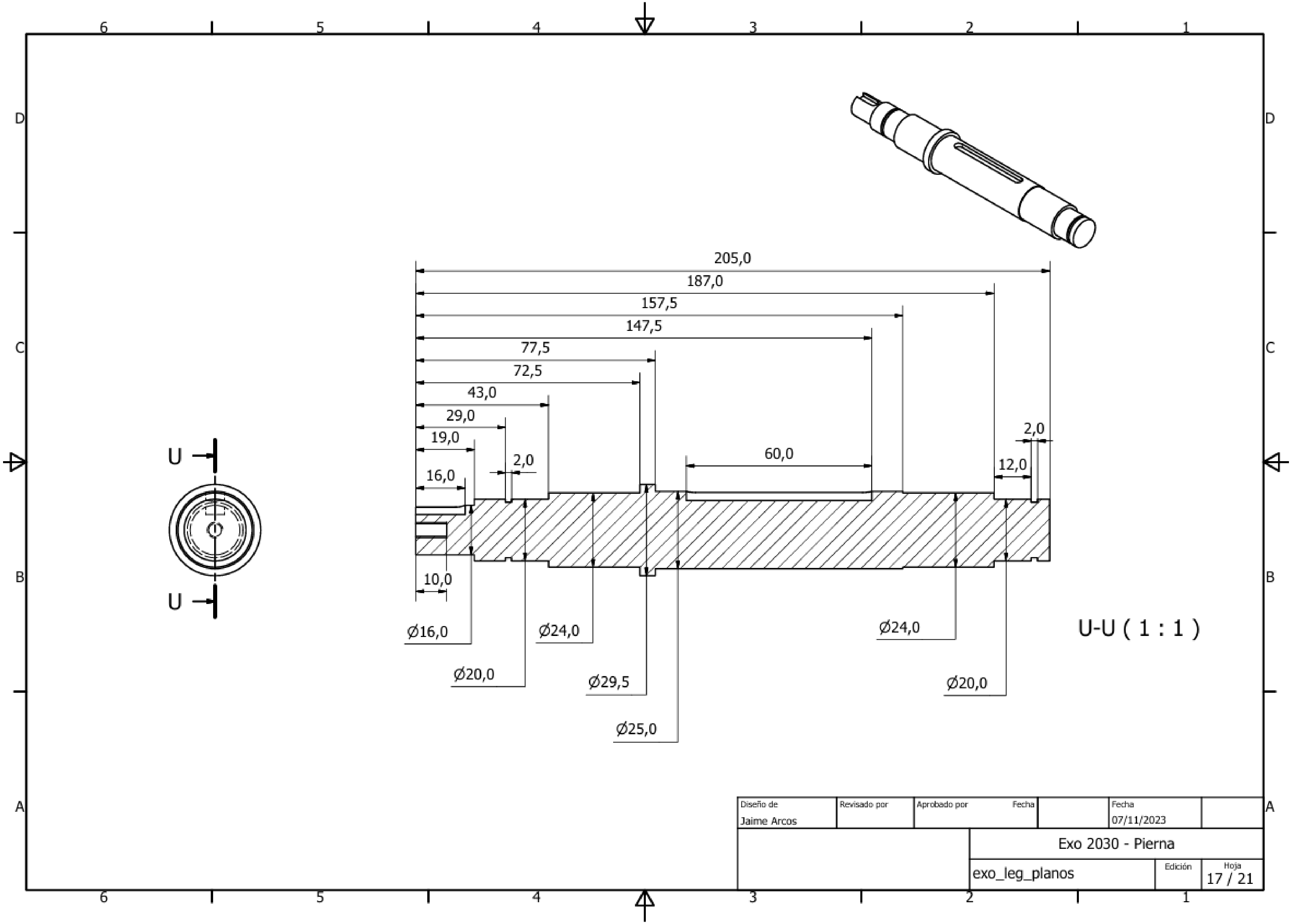
205,0
187,0
157,5
147,5
77,5
72,5
43,0
29,0
19,0
16,0
2,0
60,0
2,0
12,0
10,0
Ø16,0
Ø20,0
Ø24,0
Ø29,5
Ø25,0
Ø24,0
Ø20,0
U
U
U-U (1 : 1)
Diseño de
Jaime Arcos
Revisado por
Aprobado por
Fecha
Fecha
07/11/2023
Exo 2030 - Pierna
exo_leg_planos
Edición
Hoja
17 / 21

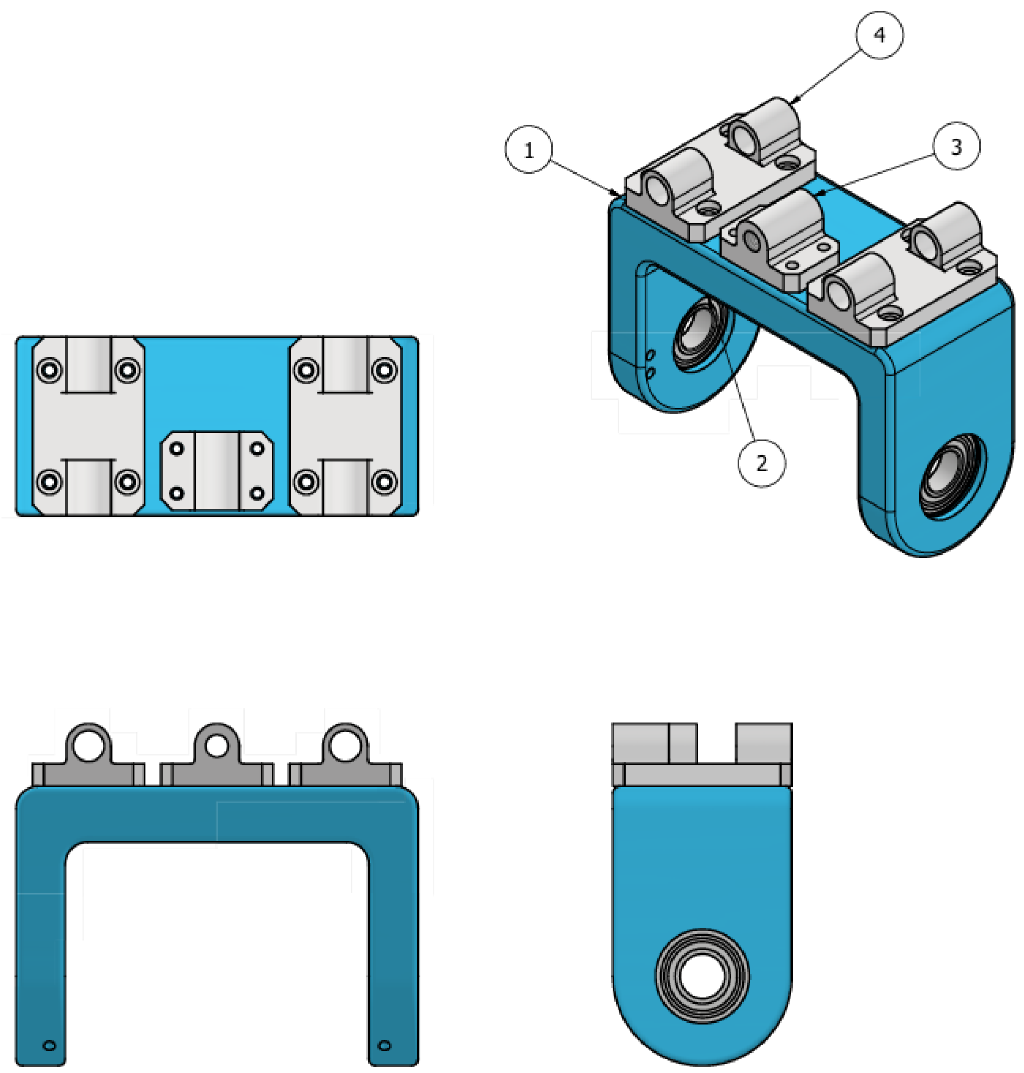

LISTA DE PIEZAS		
ELEMENTO	CTDAD	Nº DE PIEZA
1	1	base_cadera
2	2	SKF_6004-2RSH
3	1	tuerca
4	2	corredera

Diseño de	Revisado por	Aprobado por	Fecha	Fecha
Jaime Arcos				07/11/2023

Exo 2030 - Pierna

exo_leg_planos | Edición | Hoja 18 / 21

LISTA DE PIEZAS		
ELEMENTO	CTDAD	Nº DE PIEZA
1	1	amarre_barras_2
2	1	tornillo_cadera
3	1	amarre_barras_1
4	2	barra_cadera
5	4	DIN 7984 - M4 x 6
6	1	pasador_tornillo_fino
7	1	DIN 471 - 6x0.7

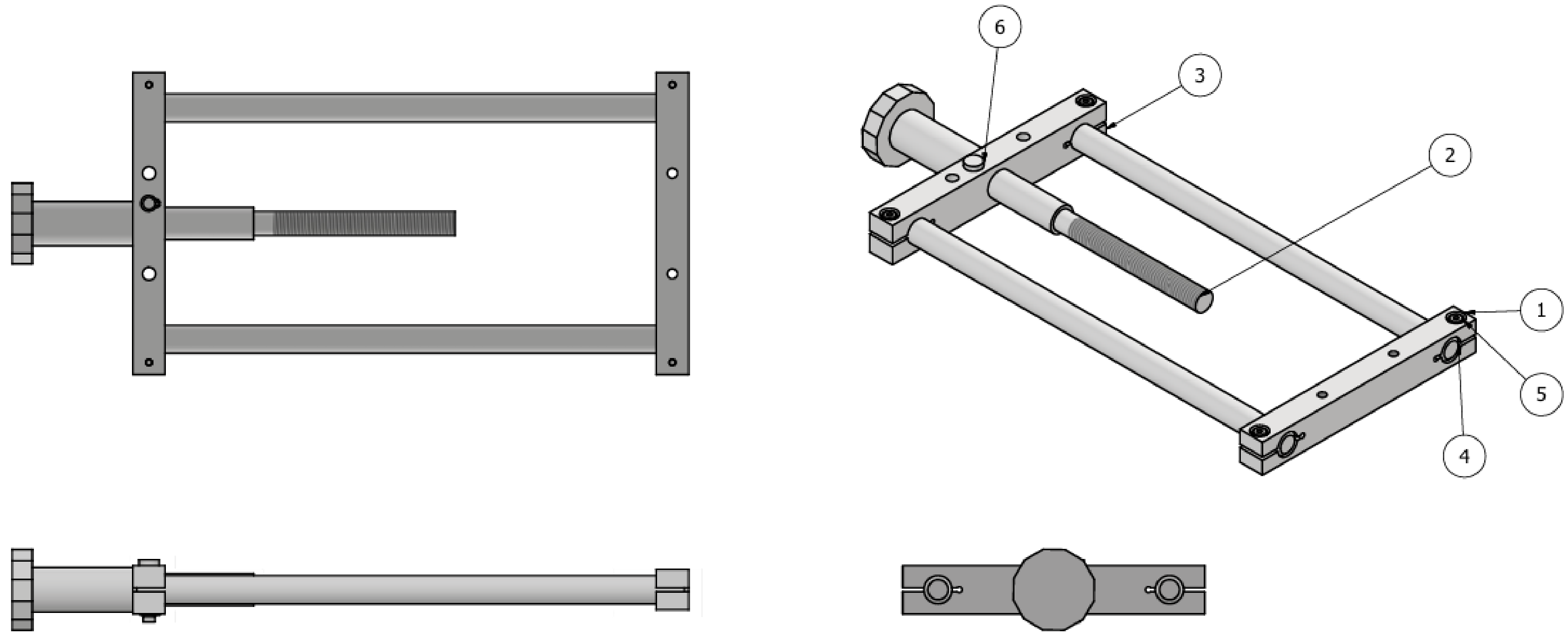

Diseño de	Revisado por	Aprobado por	Fecha	Fecha
Jaime Arcos				07/11/2023

Exo 2030 - Pierna

	Edición	Hoja
exo_leg_planos		19 / 21

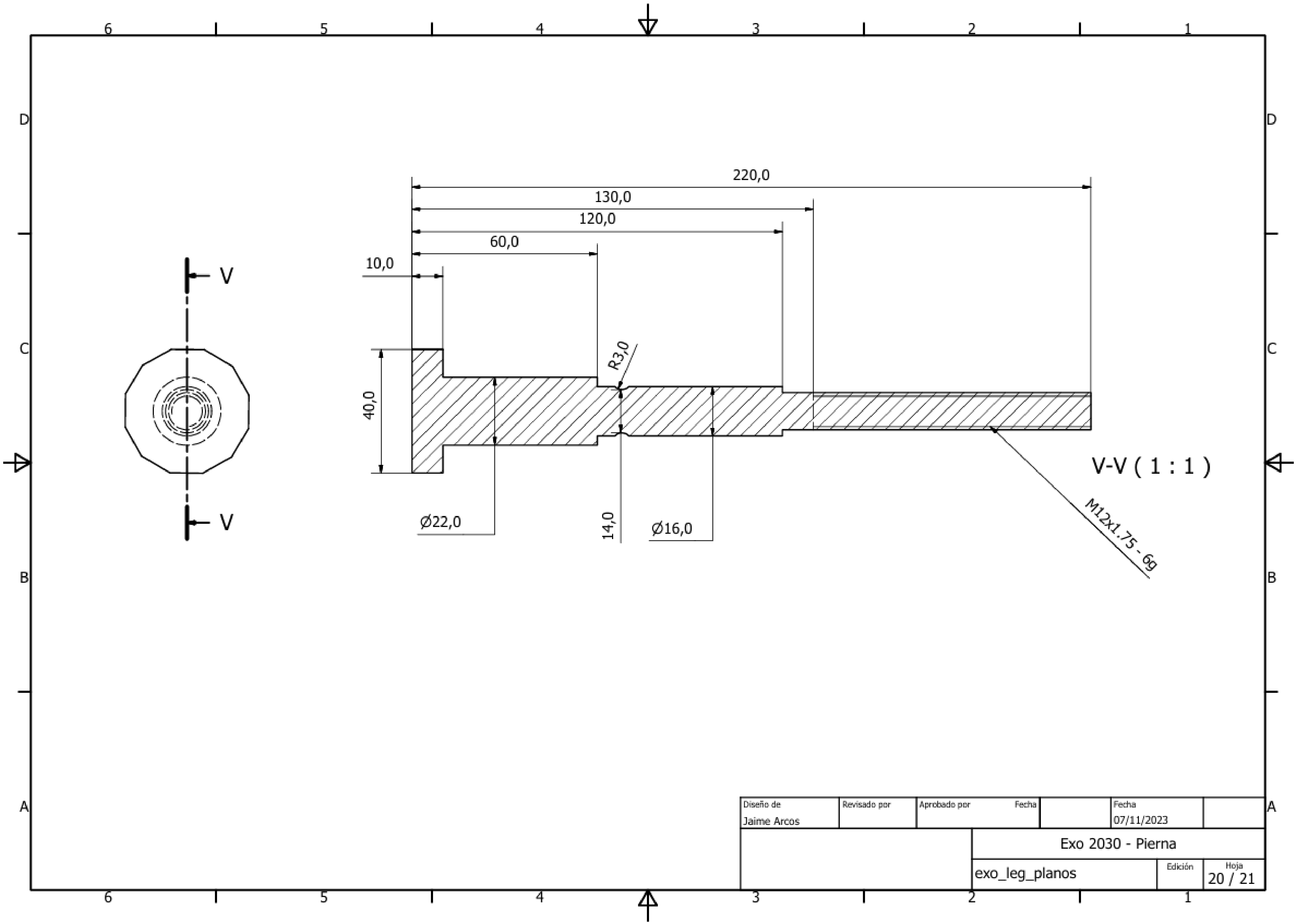
V
V
220,0
130,0
120,0
60,0
10,0
R3,0
40,0
Ø22,0
14,0
Ø16,0
V-V (1 : 1)
M12x1.75 - 6g
Diseño de
Jaime Arcos
Revisado por
Aprobado por
Fecha
Fecha
07/11/2023
Exo 2030 - Pierna
exo_leg_planos
Edición
Hoja
20 / 21

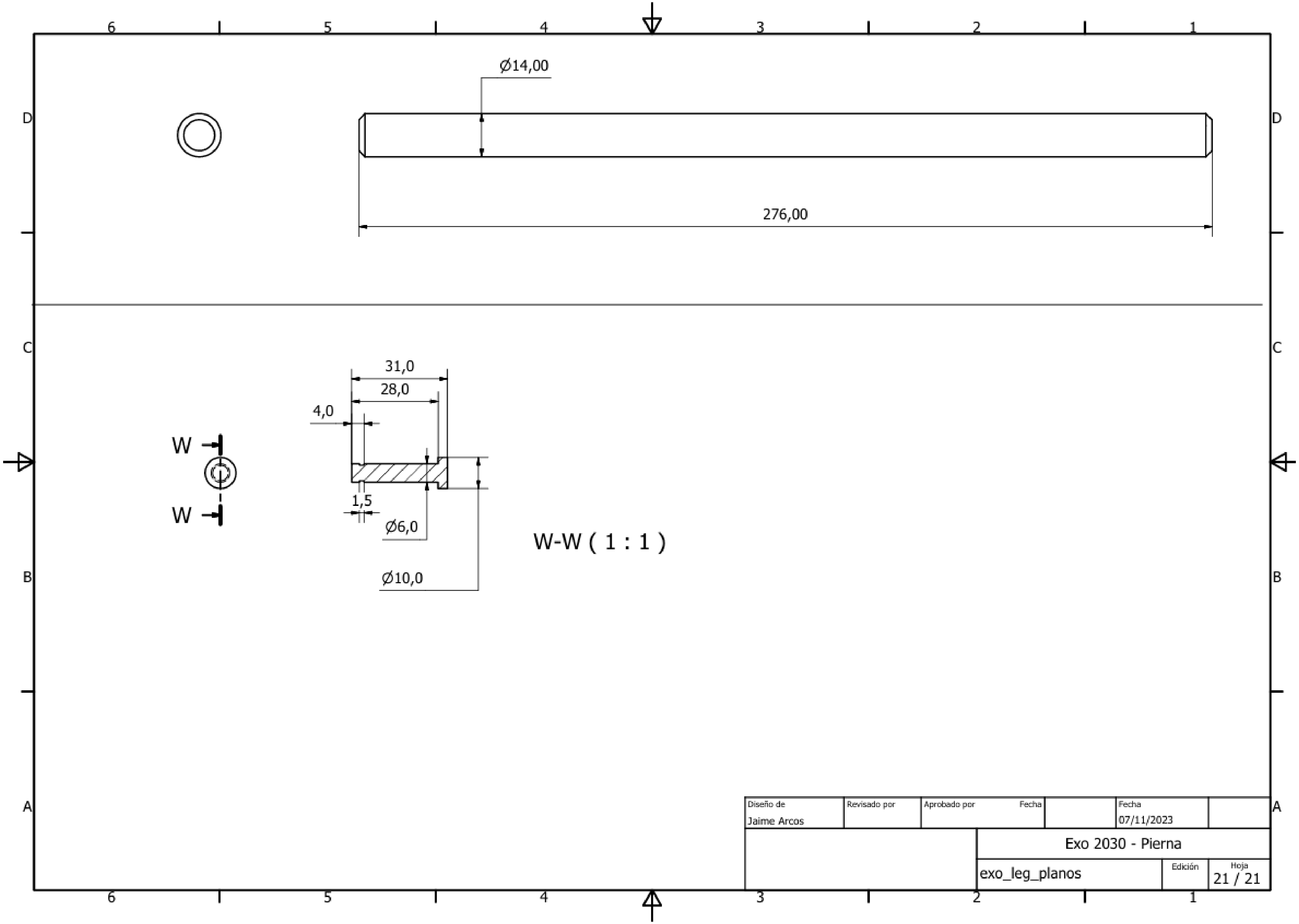

Diseño de	Revisado por	Aprobado por	Fecha		Fecha	
Jaime Arcos					07/11/2023	
	Exo 2030 - Pierna					
	exo_leg_planos				Edición	Hoja 21 / 21

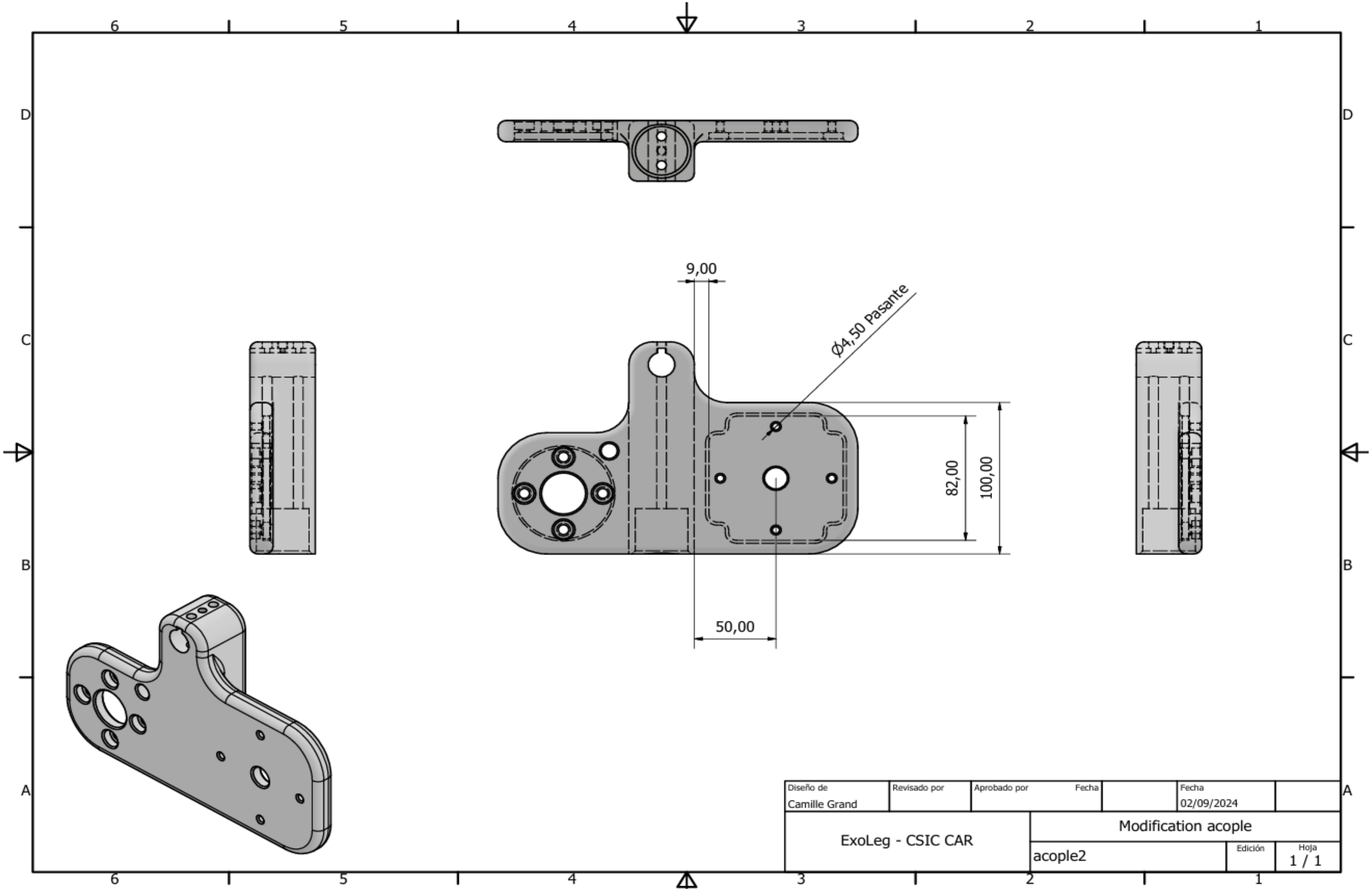
9,00
Ø4,50 Pasante
82,00
100,00
50,00
Diseño de
Camille Grand
Revisado por
Aprobado por
Fecha
Fecha
02/09/2024
ExoLeg - CSIC CAR
Modification acople
acople2
Edición
Hoja
1 / 1